



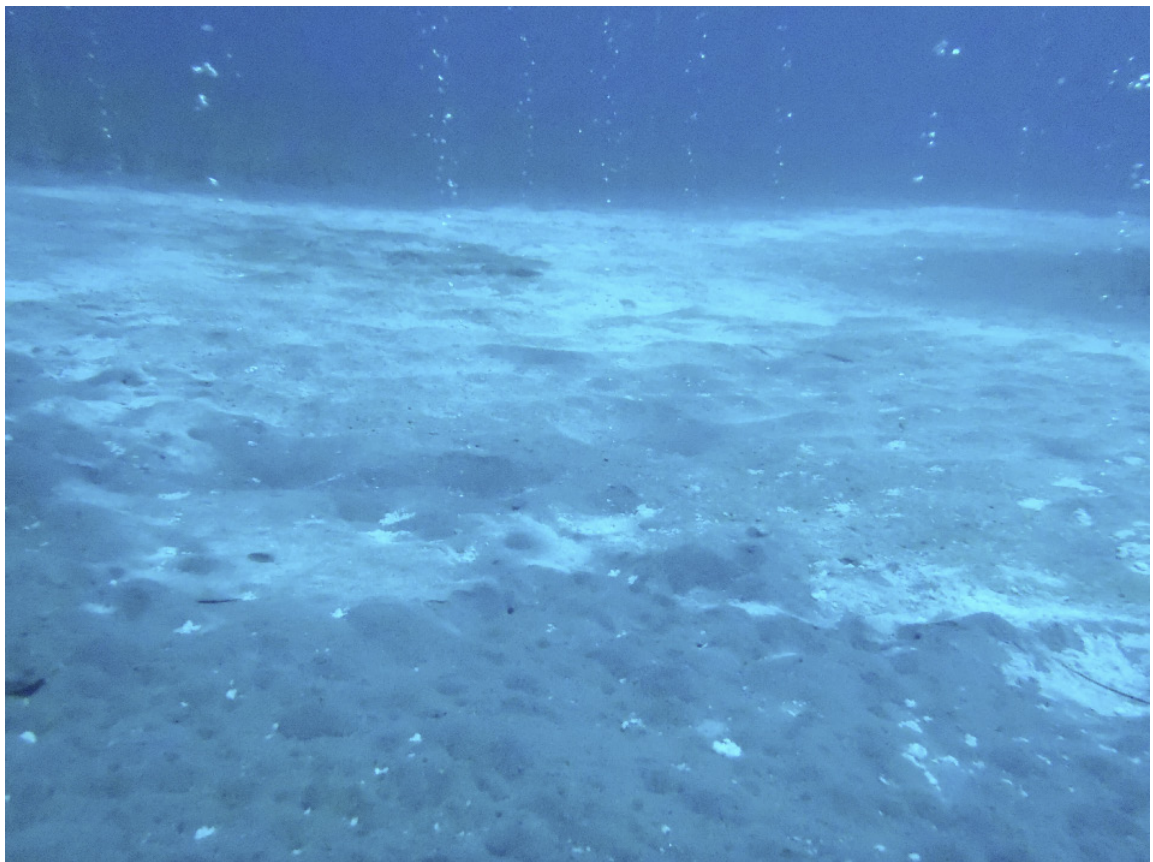
Stockholm  
University

# Master Thesis

Degree Project in  
Geochemistry 45 hp

## **A Biomarker Study of Carbon Cycling in the Shallow Submarine Hydrothermal Sediments of Milos Island (Greece)**

Alan Wiech



Stockholm 2016

Department of Geological Sciences  
Stockholm University  
SE-106 91 Stockholm  
Sweden

**Abstract**

The arsenic rich shallow submarine area surrounding Milos is affected by constant hydrothermalism, due to the subduction of the African plate under the Eurasian plate. Sediments affected by hydrothermalism in this area can be characterized into different microbial mat communities, which are affected by different physico-chemical conditions. Though these mats have been studied, the drivers of primary production, which are imperative in tracing the geochemical cycles of trace metals and for supporting life in this arsenic-rich environment, have yet to be studied in detail. This study therefore seeks to contribute to this understanding by coupling a lipid biomarker analysis to molecular microbial analysis of DNA to further constrain the processes that drive the structuring of microbial communities in the shallow submarine hydrothermal system of Milos. This together with compound specific  $\delta^{13}\text{C}$  isotope ratios of the lipid biomarkers to distinguish the dominant carbon source together with the bulk sediment of  $\delta^{13}\text{C}$ -DIC, -POC and -TOC to see if recent hydrodynamic processes are seen in the sediment records. From this a comprehensive lipid biomarker interpretation is constructed from the various sediments, together with RuBisCO and rTCA abundances. This indicated that the organism's abundance and diversity increase in the periphery and the outer regions of the hydrothermal vent field. The same is seen through depth in the different regions, with the microbial mats most likely affected by the sharp temperature rise. The carbon isotope values from the two microbial mat lipids indicated that the most likely carbon source for organism's biosynthesis is dissolved  $\text{CO}_2$ . Furthermore, this study showed for the first time that the main carbon fixation pathway in all sediment sites was the RuBisCO (form II) for the chemoautotrophic and photoautotrophic organisms. This is an important finding as the most active carbon fixation pathway in deep-sea hydrothermal systems is the rTCA cycle. For future studies involving carbon fixation pathways in submarine hydrothermal vent systems, the hydrothermal vent field around the island of Milos is an ideal research location with high RuBisCO (II) activities. If there is a connection between RuBisCO (II) and arsenic in the environment these future studies could give a better understanding of how organisms survived in the early Earth environments.

## Contents

1. Introduction .....	4
2. Background .....	6
2.1. Study Area & Shallow Submarine Hydrothermal Vent Systems of Milos Island .....	6
2.2. Biomarkers as proxies of life in geological environments.....	7
2.3. Classification of organisms based on their metabolism .....	10
3. Objectives .....	14
4. Material and methods.....	15
4.1. Core sampling.....	15
4.2. Sediment carbon isotope analysis, dissolved inorganic carbon ( $\delta^{13}\text{C}$ -DIC), particulate organic carbon ( $\delta^{13}\text{C}$ -POC) and total organic carbon ( $\delta^{13}\text{C}$ -TOC) .....	17
4.3. Reference pure microbial culture analysis .....	17
4.4. Extraction of lipids from reference microbial cultures.....	18
4.5. Sediment lipid extraction .....	19
4.6. Solid phase chromatography .....	19
4.7. Methylation and Silylation .....	21
4.8. Gas-chromatography Mass Spectrometry (GC-MS) .....	22
4.9. Lipid calculations .....	22
4.10. Isotopic ratio mass spectrometer (IRMS).....	23
4.11. High Performance Liquid chromatography mass spectrometry (HPLC-MS) .....	23
4.12. Gene abundances involved in carbon fixation pathways .....	24
5. Results.....	25
5.1. TOC.....	25
5.2. $\delta^{13}\text{C}$ of DIC and POC.....	26
5.3. Lipid analysis on collected samples .....	29
5.4. Lipid distributions .....	29
5.5. Lipid analysis of bacterial and archaeal pure cultures .....	33
5.6. Archaeol and GDGTs obtained with HPLC-MS.....	34
5.7. Isotopic signature of lipids (IRMS data) and their isotopic fractionation.....	36
5.8. rTCA, RuBisCO (I) and RuBisCO (II) signatures .....	36
6. Discussion.....	40
6.1. DIC and POC.....	40
6.2. Lipid abundances affected by hydrothermal transition zones.....	40
6.3. The presence of Sterols. ....	42
6.4. The presence of Hopanoids.....	43
6.5. The identified GDGTs.....	43

6.6. Culture lipid analysis .....	45
6.7. Isotopic lipid signatures indicating a mixed source from methanotrophs .....	45
6.8. RuBisCO (II) dominated throughout the sites .....	47
7. Conclusions .....	49
8. Acknowledgements.....	50
9. References .....	51
10. Appendix .....	61

## 1. Introduction

Marine hydrothermal vent systems, usually represented by high biological productivity (Nakagawa & Takai 2008), occur near seismically and volcanically active sea-floor spreading regions such as the East Pacific Rise (e.g. Amend et al 2011; Bennett et al 2011), the Mid-Atlantic Ridge (e.g. Kelley et al., 2001; Amend et al 2011) and the Volcanic arc in Mediterranean (e.g. Kiliyas et al., 2013; Price et al., 2013a, 2013b; Godelitsas et al., 2015). One of the most seismically active regions on Earth is situated in the Aegean Sea. This activity, which is a result of the subduction of the African plate

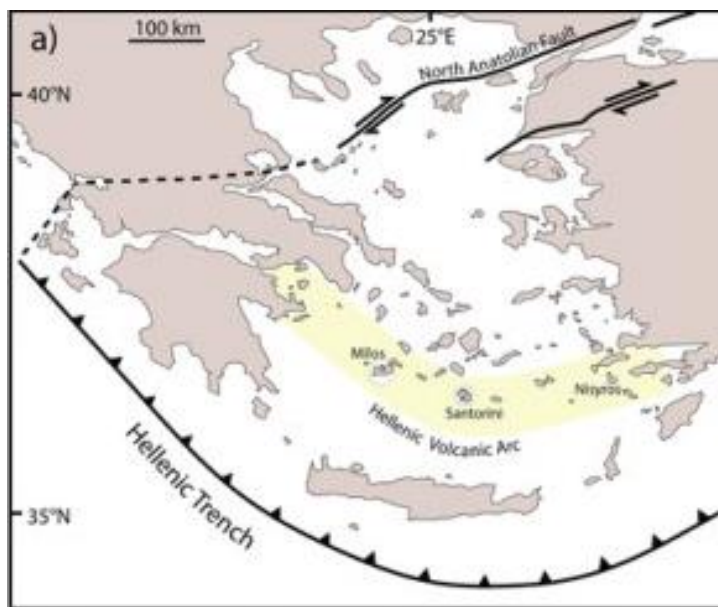


Figure 1. Hydrothermalism is affecting the regions where the Hellenic Volcanic Arc is situated. This is due to the subduction of the African plate at the Hellenic trench area (reprinted from Gilhooly et al. 2014).

under the Eurasian plate (Dando et al., 1994), produces hydrothermal activity and gas venting along the Hellenic Volcanic Arc (HVA) (figure 1), dating to at least five million years ago (Kiliyas et al., 2013).

Here different shallow submarine hydrothermal vent systems are affecting many of the islands in this region.

Greece's island of Milos, situated on the HVA, is characterized by the largest known shallow submarine

hydrothermal system that mainly expels carbon dioxide arsenic-rich fluids, along with minor traces of  $H_2$ ,  $H_2S$  and  $CH_4$  (Dando et al., 1995; Breuer and Pichler, 2013; Price et al., 2013a, 2013b; Godelitsas et al., 2015). These submarine low-temperature venting systems have in some cases precipitated iron and manganese oxides (Cronan et al., 1995; Hein et al., 2000; Chi Fru et al., 2013; 2015), leading to an enrichment of nutrients such as  $Na^+$ ,  $Ca^{2+}$ ,  $K^+$ ,  $SiO_2$ ,  $Mn^{2+}$  and  $NH_3$  (Fitzsimons et al., 1997), which are essential for stimulating microbial life. However, the hydrothermal fluid that is expelled from these systems is a net source of arsenic in these environments (Godelitsas et al., 2015).

In shallow submarine hydrothermal areas of Milos, there are sediments that can be characterized into different group types containing Yellow-, White- and Brown- mats.

These mats are a result of different hydrothermal conditions, which cause different precipitations at the sediment-water interface and are often associated with microbial mats (Dando et al., 1995a; Price et al., 2013a). The yellow mat, located in the most hydrothermally active area, is mainly composed of elemental sulfur, which is condensed on sand grains, at temperatures of up to 95°C at 2 cm sediment depth (Dando et al., 1995b). Usually the yellow mat is surrounded by a white mat, which has a lower temperature range of 40 to 95°C, composed of precipitated white amorphous silica and sulfur (Dando et al., 1995a; Fitzsimons et al., 1997; Wenzhöfer et al., 2000). The precipitated white mats are assumed to be linked to microbial activity with sulphide-tolerant species. Moving outwards from the white mats are the brownish mats, which are also affected by the hydrothermal activity but with a lower temperature range, with values below 40°C at 2 cm sediment depth (Dando et al., 1995b; Wenzhöfer et al., 2000). Ranging between 0.5 and 6 meters in diameter, these brownish mat areas are comprised mainly of Mn-oxides and arsenic sulfides precipitated from the hydrothermal vents (Dando et al., 1995b; Wenzhöfer et al., 2000; Price et al., 2013b).

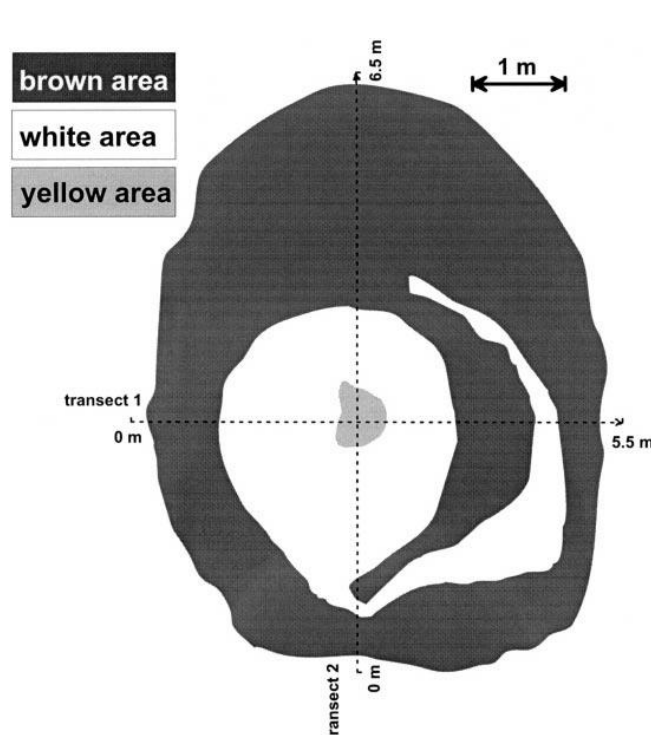
The diversity of the microbial communities varies across the different mats (Sievert et al., 1999; Price et al., 2013a). However, the drivers of primary production, which are imperative in tracing the geochemical cycles of trace metals and for supporting life in this arsenic-rich environment, have yet to be studied in detail. Though Price et al 2013a suggested that specific Alpha- and Beta-proteobacteria could play an important role in the arsenic cycling. Moreover, understanding the issues concerning the effect of toxic levels of arsenic on microbial community structures distribution and function, both in the sediments and the water column is far from complete. Although Milos is the largest known shallow submarine hydrothermal system (Dando et al., 1995a), no related biomarker studies coupled with carbon fixation pathways has been produced from these areas. This study therefore seeks to contribute to this understanding by coupling a lipid biomarker analysis to molecular microbial analysis of DNA to further constrain the processes that drive the structuring of microbial communities in the shallow submarine hydrothermal system of Milos. Importantly, some hydrothermal deposits of Milos contain deposits that have been proposed as modern banded iron formation (BIF) analogues attributed to microbial processes (Chi Fru et al., 2013, 2015). Therefore a deep understanding of the microbial activity in the hydrothermal vent fields may reveal new insights into our understanding of

biogeochemical processes that operated in the Precambrian oceans, 3.8-1.8 billion years ago when BIFs formed (Bekker et al., 2010).

## 2. Background

### 2.1. Study Area & Shallow Submarine Hydrothermal Vent Systems of Milos Island

Beneath the Mediterranean the African plate is continuously being subducted underneath the Eurasian plate, forming a Volcanic Arc with hydrothermal vent systems. Out of all the hydrothermal systems in the Aegean Sea (Kiliyas et al., 2013), the areas surrounding the island of Milos are the most studied (e.g. Dando et al., 1995; Breuer and Pichler, 2013; Price et al., 2013a, 2013b; Godelitsas et al., 2015), mainly due to the diversity of hydrothermal vents, and the easy accessibility for sampling and researching in-situ processes. Price et al., (2013b) has shown that these low temperature hydrothermal vent systems are primary sources of arsenic, this because the fluid discharges have high arsenic (As) concentrations. Price et al., (2013b) analyzed pore fluids and sediments from diffuse hydrothermal venting in both Palaeochori and Spathi Bays, Milos, with both high and low saline hydrothermal fluids, and recorded the highest As concentrations for any submarine hydrothermal system (as high as  $78 \mu\text{M}$  in the low saline fluids). In addition to arsenic, these systems also expel large volumes of gases in the form of carbon dioxide ( $\text{CO}_2$ , 54 - 90%), with minor signals of hydrogen ( $\text{H}_2$ ), hydrogen sulfide ( $\text{H}_2\text{S}$ ) and methane ( $\text{CH}_4$ ), due to slab and mantle subduction, and



degassing of carbonates in the sediments (Dando et al., 1995a & 1999). Moreover, the seep fluid is enriching the areas with  $\text{Na}^+$ ,  $\text{Ca}^{2+}$ ,  $\text{K}^+$ ,  $\text{SiO}_2$ ,  $\text{Mn}^{2+}$  and  $\text{NH}_3$ , encouraging microbial conditions, as they use these as nutrients in their metabolic processes (Dando et al., 1995; Fitzsimons et al., 1997).

Figure 2. Conceptual model of venting zones, with the highest temperature in the middle yellow area (reprinted from Wenzhöfer et al., 2000).

Dando et al (1995a) & Fitzsimons et al (1997) discovered three geochemically distinct zones in the Milos hydrothermal system, with each being characterized by distinct temperature zones (figure 2). These are the yellow-, white- and brown areas, and due to the dynamic hydrodynamics in these oceans (e.g. tides, currents and micro-earthquakes) the mats are constantly disappearing and re-appearing (Yücel et al., 2013). The yellow area is in the inner vent area and is influenced by the most hydrothermal activity, out of the three zones (Dando et al., 1995a; Fitzsimons et al., 1997; Wenzhöfer et al., 2000), though this was not present in this study. For the white area, in the sharp interface between hot fluid seepage and cold-seawater, Yücel et al. (2013) revealed that this (white) area had the strongest vent fluid influence and an overlap of O<sub>2</sub> with free sulfide at the surface sediment, which are conducive for the growth of sulfur-oxidizing bacteria (Yücel et al., 2013). Amorphous silica with silica nodules and elemental sulfur forms a white precipitate presumably together with microbial processes (Dando et al., 1995b). Using in situ micro-sensors Wenzhöfer et al (2000) presented evidence for a microcirculation in the hydrothermal vent outlet, this through the convective cells, caused by the gas seepage, sucking down O<sub>2</sub> leading to oxidation of the upstreaming H<sub>2</sub>S. Finally, further away where the induced circulation is reduced, the brown area is present. This area is characterized by even less hydrothermal activity and having MnO<sub>2</sub> be partly responsible for the brown precipitate (Wenzhöfer et al., 2000). Even though these areas, affected by dynamic hydrodynamics (Yücel et al., 2013), have been studied, the organisms metabolic processes have yet to be researched and understood.

## 2.2. Biomarkers as proxies of life in geological environments

Life on Earth is diverse, the most abundant being microbial organisms. Capable of surviving in the most unique environments, microbes are divided into three domains of life in the phylogenetic tree (figure 3). These include: Eukarya; and the prokaryotes Bacteria and Archaea (Woese et al., 1990). The eukaryotic domain consists of organisms with membrane-bound nuclei and complex organelles (Woese et al., 1990), whereas the prokaryotes are mainly characterized by single-cells (unicellular organisms) with no membrane-bound cell nucleus or organelles (Starr et al., 1981). To protect intercellular structures from the harsh extracellular conditions of the environment, all organisms have lipid membranes surrounding their cellular structures. Lipid membranes allow the passage of water; inorganic ions; consumption (carbon fixation); and waste byproducts

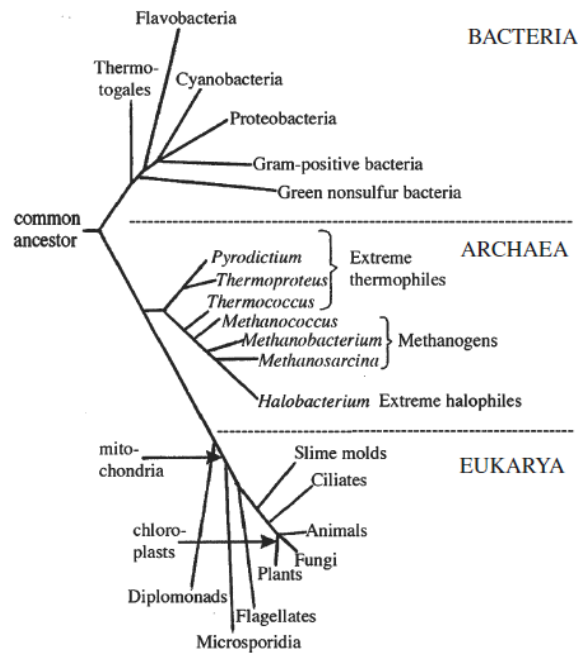


Figure 3. A 16S rRNA gene phylogenetic tree showing the three key domains of life (Stan-Lotter and Fendrihan, 2012).

(usually a double layered hydrocarbon chain), with a glycerol backbone and ester-bonds. However, archaeal lipids can have either a mono- or double layered hydrophobic core with ether-bonds on the hydrocarbon chain connecting to the glycerol and polar head group (figure 4) (Peters et al., 2005).

Organisms have evolved differently to adapt to changes in temperature. Bacteria and eukaryota have fatty-acid tail groups connecting to their head group in the phospholipid. To adapt to higher temperatures, the lengths of the fatty acids are often regulated, unsaturations and/or cyclic lipids are introduced. Conversely lipid chains are often longer when the organisms need to adapt to/tolerate higher temperatures. Bacteria insert hopanoids as their cyclic lipids, while eukaryotes insert sterols, both of which increase membranes stiffness and stability (Timmis 2010). Another mechanism which increases the fluidity in the membrane, are iso or anteiso branched-chain acids in the phospholipids (Harwood & Russel, 1984). Archaeal organisms introduce isoprenoid sidechains, which are comprised of a five carbon structure with different lengths, as the main structural compounds in their phospholipids (figure 4). To increase the resistance and to become more thermally stable the addition of cyclopentyl rings are introduced (in the tail part of the phospholipid). This makes them more densely packed and more rigid, which in turn increases their tolerability to higher temperatures (Peters et al.,

from internal reactions (Peters et al., 2005). Almost all organisms have a lipid bilayer surrounding the cell membrane and nucleus (figure 4). At opposite ends of the lipid bilayer are hydrophilic polar head groups (phosphate-based) connected to a glycerol, with either an ester or ether bond, connected to the two non-polar tail groups (hydrophobic hydrocarbon chains), all together called phospholipids (Peters et al., 2005). For bacteria and eukaryotic organisms the head groups are connected to the hydrophobic core

2005). Identifying specific lipid structures, recovered from the hydrothermal vent field in Milos, could give a better understanding on how well the organisms have adapted to these environment and also indicate which environments are the most habitable.

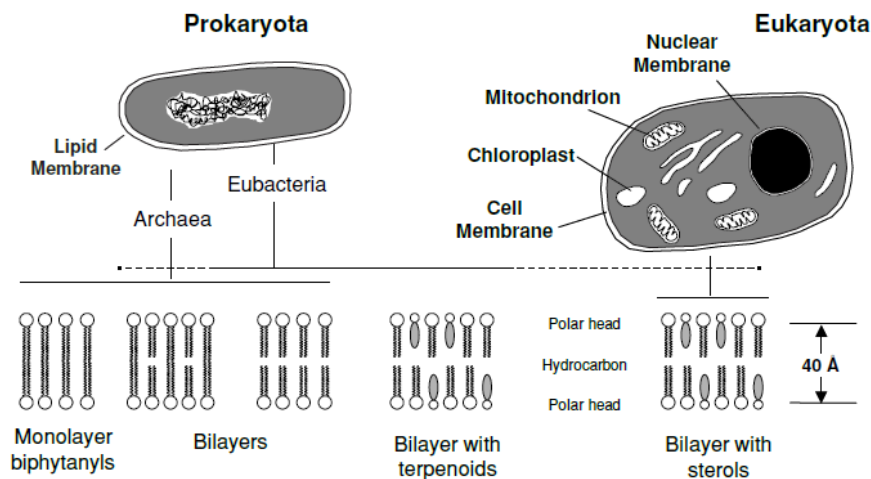


Figure 4. Lipid membrane structure of prokaryotes and eukaryotes. Almost all organisms have bilayer membranes. However, some prokaryotes have monolayers (reprinted as seen in Peters et al., 2005).

One of the ways to investigate the preservation of organic matter in soils and sediments is by analyzing lipid biomarkers. Lipid biomarkers are preserved due to their high resistance to biodegradation, either through sedimentation or diagenesis, where the organic matter undergoes a chemical, physical, or biological change after its deposition. Due to the strong carbon to carbon bonded lipid membranes, the lipids retain enough information to link compounds such as steranes (sterols) and hopanes (hopanoids) to eukaryotes and bacteria, respectively (Mackenzie et al., 1982). E.g. cholesterol are biosynthesized predominantly by animals while phytosterols (sitosterol or stigmasterol) by plants (Galea & Brown 2009). Moreover, to be able to synthesize sterols in any case, the presence of oxygen is an absolute requirement (Galea & Brown 2009). Hopanes, on the other hand, do not need oxygen in their synthesis. Using a lipid extraction method these lipids could bring light on what kind of organisms (eukaryotes or prokaryotes) are dominantly present in Milos's hydrothermal vent area.

For archaeal lipid traces, isoprenoid glycerol dialkyl glycerol tetraethers (GDGTs) and isoprenoid glycerol dialkanol diethers (GDDs) are used to identify archaeal biomass and information on how they were preserved (Liu et al., 2012; Lincoln et al., 2013).

Structured in isoprenoid chains, GDGTs can contain both cyclopentane and cyclohexane moieties. E.g. the non-thermophilic Crenarchaeota, classified as Thaumarchaeota (Smittenberg et al., 2005b; Schouten et al., 2013), can biosynthesize GDGTs containing

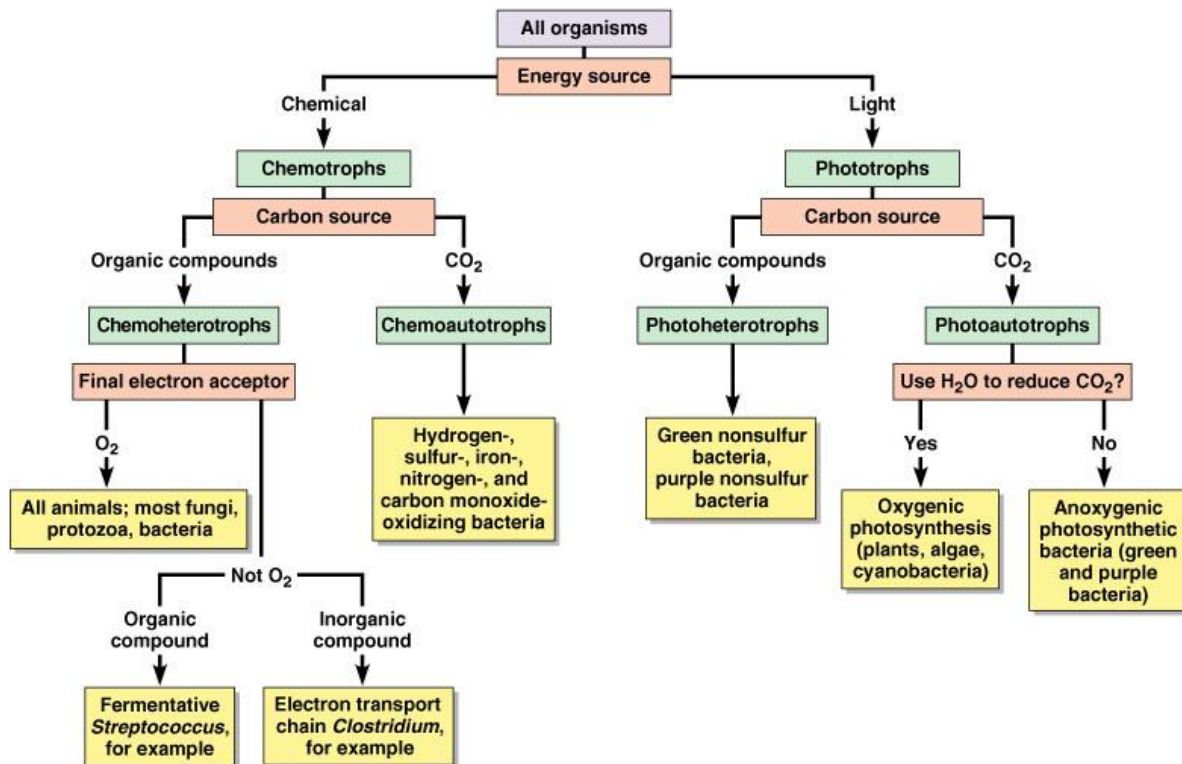
0-; 1-; 2-; and 3- cyclopentane moieties in conjunction with a crenarchaeol and its region-isomer (both containing four cyclopentane moieties and a cyclohexane moiety), and has been found in marine, lacustrine and terrigenous settings (Lincoln et al., 2013; Smittenberg et al., 2005b; Pearson et al., 2008). However, it has also been suggested that the crenarchaeol may also be a biomarker for the biosynthesis of a thermophilic ammonia oxidizing crenarchaeon "*Candidatus Nitrosocaldus yellowstonii*", which grows optimally at 72°C and under slightly alkaline conditions, producing high abundances of crenarchaeol (Pearson et al., 2008; Lincoln et al 2013), which is more suitable for this hydrothermal area. By identifying these GDGTs from the sediments from the hydrothermal vent area of Milos, these could shed light on which archaeal organisms are present in the systems. However, it is worth noting that recent studies suggest that GDGTs are not limited to archaea, but can also be produced by bacteria, producing branched GDGTs (Schouten et al., 2013 & references therein).

Lipids are vital components of cell membranes, which provide structural support for microbial cells (Jungblut et al., 2009). Some lipids are ubiquitous while other are specific to certain microorganisms (Casteñada & Schouten, 2011). Therefore, certain lipids found in the geological environments can be traced back to a group of organisms or specific processes (e.g. Zimmerman & Canuel, 2000; Coolen et al., 2004; Smittenberg et al., 2005). This will be one of the main focusses in this study.

### 2.3. Classification of organisms based on their metabolism

Organisms can further be classified based on their primary energy-consuming mechanisms: autotrophic, heterotrophic, phototrophic, chemotrophic, or by a compound using multiple terms (figure 5). Autotrophs reduce carbon dioxide (inorganic carbon) with energy obtained either from a light- (photoautotroph) or a chemical source (chemoautotroph). Chemoautotrophs utilize electron donors from inorganic chemical sources (e.g. H<sub>2</sub> or H<sub>2</sub>S) to synthesize organic compounds from CO<sub>2</sub>, making them primary producers in extreme environments such as hydrothermal vent systems (Nakagawa & Takai 2008). On the other hand, heterotrophs gain their carbon from organic compounds, where light is used as an energy source for photoheterotrophs, through anabolic (requiring energy) or catabolic (releasing energy) reactions, and chemoheterotrophs use aerobic (oxygen) or anaerobic (in the absence of oxygen) reaction pathways (Peters et al., 2005). There are also examples of lithotrophs that use inorganic substrates in their biosynthesis, and organotrophs that use organic substrates,

both of which can either be photo- or chemotrophs (Kuenen 2009). It is still unknown if phototrophs are an important process in the recycling of carbon in the shallow submarine hydrothermal vent systems of Milos, though this study can promote a better understanding of this, as the sediment surface is in the photic zone (where light can reach).

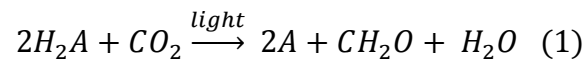


Copyright © 2004 Pearson Education, Inc., publishing as Benjamin Cummings.

Figure 5. A simplified classification of organisms based on their metabolic pathways (Brüchert seminar: Biogeochemistry org geochem-OM-biosynthesis-Tuesday, 2015).

The main primary producers of organic matter utilize photosynthetic pathways to grow, and many other organisms (e.g. heterotrophic bacteria) reuse the carbon originally produced by photosynthetic organisms (Peters et al., 2005 & references therein). Heterotrophs are also actively supported by chemoautotrophs (in the absence of phototrophs), which also produce organic carbon. This could be the case in the hydrothermal systems, where chemical energy is abundant and chemoautotrophs tend to be plentiful (e.g. Sievert et al., 1999; Giovannelli et al., 2013). By analyzing the different microbial mat systems, in Milos's submarine hydrothermal vent system, a better insight can be understood on which primary producers are dominating the system.

Organisms that photosynthesize (phototrophs) e.g. green plants and some bacteria (e.g. green-; purple bacteria; and cyanobacteria), biosynthesize through this simplified reaction (1):



Reaction 1. Here  $H_2A = H_2O$  and  $2A = O_2$ , for cyanobacteria and green plants; while for bacteria  $H_2A$  is some oxidizable substrate and  $2A$  is the product of the oxidation (reprinted as seen in Peters et al., 2005).

Reaction (1) can either be used by aerobic (oxygenic photosynthesis) or anaerobic (anoxygenic photosynthesis) organisms (Peters et al., 2005). In addition to light energy sources, for photosynthesis to occur, the presence of nutrients, such as fixed nitrogen, phosphates and key metals are important, thus limiting photosynthetic organisms to terrestrial and the photic zones in lakes and oceans where relevant nutrients are abundant. Because the main input of nutrients into aquatic environments are through runoff, lakes usually have more nutrients than oceans, as they are enclosed by land, and hence have a higher primary productivity (Lerman & Baccini 1978). The Earth is in a sense balanced by photosynthesis- and respiration reactions, which is essentially reaction 1 in the opposite direction (Peters et al., 2005).

Although most organisms that we are familiar with occur in “normal” or “moderate” environments, and grow optimally in ~20-45°C (mesophiles), many other organisms have adapted to grow optimally in environments considered as “extreme” (Stan-Lotter & Fendrihan 2012). Extreme environments can be characterized by one or several physico-chemical parameters (e.g. high/low temperature, pH and pressure). The organisms in these environments are called extremophiles, meaning that they thrive in extreme environmental conditions (Stan-Lotter & Fendrihan 2012). Of the three main domains, archaea are the organisms most commonly inhabiting extreme environments (figure 3), although they have also been found in “moderate” environments, as non-extremophiles (DeLong, 1998). Being that Milos’s hydrothermal vent areas are influenced by physico-chemical zones, these environments should be ideal for some extremophiles, which will be analyzed using a lipid extraction of the sediments.

Photoautotrophs and chemoautotrophs store different energy sources (light or reduced mineral) for work in their cellular structures in the form of ATP (Adenosine

triphosphate) and NADPH (reduced nicotinic adenosine phosphate). This energy is utilized for the fixation of carbon. For example in phototrophic organisms such as plants and cyanobacteria, CO<sub>2</sub> is fixed through the use of the Calvin Benson cycle (Calvin-Benson-Bassham Cycle (CBB)). Chemoautotrophs, like those inhabiting hydrothermal vent ecosystems, can use several metabolic pathways for CO<sub>2</sub> fixation, including the Calvin Benson cycle, reductive tricarboxylic acid cycle (rTCA or reverse Krebs cycle), acetyl-CoA pathway, dicarboxylate/4-hydroxybutyrate cycle and 3-hydroxypropionate/4-hydroxybutyrate cycle (some of which have been measured in this study) (Minic & Thongbam 2011 & references therein). In hydrothermal vent systems, the carbon fixation through the assimilation of CO<sub>2</sub> is an important biosynthesizing process for autotrophs (Oulas et al., 2016). As seen in figure 6, the Calvin Benson cycle uses the enzyme Ribulose 1,5-bisphosphate carboxylase/oxygenase (RuBisCO) to fix CO<sub>2</sub> into organic carbon, which can come in four forms (Berg et al., 2010; Nakagawa & Takai 2008). RuBisCO (I), (II) and (III) synthesize CO<sub>2</sub> in the same way, by the use of RuBisCO and the difference between them being the sizes and amounts of subunits in the cycle. RuBisCO (IV) is a RuBisCO-like protein which is not involved in the CO<sub>2</sub> fixation (Nakagawa & Takai 2008). Moreover, RuBisCO (II) is usually abundant in high CO<sub>2</sub> environments (Hayes 2001) which could be the case in the hydrothermal area of Milos, as the gas venting is mainly composed of CO<sub>2</sub>. Though there is no information for the presence of RuBisCO in this area, this study will attempt to provide the first results of RuBisCO activities in the shallow submarine hydrothermal system of Milos. Elsaied & Naganuma (2001) recorded activities from different organisms utilizing RuBisCO (form I and II) in deep-sea and deep-sea hydrothermal vents, proving that there is a presence of primary producers utilizing the CBB cycle.

The rTCA cycle (figure 6) is an alternative strategy to the Calvin Benson cycle, used when the energy source is limited (low energy environments). This since the CBB cycle requires more ATP molecules (nine) than that of the rTCA cycle (five). Campbell & Cary's (2004) study showed higher activities of the rTCA pathway from free-living microorganisms in deep-sea hydrothermal vent systems. This because the cycle requires significantly less ATP in its CO<sub>2</sub> fixation, thus playing an important role in hydrothermal vent environments where the energy availability is limited (Oulas et al., 2016). Differences in the carbon fixation pathways will be explored in this study, together with the use of stable carbon isotope analysis of lipid, to see if these shallow submarine

hydrothermal vent system's main biosynthetic pathways differ from the deep-sea hydrothermal systems, where rTCA is most promptly seen (e.g. Campbell & Cary 2004; Elsaied & Naganuma 2001).

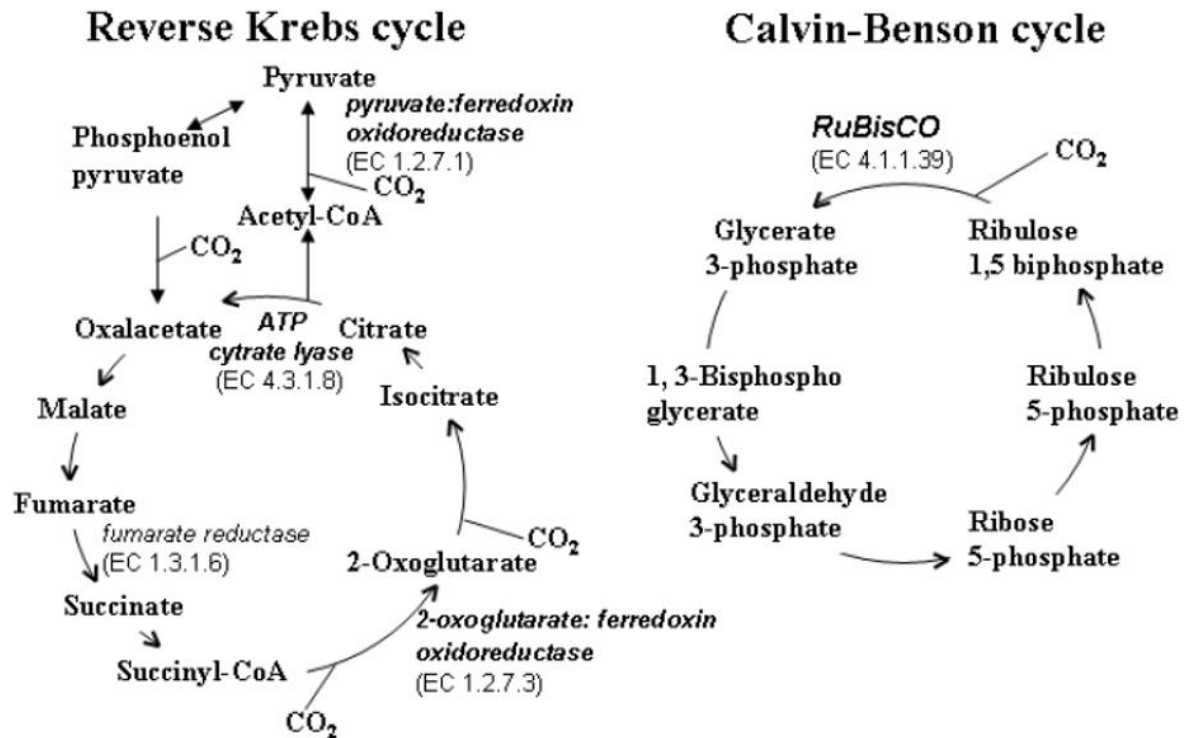


Figure 6. Two of the autotrophic CO<sub>2</sub> fixation pathways, rTCA (reverse Krebs cycle) and CBB (Calvin Benson cycle). The main enzymes in these pathways are coenzyme A and RuBisCO, respectively (Minic & Thongbam 2011).

### 3. Objectives

The main objective of this study is to create the first comprehensive lipid biomarker interpretation of sediments from the microbial mats in the shallow submarine hydrothermal system of Milos, Greece. To help unveil ongoing microbial metabolic processes and temporal dynamics through time, lipid biomarkers together with compound specific isotopes (as they are often well preserved), in different sediment types, and different carbon fixation activities will be analyzed. Through this they will be linked to organisms and/or particular processes from the environment in which the lipids had been deposited in (Peters et al., 2005; Castañeda and Schouten 2011). Subsequently, a better understanding of how these organisms are affected by changes in the hydrothermal system can be understood and thus fluctuations related to hydrothermal activity can be reconstructed. This will also increase existing knowledge

on microbial contribution to hydrothermal vent field biogeochemical processes, which expected to further provide potential insights into biological activity that may have prevailed early Earth's oceans that were at least 3-4 times more hydrothermally active than today (Baross & Hoffman 1985).

These objectives will be answered by:

1. Identifying and measuring the abundances of lipid biomarkers from distinct sedimentary habitats characterized by visually different mat covers.
2. Generating preselected quantitative polymerase chain reactions of key gene sequences from this hydrothermal system, to understand recent and past biological processes.
3. Measuring compound specific  $\delta^{13}\text{C}$  isotope ratios of the lipid biomarkers to distinguish the dominant carbon source together with the bulk sediment of  $\delta^{13}\text{C}$ -DIC, -POC and -TOC to see if recent hydrodynamic processes are seen in the sediment records.

#### 4. Material and methods

##### 4.1. Core sampling

At the Spathi bay, located at 36°40'N; 24°31'E, on the southeast region of Milos Island (figure 7), a total of three areas were sampled, the white and brown microbial mats, and a sandy reference area which was not visibly affected by the hydrothermal emissions. Samples were collected with polycarbonates push core tubes and capped with rubber stoppers underwater by a scuba diver. Duplicate cores were acquired for geomicrobiological survey and three replicates for chemistry, with pre-drilled polycarbonate tubes for pore water extraction for geochemical and isotopic analysis. In the field, each core was sliced, under anoxic conditions, using  $\text{N}_2$  gas, in an anaerobic glove bag. Sections were taken every 2 cm and stored in 50ml Falcon tubes on dry ice, transported and frozen at -80°C in the laboratory at Stockholm University. Porewater was extracted using rhizones pore water samplers attached to depressurized exetainer bottles. These samples were stored upside down at 4°C until they were analyzed for DIC carbon isotopic composition. Following this, one push core per site was sliced in the anaerobic glove bag every 2 cm for bulk  $\delta^{13}\text{C}$  isotopic analysis and C:N ratios. These were also placed in 50 ml Falcon tubes and stored under  $\text{N}_2$  in an anoxic bag, which was frozen on dry ice, shipped and frozen at -20°C in the laboratory at Stockholm University.

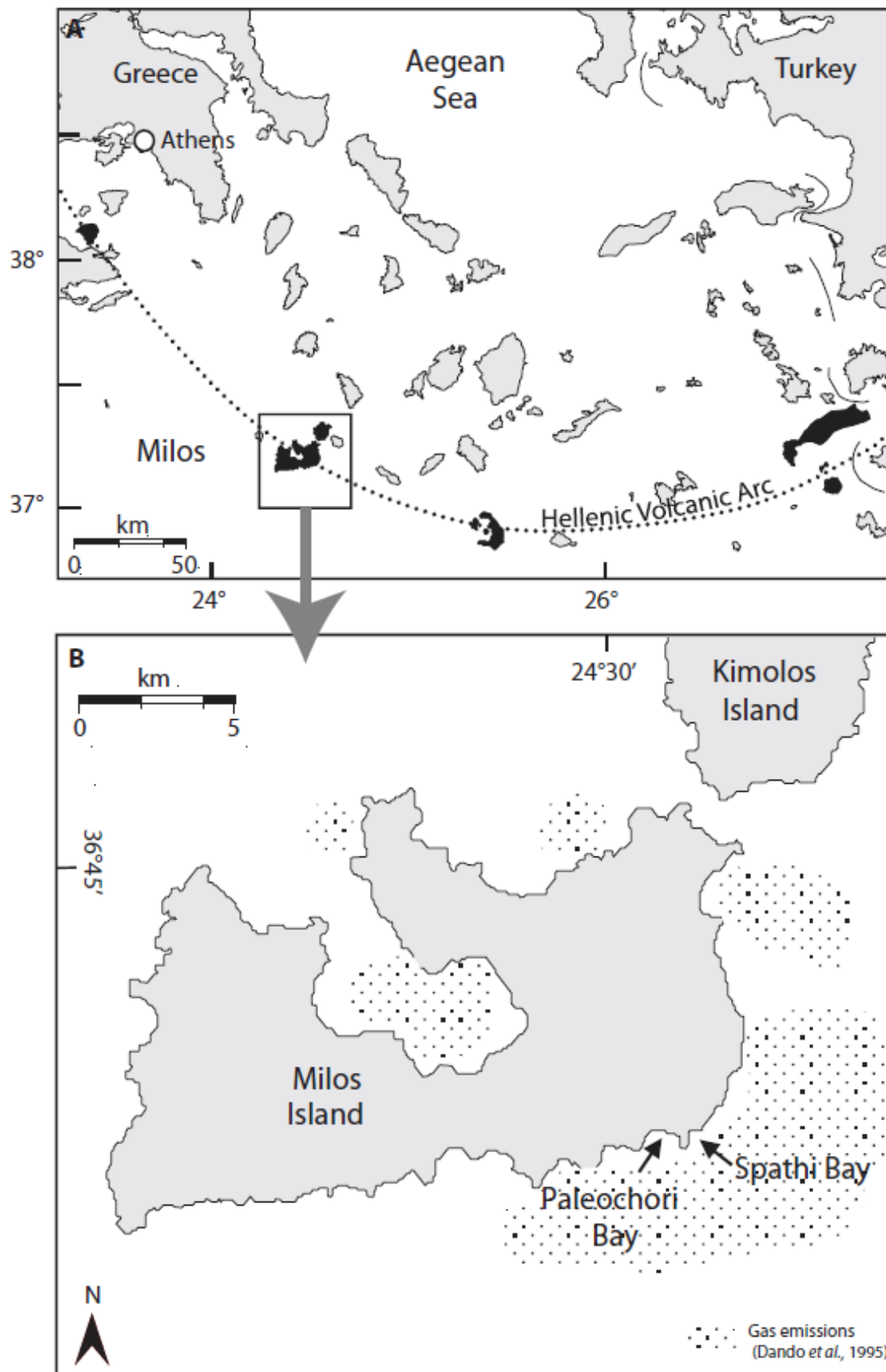


Figure 7. Map of the island of Milos, Greece. Arrows depict sampling area and gas emissions, from Dando et al. (1995) are depicted by dots (modified from Price et al., 2013).

#### 4.2. Sediment carbon isotope analysis, dissolved inorganic carbon ( $\delta^{13}\text{C-DIC}$ ), particulate organic carbon ( $\delta^{13}\text{C-POC}$ ) and total organic carbon ( $\delta^{13}\text{C-TOC}$ )

By measuring the bulk sediments different carbon isotopes and the specific lipid compounds an interpretation will be made to understand the carbon source for organisms in each site. The  $\delta^{13}\text{C-DIC}$  and  $\delta^{13}\text{C-POC}$  were analyzed in Denmark, at the Nordic Center for Earth Evolution, while the  $\delta^{13}\text{C-TOC}$  was analyzed at Stockholm University using a duplicate core (taken from close proximity of the first cores) that would be used for the total lipid extraction method. Using a GC-IRMS (Thermo-Scientific – Delta plus) each sample was measured compared with the internal bicarbonate standard together with international standards (IAEA NBS-18-Calcite (of  $-5.014\text{‰}_{\text{VPDB}} \pm 0.035$ ) and IAEA-LSVEC Lithium Carbonate (of  $-46.6\text{‰} \pm 0.2$ )). The ratios of the carbon isotopes ( $^{13}\text{C}/^{12}\text{C}$ ) were reported in delta ( $\delta$ ) notations with respect to Vienna-PeeDee Belemnite (VPDB). The delta notation is in units per mil (‰) following formula (2):

$$\delta(\text{‰}) = \left( \frac{R_{\text{sample}}}{R_{\text{standard}}} - 1 \right) * 1000 \quad (2)$$

Here R= the isotopic ratio, i.e.  $^{13}\text{C}/^{12}\text{C}$ .

For the TOC and POC the samples were freeze-dried, homogenized and acid-treated with hydrogen chloride (HCl) to ensure that no carbonate carbon would contaminate the results of the analysis. The POC samples were then analyzed on an EA-IRMS (Thermo–Delta V Advantage Isotope Ratio MS, EA Flash 2000 Organic elemental analyzer, SDU Odense), compared to IVA standard Protein ( $\delta^{13}\text{C}_{\text{VPDB}} = -26.98$  and IVA standard Urea  $\delta^{13}\text{C}_{\text{VPDB}} = -45.38$ ). While the TOC samples were run on a Carlo Erba NC2500 elemental analyzer, coupled to a Finnigan MAT Delta+ mass spectrometer, at Stockholm University. The  $\delta^{13}\text{C}_{\text{org}}$  was reported in parts per mil (‰) relative to Vienna Pee Dee Belemnite (VPDB) as seen in formula (2), and the total organic carbon was reported in %.

#### 4.3. Reference pure microbial culture analysis

The microbial cultures selected here have been found in the HVA and will be correlated with the lipids found in the different sediment sites.

Cultures selected for analysis:

**Archaea:** *Methanoculleus bourgensis* strain MAB1 (courtesy given by Anna Neubeck) methanogen.

**Bacteria:** *Geobacter Sulfurreducens* (DSM number 12127) Fe and metal reducing,  
*Marinobacter santoriniensis* (DSM number 21262) As (III)-oxidizer and  
As (V) reducer.  
*Mariprofundus ferrooxydans* (DMS number 23021) Fe-oxidizer.

The cultures were grown at Stockholm University in the Department of Geological Sciences following the protocols provided from DSMZ [Deutsche Sammlung von Mikroorganismen und Zellkulturen; microbial organism institute]. Biomass harvesting was followed by centrifugation (20 min at 11000g) and supernatant removed using a pipette. Less than 1 gram biomass was recovered and freeze-dried.

#### 4.4. Extraction of lipids from reference microbial cultures

To compare the lipids from the different sites with the microbial cultures that had been identified in the HVA, an extraction method was implemented (modified from Yamoah et al., 2016). The freeze-dried cultures were placed into combusted vials that had been rinsed with dichloromethane (DCM) beforehand to ensure that no residue contaminants would affect the sample results. For the extraction of the total lipid extracts, a 1ml solvent solution, consisting of DCM/MeOH (methanol) (2:1 volume to volume [v/v]), had been added into each vial. The cultures were then placed in an ultrasonicator for 15min, to agitate the extracts. The solvent was then extracted into new vials and the procedure was repeated 5 times. The extracted solvent from the cultures extracts was then blown down, using nitrogen gas fitted to a heated plate (set to about 25°C) to concentrate the extracts prior to storage in the freezer where they awaited further analysis.

Because the extracted cultures may have sulfur in them, it has to be removed from the samples prior to analysis. This since the sulfur will affect the background in the GCMS analysis. Also to effectively recover fatty acids and alcohols from the extracts a methylation method (adding methyl esters to compounds) and silylation method (replacing a proton with a trimethylsilyl group) had been performed on these samples. The sulfur removal, methylation- and silylation- methods would additionally be done on the Milos site samples and are thus be covered in detail below (section 4.6. & 4.7.).

#### 4.5. Sediment lipid extraction

A lipid analysis was performed to obtain information about the microbial presence in the different sites in Milos. The lipid extraction method for the site samples followed a similar method description to Smittenberg et al (2005; 2005b) and Yamoah et al. (2016). Each sample was freeze-dried, weighed and placed into vials that had been combusted and pre-rinsed with DCM (same as the cultures). The samples that were selected are denoted below in table 1. The extraction of each sample was made by adding a known volume of DCM/MeOH (2:1 v/v), about 3 times more than the sediment volume, and was followed by vortexing the contents and placing them in the ultrasonicator for 15min and finally centrifuged for 2min. The solvents were then extracted into new vials and the procedure was repeated 4 more times. Finally the samples were blown down using nitrogen gas fitted with a heated plate (25°C). The samples were then weighed, to record the dry weight of the extracts, and then kept in the freezer.

Table 1. Depth and weight of samples from each sampled area.

<b>Sand sed.</b>	<b>Weight [g]</b>	<b>Brown mat</b>	<b>Weight [g]</b>	<b>White mat</b>	<b>Weight [g]</b>
0-2 cm	8.287	0-2 cm	8.038	0-2 cm	5.075
6-8 cm	7.230	6-8 cm	7.452	6-8 cm	7.592
10-12 cm	8.613	16-18 cm	8.512	12-14 cm	8.422

#### 4.6. Solid phase chromatography

The solid phase extraction is performed to separate the different compounds in the extracts and make the analytical testing more successful. This was done by eluting the extracts into different polarity fractions going from least polar compounds (hydrocarbons) to more polar compounds (fatty acids) (figure 8). Before the solid phase chromatography could proceed, two methods had to be set up prior to the solid phase chromatography. 1<sup>st</sup> the Back Extracted Water: Pouring together a mixture of deionized (MilliQ) water and DCM, with a ratio of 15:1 (v/v) respectively, in a large separation funnel. Carefully, due to buildup of overpressure, the funnel is shaken to mix these together, then letting the phases separate and draining the DCM out. This method was repeated again twice and then the back extracted water was ready and placed in a bottle

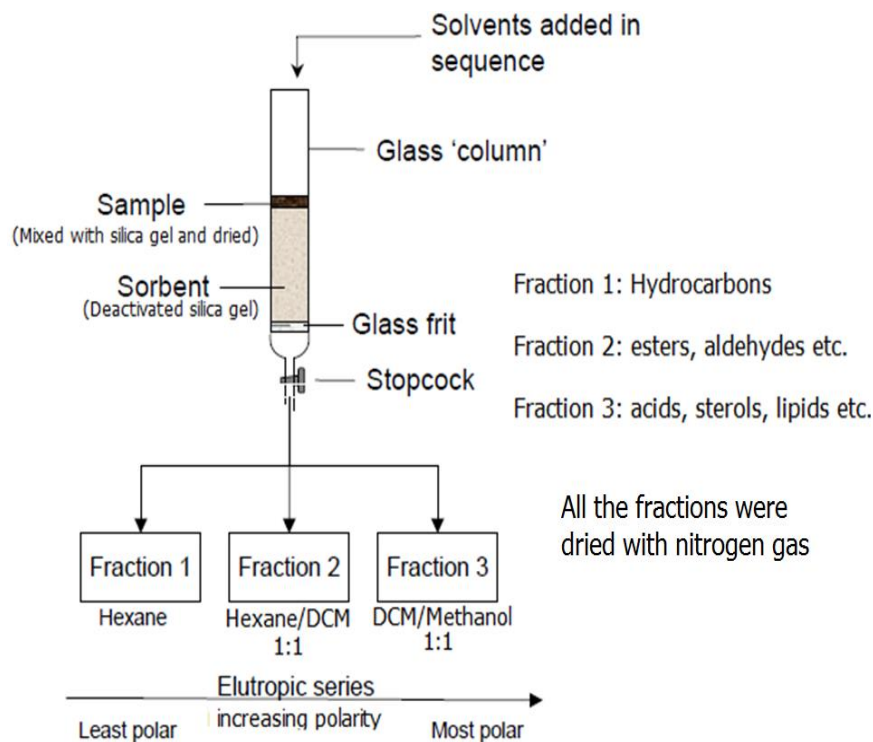


Figure 8. Schematic figure of a solid phase chromatograph (made by Kweku Afrifa Yamoah).

with a lid. This is done to ensure that the water used in the solid phase chromatograph does not have any organic compounds. 2<sup>nd</sup> was the 5% deactivated silica gel. Weighing a 19:1 (v/v) amount of pre-combusted silica gel together with back extracted water in a bottle. The bottle was then

shaken and left to equilibrate overnight. This will give better defined chromatographic zones from the fraction separation (Cahnman 1957).

The extracted samples were dissolved in a small amount of DCM. To this a small amount of 5% deactivated silica gel was added to ensure that all the extracts would be absorbed into the silica gel, which was followed by drying the gel using only a heated plate. From here pipette columns were prepared, using cotton wool to plug the bottom, then adding 5% deactivated silica gel. These were then rinsed using three solvents (MeOH, DCM and finally hexane), to ensure as much as possible, that no contaminants would be present. After this, the absorbed silica gel was added to the column. Here the extracts would be separated into three fractions going from least polar and then increasing the polarity to more and more polar. 1<sup>st</sup> Fraction (F1) was eluted using only hexane, 2<sup>nd</sup> Fraction (F2) was eluted using hexane/DCM (1:1 v/v) and the 3<sup>rd</sup> Fraction (F3) was eluted using DCM/MeOH (1:1 v/v). Each fraction was eluted 3 times into the same fraction vial, and then blown down using nitrogen gas.

To remove the sulfur mentioned earlier, from F1, F2 and the cultures, they had to be cleaned using copper. This was done by filling a column with cotton wool, at the

bottom, and adding about 2cm depth of copper powder. To activate the copper it was rinsed with 1N HCL and then rinsed once with distilled water, three times with MeOH, DCM and then finally with hexane. Separately F1 and F2 were then pipetted on and rinsed with hexane/ethyl acetate (1:1 v/v), blown down again and finally a fixed amount of hexane/ethyl acetate was added into each vial and thus ready for the analysis on the GCMS.

#### 4.7. Methylation and Silylation

To be separate the alcohols and fatty acids, the F3 fraction samples and the bacteria/archaea cultures were all methylated and silylated. Methylation was performed to make the samples less reactive (Sjöberg 2014), by adding a methyl ester group (CH<sub>3</sub>-group) to the fatty acids present in the samples, thus making it easier to separate and detect the peak compounds on the GCMS. A simplified reaction of the methylation reaction is shown in reaction (3).



Methylation of fatty acids (HTML 1).

The methylation procedure started by re-dissolving the samples (both the F3 samples and bacterial/archaeal cultures) in 0.2 ml DCM, then an addition of 1.5 ml MeOH and 0.3 ml of HCL (8% conc.). The samples were then vortexed and incubated overnight at 45°C. After this, 0.5 mg of pre-combusted Na<sub>2</sub>CO<sub>3</sub> was added together with 1ml of hexane and 1 ml of back extracted water, followed by a vortex of the samples and finally left to let the phases separate. From this the upper hexane layer was transferred into new vials and blown down.

To separate the fatty acid methyl esters (FAMEs) from the alcohols, one more step had to be made before the silylation. This was only done with the F3 from the sediment samples due to the complexity of the samples in comparison to the cultures. A column was filled with a small piece of cotton wool in the bottom and 5% deactivated silica gel to about 2/3 of the column, then adding the methylated F3 absorbed extract to the column. The column was then eluted with solvents to produce a F3a fraction and a F3b fraction. For F3a (which holds the FAMEs) it was eluted three times with hexane/DCM (1:1 v/v), and for F3b (alcohols and tetra-ethers) it was eluted three times with pure ethyl acetate. The F3a samples were then blown down and a known amount of

hexane/ethyl acetate (1:1 v/v) was added. After this the F3a samples were now ready for the GCMS analysis.

F3b and the culture samples finally went through the silylation procedure before they were analyzed. Silylation introduces the replacement of a proton with a silyl group ( $R^1R^2R^3Si-O-R^4$ , where  $R^4$  is an alkyl group), to enhance the volatility of the compounds. However, the trimethylsilyl esters that are introduced are sensitive to any traces of water (as water may slow or completely stop the reaction) and it is imperative that there are no traces of water in the sample before or after the procedure. This is also done to simplify the detection and separation of the lipid peaks in the GCMS.

The procedure was started by transferring the samples into GCMS vials and then being blown down. After this 20  $\mu$ l of pyridine was added along with 20  $\mu$ l of BSTFA (N,O-bis [trimethylsilyl] trifluoroacetamide). Samples were then placed in a 60°C oven for 25 min. After this, a known amount of hexane/ethyl acetate was added and subsequently the samples were ready for the GCMS analysis.

#### 4.8. Gas-chromatography Mass Spectrometry (GC-MS)

For the identification of individual lipids the samples were analyzed using a Shimadzu GCMS-QP2010 Ultra, equipped with an AOC-20i auto sampler and a split-splitless injector operated in splitless mode. A Zebron ZB-5HT Inferno GC column (30 x 0.25 mm x 0.25  $\mu$ m) was used for separation using pure helium as the carrier gas. Each sample was injected into the GC at an oven temperature of 60°C. After 2 min, the oven temperature was raised to 180°C at a rate of 15°C minute<sup>-1</sup>, and then raised again to 320°C at a rate of 4°C minute<sup>-1</sup>, where it was held for 20 min.

A selected ion monitoring (SIM) method was used for analysis, as the detection of the instrument is enhanced and selective for only specific ions. In the SIM scan the selected ions were indicative of a specific hopanoid lipid fragment of m/z 191 over the entire run time.

#### 4.9. Lipid calculations

To calculate the relative concentrations of the lipids in the samples, a standard, with a known concentration of 40 ng  $\mu$ l<sup>-1</sup>, was analyzed together when the samples were run on the GCMS. This standard was composed of n-alkanes from C<sub>21-40</sub> and was run three times at different intervals. The concentration calculated is relative to the standard because there are no specific standards for the lipid biomarkers that were identified.

The relative concentration of each identified lipid follows this calculation method (formula 4):

$$\text{Lipid with } C_x \text{ [ng g}^{-1} \text{ dw sample]} = \frac{\left( \frac{\text{Area of GCMS peak} * \mu\text{l injected}}{\text{Average area of GCMS peak for } C_x \text{ Standard } \left[ \frac{\text{area}}{\text{ng } \mu\text{l}^{-1}} \right] * \mu\text{l injected}} \right) * \mu\text{l Volume of sample vial}}{\text{g dw sample}} \quad (4)$$

Where x is the number of the carbons; and dw is the dry weight.

#### 4.10. Isotopic ratio mass spectrometer (IRMS)

By measuring the carbon isotope signatures of specific lipid compounds (fatty acids), the fractionation factor could be measured and correlated to carbon fixation pathways (section 4.12.). For stable carbon isotopic signatures of specific lipid compounds, the samples were run using an IRMS that measures differences in the abundances of the  $^{13}\text{C}/^{12}\text{C}$  of specific lipid compounds. Because the samples had been methylated ( $\text{CH}_3$ ), isotopic signature was corrected from the biomarkers to get an accurate  $\delta^{13}\text{C}$  result from the samples. This was done by methylating a known standard, in this case phthalic acid with  $\delta^{13}\text{C} = -29.98 \pm 0.01\text{‰}$  (relative to VPBD), and running it run through the same IRMS analysis as the samples.

As will be seen in the results, the surface samples were the ones with the highest concentration of biomarkers (high concentration is needed to detect and isolate the different biomarkers). Hence these samples, an internal standard (with known isotopic  $\delta^{13}\text{C}$  signatures) and the phthalic acid standard were all analyzed for  $\delta^{13}\text{C}$  values, using a Thermo Finnigan Delta V Plus mass spectrometer fitted with a Trace Ultra GC 2000, GC Isolink II and Conflo IV system. With a constant flow, helium was used as a carrier gas with the gas chromatograph oven temperature programmed from 100 to 250°C at a rate of 20°C min<sup>-1</sup>, then increasing to 340°C at a rate of 5°C min<sup>-1</sup>, holding for 18 min. The peaks were then identified through the use of the GCMS peaks, and thus acquiring the  $\delta^{13}\text{C}$ . Subsequently the  $\delta^{13}\text{C}$  values were adjusted for their methylated group, by removing the values of these in the samples measured values.

#### 4.11. High Performance Liquid chromatography mass spectrometry (HPLC-MS)

Further analyzing the extracted samples on a HPLC-MS the GDGTs would be identified. Prior to the analysis the samples had been filtered in and dissolved in 9:1

(v/v) MeOH:DCM. The filtration was performed to ensure no flow problems through the HPLC columns. The samples were analyzed on a Dionex Ultimate 3000RS HPLC system coupled via an atmospheric pressure chemical ionization (APCI) interface to a Thermo Scientific TSQ quantum access MAX triple stage quadrupole mass spectrometer. Peak separation was performed on a Kinetex XB C18, 1.7  $\mu\text{m}$ , 150 x 2.10 mm column from Phenomenex, with reverse phase chromatographic setting set to: Mobile phase solution of A was MeOH with 0.04 % formic acid and mobile phase solution of B was isopropyl alcohol (IPA) with 0.04 % formic acid (Lanekoff & Karlsson, 2010; Zhu et al., 2013; Rattray et al., in prep). With a column temperature set to 45 °C and a flow rate of 0.2 ml min<sup>-1</sup>. The program of the initial composition of the mobile phases were set to 60 % of A and 40 % of B holding for 1 minute ramping to 50 % to 50 % of each mobile phases solution at 20 minutes, then held for 15 minutes and subsequently reduced to the initial starting volumes of 60 % and 40 % of A and B respectively. The samples were kept at room temperature during the analysis using an injected volume of 10  $\mu\text{l}$ , with a total run time of 45 minutes.

#### 4.12. Gene abundances involved in carbon fixation pathways

With the use of polymerase chain reactions targeting specific key gene sequences, either for RuBisCO or rTCA cycle, the detection, and diversity, of microorganisms that utilize the RuBisCO cycle and/or rTCA cycle can be made (Campbell et al., 2003; Elsaied & Naganuma 2001). Here quantitative polymerase chain reactions (qPCR) of key bacterial and archaeal 16S ribosomal (rRNA) gene copies g<sup>-1</sup> in the sediment of each site (not shown in the results or discussion) and three small key subunit (rRNA) gene sequences involved in inorganic carbon fixation (two RuBisCO [form I and II] units and one rTCA unit) was conducted by Dr. Nolwenn Callac, a postdoc at the department of geological Sciences, Stockholm University. Following this method will provide valuable information on the specific microbial taxa (not shown in results or discussion) and the metabolic pathways (Coolen and Gibson 2009) present in each site. The targeted subunit gene sequences include: *aclB*, targeting key gene subunits fragments for the rTCA cycle; and, *cbbL* and *cbbM*, targeting fragments of the genes encoding the RuBisCO form I and II in the CBB cycle, respectively,

## 5. Results.

### 5.1. TOC

Analytical results shown in table 2 indicate that the total organic carbon contents are very low (figure 9), with the highest mean values (0.04%) acquired from the sand reference sediments lacking mat cover. The brown- and white microbial mats have slightly less mean values of 0.0237% & 0.03%, respectively. The white and brown mat's TOC seem to decrease and increase at the same depths while the sands TOC behaves in the opposite direction to them. The white and brown values decrease from about 0.022 to 0.02 until 5cm, where after there is an increase in TOC to 0.03% and 0.04% (for the white and brown, respectively), that then steadily decreases with depth.

In the sand the TOC is steady at 0.03% until 5cm where it decreases to 0.022% and then increases to 0.026% and then decreases slightly to 0.023%. All sites are depleted in  $\delta^{13}\text{C}$ -TOC, with the sand sediment having the most depleted  $\delta^{13}\text{C}$  (-20.13‰), though not far from the brown- and white microbial mat values that averaged -19.69‰ & -19.96‰, respectively.

Table 2. Bulk total carbon isotope results from the three investigated sediment types.

	<u>Average</u>		<u>Average</u>	
	$\delta^{13}\text{C TOC vs PDB [‰]}$	+/-	TOC [%]	+/-
<b>Sand sediment</b>	-20.13	0.672	0.04	0.004
<b>Brown mat</b>	-19.69	1.105	0.0237	0.008
<b>White mat</b>	-19.96	0.990	0.03	0.003

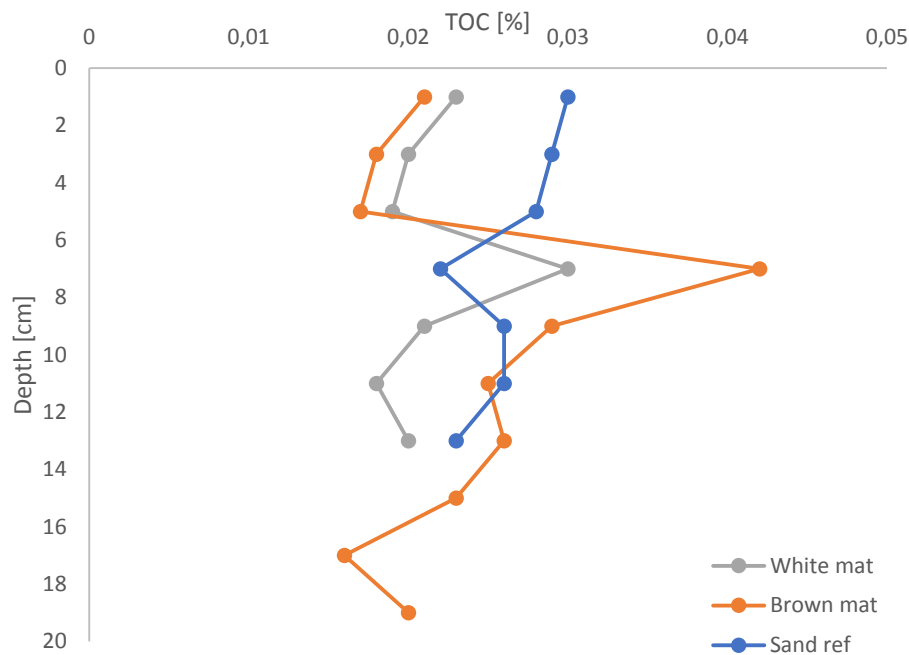


Figure 9. TOC [%] through depth [cm] for the three sediment types.

## 5.2. $\delta^{13}\text{C}$ of DIC and POC

A detailed list of the isotopic carbon  $\delta^{13}\text{C}$  values of the DIC and POC is presented in table 3 (also see figure 10).

The  $\delta^{13}\text{C}$ -POC stays rather uniform in the range of  $-18\text{‰}$  to  $-20\text{‰}$ , through depth both the microbial mats, while the sand sediment stays uniform with  $\delta^{13}\text{C}$ -POC values of  $-17\text{‰}$  to  $-19\text{‰}$ , though there is a depletion in the deepest point going to  $-36\text{‰}$ . However, in the  $\delta^{13}\text{C}$ -DIC the values differ more. In the white microbial mat site, the  $\delta^{13}\text{C}$ -DIC becomes more enriched with depth, going from  $\delta^{13}\text{C}$ -DIC  $0.64\text{‰}$ , at the surface, to  $\delta^{13}\text{C}$ -DIC of  $14\text{‰}$  in the deepest point. The trend is similar in the brown microbial mat site though not as extreme as in the white core. Here the surface values are at  $3.94\text{‰}$  while at the deepest point is enriched with  $\delta^{13}\text{C}$ -DIC values of  $10.7\text{‰}$  which is lower but still enriched and higher than the white mat. The sand reference site was more stable and uniform with  $\delta^{13}\text{C}$ -DIC value in the range of to  $4.67\text{‰}$  in the surface, to  $3.62\text{‰}$  in the deepest point. When comparing the  $\delta^{13}\text{C}$  values of the DIC and POC there seems to be a clear increase in the microbial mats, while the sand sediment stays uniform. In the white the  $\Delta^{13}\text{C}$  (difference between the  $\delta^{13}\text{C}$  values of DIC and POC) increases rapidly with depth, the brown mat shows the same though not as extreme (table 3).

Table 3.  $\delta^{13}\text{C}$  [permil] vs PDB of the DIC and POC through depth for the three different sediment types.

Depth [cm]	<u>White mat</u>			<u>Brown mat</u>			<u>Sand Sediment</u>		
	$\delta^{13}\text{C}_{\text{POC}}$	$\delta^{13}\text{C}_{\text{DIC}}$	$\Delta^{13}\text{C}$	$\delta^{13}\text{C}_{\text{POC}}$	$\delta^{13}\text{C}_{\text{DIC}}$	$\Delta^{13}\text{C}$	$\delta^{13}\text{C}_{\text{POC}}$	$\delta^{13}\text{C}_{\text{DIC}}$	$\Delta^{13}\text{C}$
0	-19.17	0.64 ±1.02	19.81				-16.32	4.67 ±0.44	20.98
1	-19.12	0.43 ±0.52	19.55	-17.97	3.94	21,91	-17.76	2.45 ±0.20	20.21
3	-19.43	2.52 ±0.21	21.95	-18.98	5.91	24,90	-18.91		
5	-19.78	7.98 ±5.26	27.76	-19.18			-17.84	2.44 ±0.30	20.28
7	-18.97	11.21 ±4.81	30.18	-18.88		15,95	-18.46		
9	-18.62	10.68 ±0.41	29.31	-19.04			-17.95		
11	-20.31	11.62 ±0.98	31.93	-18.69			-18.43		
13	-20.31	14.48 ±1.49	34.80	-19.08	11.56	30,63	-18.69		
15				-18.49	9.32	27,81	-18.67		
17				-18.81	10.68	29,49	-18.78		
19				-18.76	11.13	29,90	-18.83	2.06 ±0.42	20.89
21				-18.62	10.71	29,32	-36.26	3.62 ±0.45	39.88

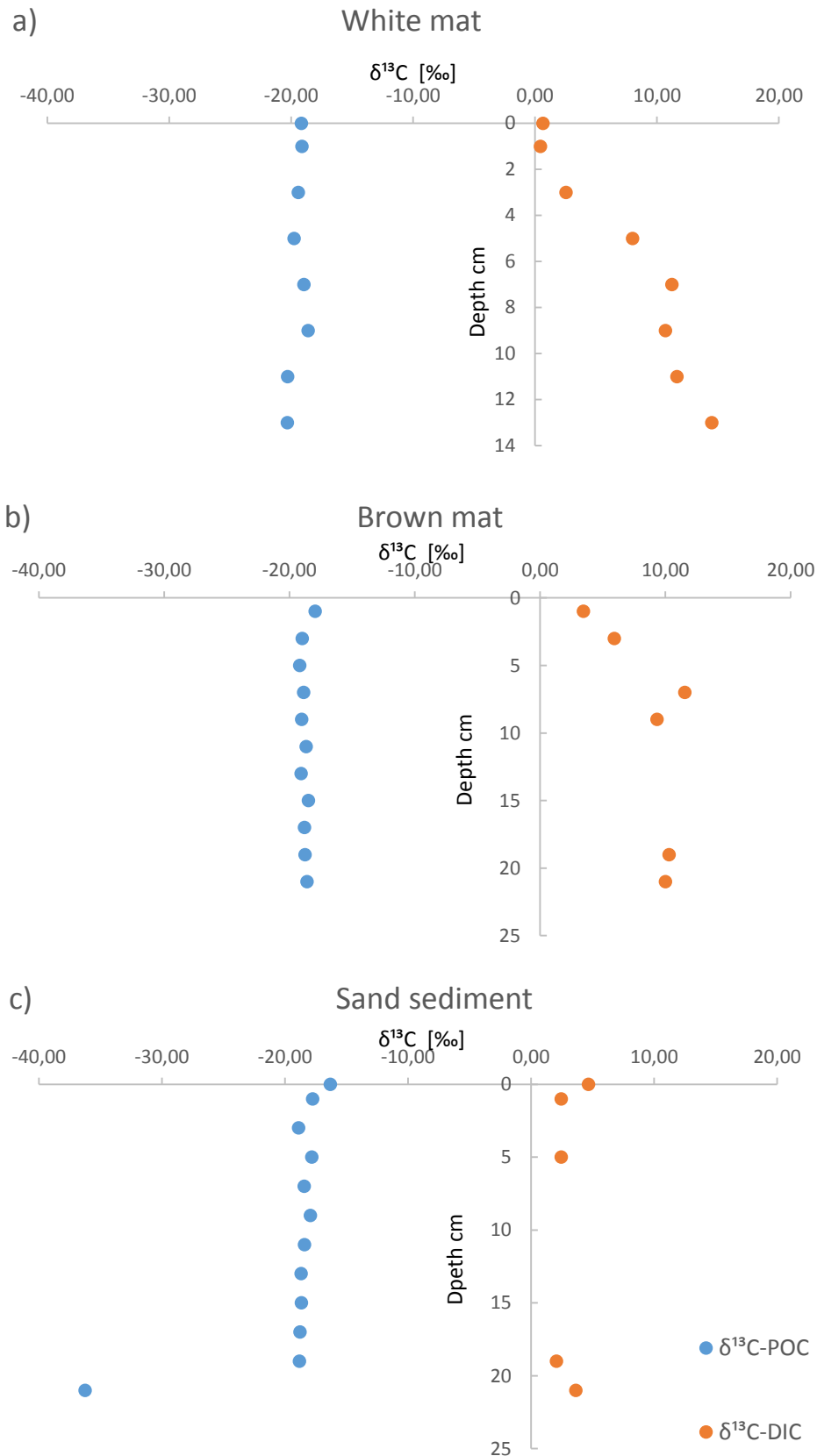


Figure 10 a;b;c. Carbon isotope ( $\delta^{13}\text{C}$  vs PDB [permil]) trends for DIC and POC through depth for the three sediment types investigated, a) the white mat; b) brown mat; and c) sand sediment reference.

### 5.3. Lipid analysis on collected samples

The least polar fractions (1 and 2) did not yield any results and are thus excluded from further consideration. However, all sites had a significant number of polar compounds which were identified in fractions 3a and 3b (from Material and Methods 4.9.), with the highest quantity found in the surface samples at all sites. Tables 8, 10 & 12 (appendix) show a detailed lists of surface lipid biomarkers found from fraction 3a, while tables 9, 11 & 13 (appendix) show lipid biomarkers found in fraction 3b from surface mats of the three investigated sediment types (appendix figures 30, 31 & 32 are the chromatographs for the brown-, sand- and white- areas respectively).

Identification of the compounds was done by investigating significant  $m/z$  (mass to ratio) ions and using different mass spectra libraries. The most significant lipids identified were normal, iso- and anteiso- fatty acid lipids (denoted as i or ai, respectively); monoenoic fatty acids; sterols; and finally the hopanoids. These all have specific spectra particular to that group and only varying slightly depending on their carbon numbers (tables seen in appendix). The appendix has a more detailed description on the identification and abundances of the lipids identified.

### 5.4. Lipid distributions

The lipid biomarkers identified and found in all surface samples (appendix tables 8 to 13) include:

- Straight chain fatty acids: *hexadecanoate and octadecanoate*.
- Unsaturated fatty acids: *9-hexadecenoate (9-16:1)*.
- *squalene and glycerol*
- Esters: *hexadecanoic acid 2,3-bis[(trimethylsilyl)oxy] propyl ester (C<sub>16</sub> monoglyceride) and octadecanoic 2,3-bis[(trimethylsilyl)oxy] propyl ester (C<sub>18</sub> monoglyceride)*.
- Sterols: *cholesterol, sterol, stigmasterol and beta sitosterol (appendix table 6 & figures 25 to 28)*.
- Hopanoids: *17 $\beta$ H, 21 $\beta$ H-homohopanoic fatty acid, 17 $\alpha$ H, 21 $\beta$ H-bishomohopanoic fatty acid, 17 $\beta$ H, 21 $\beta$ H-bishomohopanoic fatty acid and diploptene (appendix table 7 & figure 29)*.

Although the surface samples at all sites had significant lipid biomarkers, the sand sediment samples had the highest concentrations of lipids both at the surface and down core. The brown and white microbial mats both had lower amounts of lipid biomarkers in the surface sediment as well as down core, though there were some that were also found in the deeper samples as well. These are summarized in table 4 (page 38).

The sand sediment had the most lipid biomarkers found through depth (figure 11, 12 & 13). These include: 12-methyl-tetradecanoate (*aiC<sub>12:0</sub> 15Me*), octadecanoate ( $C_{18}$ ), 15-methyl-hexadecanoate (*iC<sub>15:0</sub> 17Me*), 9-hexadecenoate (9-16:1) (monoenoic), tetradecanoate ( $C_{14}$ ), glycerol, hexadecanoic acid 2,3-bis[(trimethylsilyl)oxy] propyl ester, octadecanoic acid 2,3-bis[(trimethylsilyl)oxy] propyl ester, cholesterol, sterol, stigmasterol and beta sitosterol. For figure 11 biomarkers that deviate from the rest are the hexadecanoic acid 2,3-bis[(trimethylsilyl)oxy] propyl ester and octadecanoic acid 2,3-bis[(trimethylsilyl)oxy] propyl ester, which both increase with depth. Glycerol increases as well through depth. 12-methyl-tetradecanoate, octadecanoate and cholesterol, all decrease through depth. The other biomarkers mentioned above behave differently in that they decrease rapidly and then increase slightly through depth. This is especially particular due to the other sterols acting differently from the Cholesterol.

The brown mat samples had a lower diversity of biomarkers identified down core (figures 11, 12 & 13). These include: glycerol, hexadecanoate ( $C_{16}$ ), octadecanoate ( $C_{18}$ ), hexadecanoic acid 2,3-bis[(trimethylsilyl)oxy] propyl ester and octadecanoic acid 2,3-bis[(trimethylsilyl)oxy] propyl ester. Here, hexadecanoate decreases progressively with depth, unlike glycerol that seems to almost have an opposite increasing trend. Octadecanoate increases from the surface point to the middle point, then decreases rapidly at the deepest point. Hexadecanoic acid 2,3-bis[(trimethylsilyl)oxy] propyl ester and octadecanoic acid 2,3-bis[(trimethylsilyl)oxy] propyl ester both increase with depth. Biomarkers found in the two upper samples include: 9-hexadecenoate (9-16:1) (monoenoic), tetracosanoate (normal  $C_{24}$ ), cholesterol, sterol, stigmasterol and beta sitosterol. These biomarkers all decrease down core and are not found at the lowest depth.

The white mat samples had even less biomarkers found through depth (figures 11, 12 & 13). These include: glycerol, hexadecanoate ( $C_{16}$ ), octadecanoate ( $C_{18}$ ), hexadecanoic acid 2,3-bis[(trimethylsilyl)oxy] propyl ester, octadecanoic acid 2,3-

bis[(trimethylsilyl)oxy] propyl ester and cholesterol. Excluding the cholesterol, all biomarkers decrease with depth. Cholesterol on the other hand decreases and then increases slightly again, following the same trend as the other sterols in the sand sediment (though not the sand's cholesterol specifically).

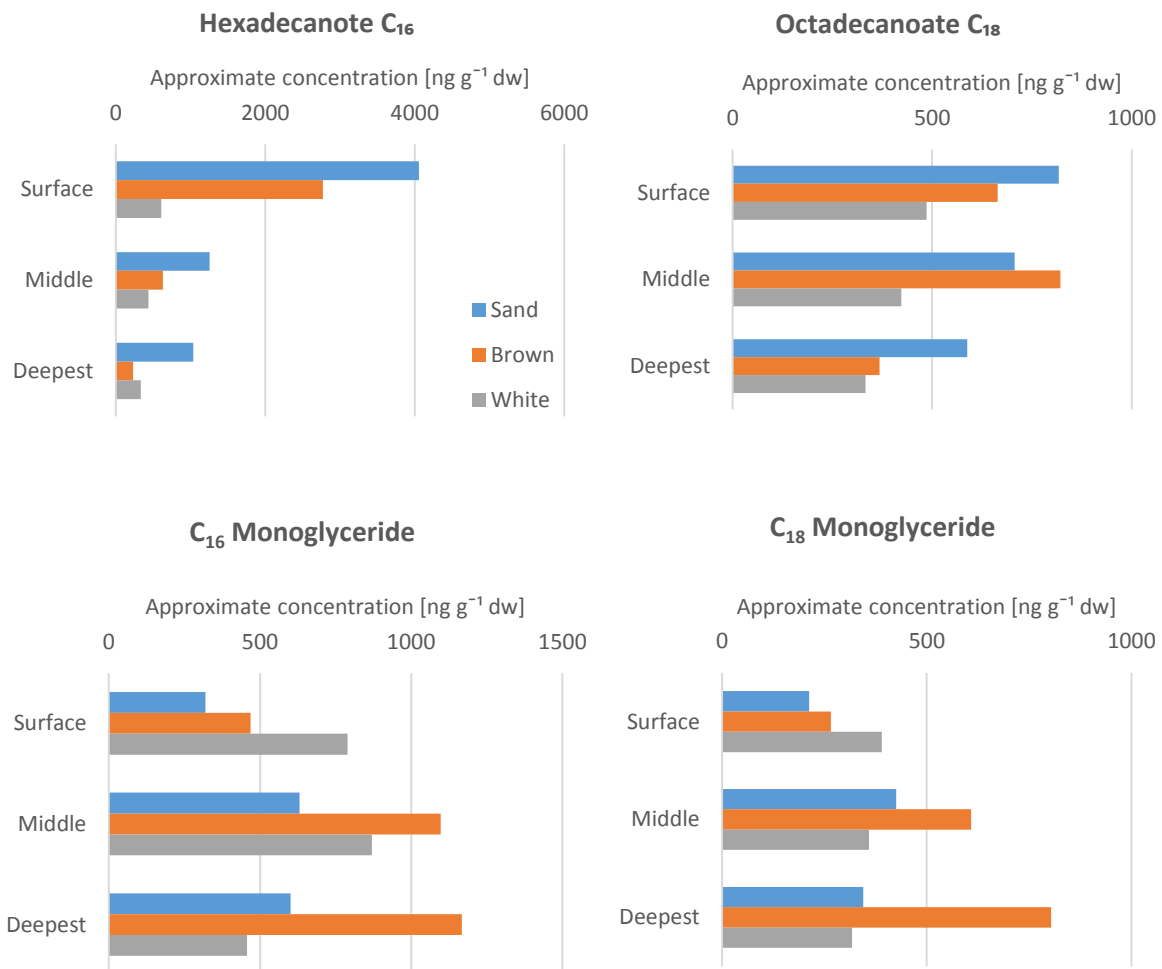


Figure 11.  $C_{16}$ ,  $C_{18}$  and propyl esters approximate concentration [ $\text{ng g}^{-1} \text{ dw}$ ] relative to n-alkane standard through depth. Colors: Sand references site=blue; Brown microbial mat= orange; and White microbial mat= grey. Depths: Surface= 0-2cm; Middle= 6-8cm; and Deepest= 10-11cm for Sand; 16-18cm for Brown; and 12-14cm for White.

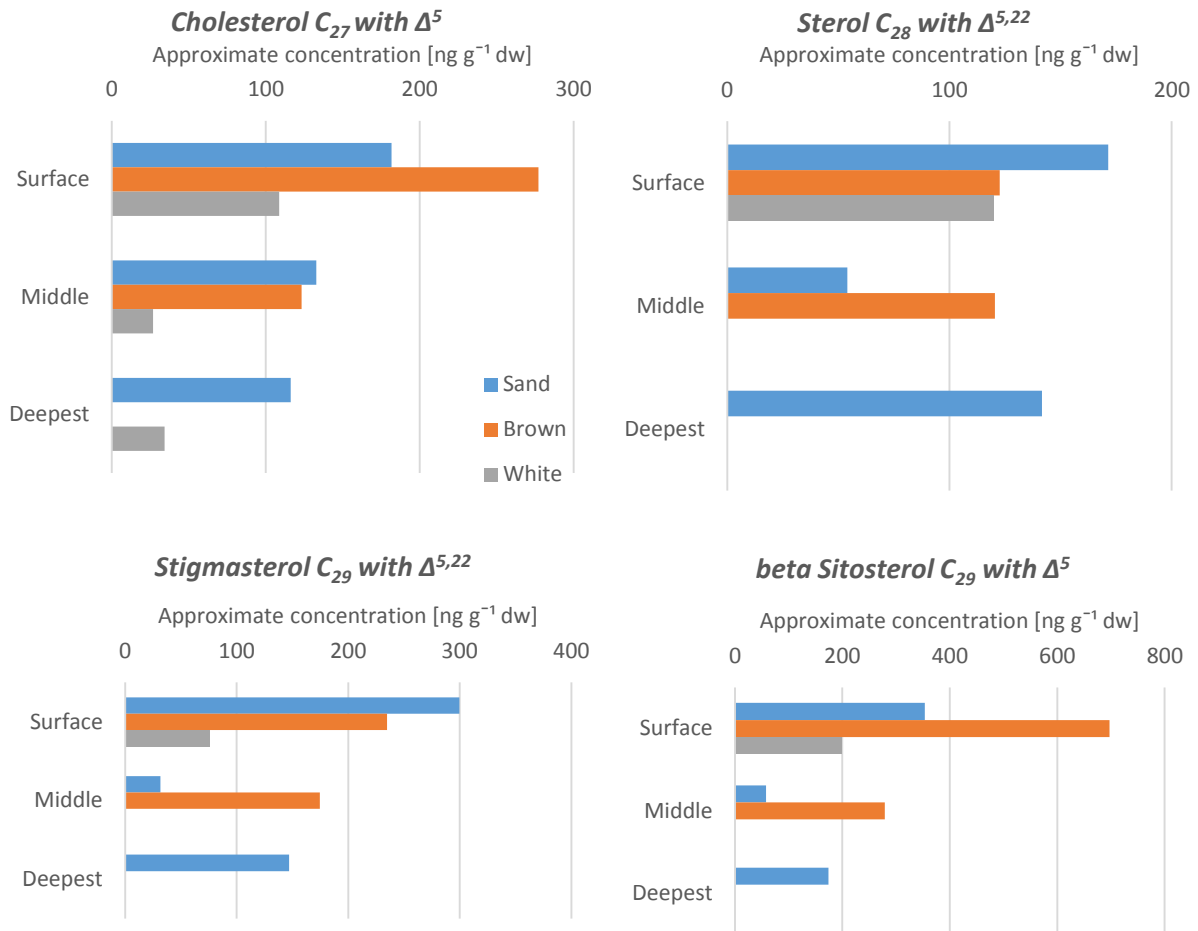


Figure 12. Sterols approximate concentration [ $\text{ng g}^{-1} \text{dw}$ ] relative to n-alkane standard through depth. Colors: Sand references site=blue; Brown microbial mat= orange; and White microbial mat= grey. Depths: Surface= 0-2cm; Middle= 6-8cm; and Deepest= 10-11cm for Sand; 16-18cm for Brown; and 12-14cm for White.

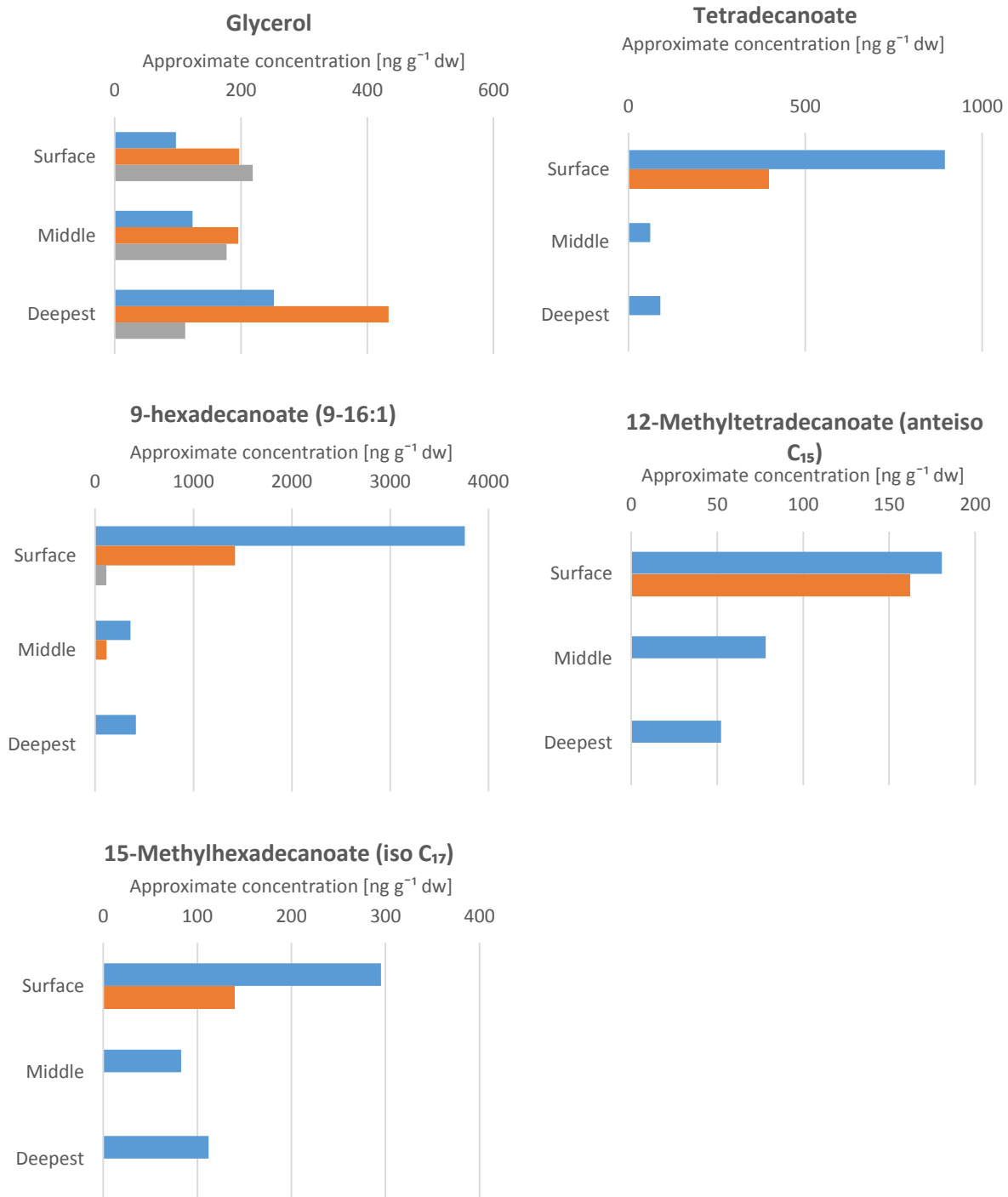


Figure 13. Glycerol, C<sub>14</sub>, 9-hexadecanoate (9-16:1), aiC<sub>12:0</sub>15Me and iC<sub>15:0</sub>17Me approximate concentration [ng g<sup>-1</sup> dw] relative to n-alkane standard through depth. Colors: Sand references site=blue; Brown microbial mat= orange; and White microbial mat= grey. Depths: Surface= 0-2cm; Middle= 6-8cm; and Deepest= 10-11cm for Sand; 16-18cm for Brown; and 12-14cm for White.

### 5.5. Lipid analysis of bacterial and archaeal pure cultures

A detailed list of the lipid biomarkers found in the cultures is presented in appendix table 14 (appendix figure 33 & 34). The most worth noting ones in the bacteria

were the hexadecanoate; octadecanoate; 9-hexadecanoate (only in the *Geobacter sulfurreducens*); hexadecanoic acid 2,3-bis[(trimethylsilyl)oxy] propyl ester and octadecanoic acid 2,3-bis[(trimethylsilyl)oxy] propyl ester, as these were all seen in the samples as well. The contaminants are cyclononasiloxane occurring at each repetitive point in the chromatograph. Even though the archaeal culture had lipid biomarkers identifiable by the GCMS, the hydrocarbons (e.g. hexadecanoate) present are because this culture was grown using yeast (appendix table 14 & figure 33).

#### 5.6. Archaeol and GDGTs obtained with HPLC-MS

There were no identified abundances of GDGTs identified in the brown microbial mat samples nor the sand reference samples. The most abundant concentration of archaeols and GDGTs were found in the archaeal culture and the white microbial mat samples (figure 14). NOTE\* the concentration of all archaeols and GDGTs from these results were calculated relative to an archaeol like standard (AStd) concentration (standard's name= 1,2,0-Dihexadecyl-rac-glycerol).

In the archaeal culture the most abundant structures, with the highest concentration first: archaeol (glycerol diphytanyl diether, henceforth Ar) (m/z: 653, 1593.13 ng g<sup>-1</sup> dw); GDGT-0 (m/z: 1302, 1477.54 ng g<sup>-1</sup> dw); GDGT-1 (m/z: 1300, 4.41 ng g<sup>-1</sup> dw); GDGT-2 (m/z: 1298, 0.29 ng g<sup>-1</sup> dw); and GDGT-3 (m/z: 1296, 0.05 ng g<sup>-1</sup> dw). Structures seen in figures 15 & 16.

In the white mat surface sample the highest concentration was the Ar with 3.94 ng g<sup>-1</sup> dw, followed by GDGT-0 with 1.42 ng g<sup>-1</sup> dw, and finally crenarchaeol with 1.11 ng g<sup>-1</sup> dw. The total amount at the surface equaled 6.71 ng g<sup>-1</sup> dw. However, the middle sample (6-8 cm) had GDGT-0, GDGT-1, GDGT-2, GDGT-3, crenarchaeol and Ar with concentration of 1.35, 1.21, 2.34, 1.36, 1.13 and 1.62 ng g<sup>-1</sup> dw respectively. The total amount at 6-8 cm equaled to 8.52 ng g<sup>-1</sup> dw.

In the deepest sample (12-14 cm) the GDGT-0, GDGT-2, GDGT-3 and crenarchaeol were present, with concentrations of 0.04, 0.29, 0.10 and 0.18 ng g<sup>-1</sup> dw respectively. The total amount at 12-14 cm (deepest sample) equaled 0.61 ng g<sup>-1</sup> dw.

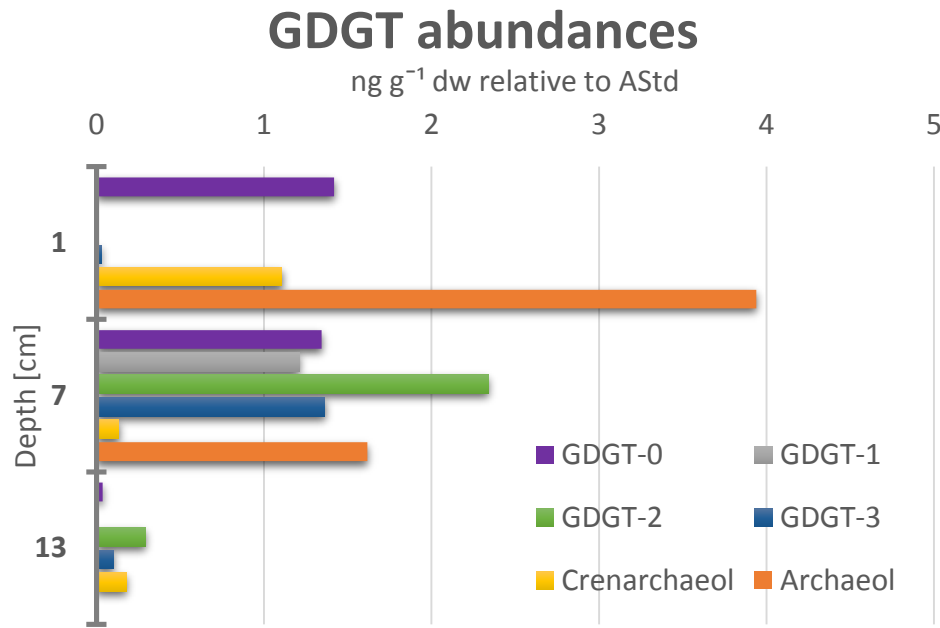


Figure 14. GDGT abundances by depth down the white mat core.

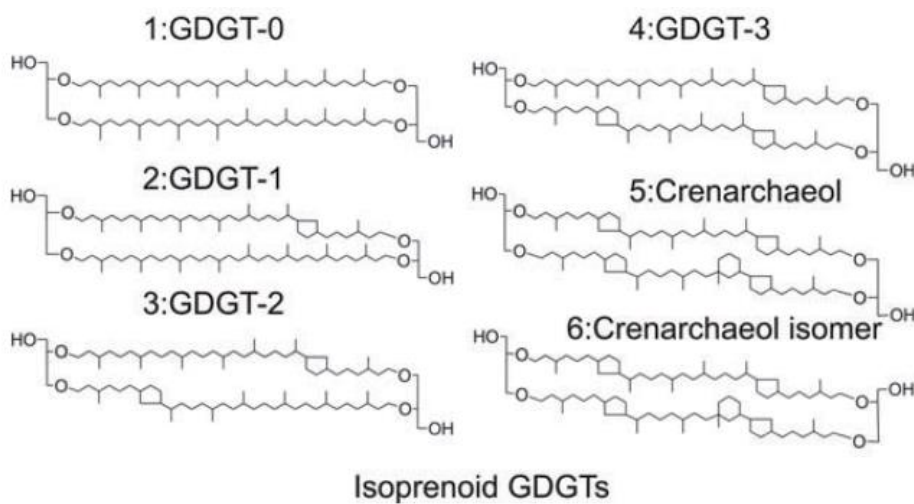


Figure 15. Molecular structure of isoprenoid glycerol dialkyl glycerol tetraethers (GDGTs) (picture from Liu 2011). 1<sup>st</sup>, 2<sup>nd</sup>, 3<sup>rd</sup>, 4<sup>th</sup> and 5<sup>th</sup> identified using HPLC-MS.

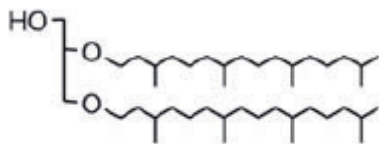


Figure 16. Structure of archaeol identified using HPLC-MS (picture from Liu 2011).

### 5.7. Isotopic signature of lipids (IRMS data) and their isotopic fractionation

To acquire reliable isotopic results the IRMS have to have higher detection limit and overload amplitude. Hence the lipids with low concentrations (e.g. hopanoids many among others) could not be measured. Fortunately, two lipids were measured in all surface sites: 9-hexadecanoate (9-16:1) and hexadecanoate. A summary of these values are in table 5.

Note all  $\delta^{13}\text{C}$  values are relative to the Vienna Pee Dee Belemnite standard. The white microbial mat had isotopic signatures ( $\delta^{13}\text{C}$ ) of -15.65‰ for the 9-hexadecanoate, and -25.51‰ for the hexadecanoate, with differences between the DIC and lipids isotopic values ( $\Delta^{13}\text{C-DIC-lipid}$ ) of 16.55‰ and 26.84‰ respectively.

The lipids from the brown microbial mat had a higher intensity of lipids which the IRMS could measure. Here the 9-hexadecanoate's isotopic signature ( $\delta^{13}\text{C}$ ) was between -29.52‰; hexadecanoate, -29.58‰; and octadecanoate, -31.63‰. The differences between the DIC and lipids isotopic values ( $\Delta^{13}\text{C-DIC-lipid}$ ) were 35.30‰; 35.37‰; and 37.55‰, for 9-hexadecanoate, hexadecanoate and octadecanoate, respectively.

In the sand sediment, because lipid peak heights were even higher than the brown microbial mat, more lipids were detectable. The lipids measured here were 12-methyl-tetradecanoate (anteiso); 15-methyl-hexadecanoate (iso); 9-hexadecanoate; hexadecanoate; and octadecanoate, with isotopic signatures of -19.73‰; -22.58‰; -19.38‰; -19.89‰; and -25.68‰ respectively for each lipid biomarker. The differences between the DIC and lipids isotopic values ( $\Delta^{13}\text{C-DIC-lipid}$ ) in the surface sand sediment were 25.51‰; 28.50‰; 25.15‰; 25.68‰; and 31.78‰, for 12-methyl-tetradecanoate, 15-methyl-hexadecanoate, 9-hexadecanoate, hexadecanoate and octadecanoate respectively (see table 5).

### 5.8. rTCA, RuBisCO (I) and RuBisCO (II) signatures

The inorganic carbon pathways quantified, according to the abundance of specific genes at the different sites, varied significantly (figure 17). In the surface samples, all sites the RuBisCO (II) was the most dominant carbon fixing enzyme, with the highest abundance recorded in the brown, followed by the white and finally the sand reference. The rTCA cycle in the surface did not change much between the different sites, however, it did have the lowest values in the brown mat and sand sediment, while the lowest

values in the white mat was that of the RuBisCO (I) pathway. The carbon pathway for RuBisCO (I) in the brown mat and sand sediment surface samples had a much higher abundance compared to its quantification in the white mat's sample.

Observing the whole core, the brown microbial mats show an increasing abundance trend of all the cycles going towards the surface. For the white microbial mat, the RuBisCO (I) seems to decrease towards the surface while the rTCA cycle has an increasing trend. The RuBisCO (II) has also an increasing trend, though not many points were obtained. The sand sediment reference seems to be fairly stable and does not have an increasing/decreasing trend. However, the RuBisCO (II) cycle is highest in all depths.

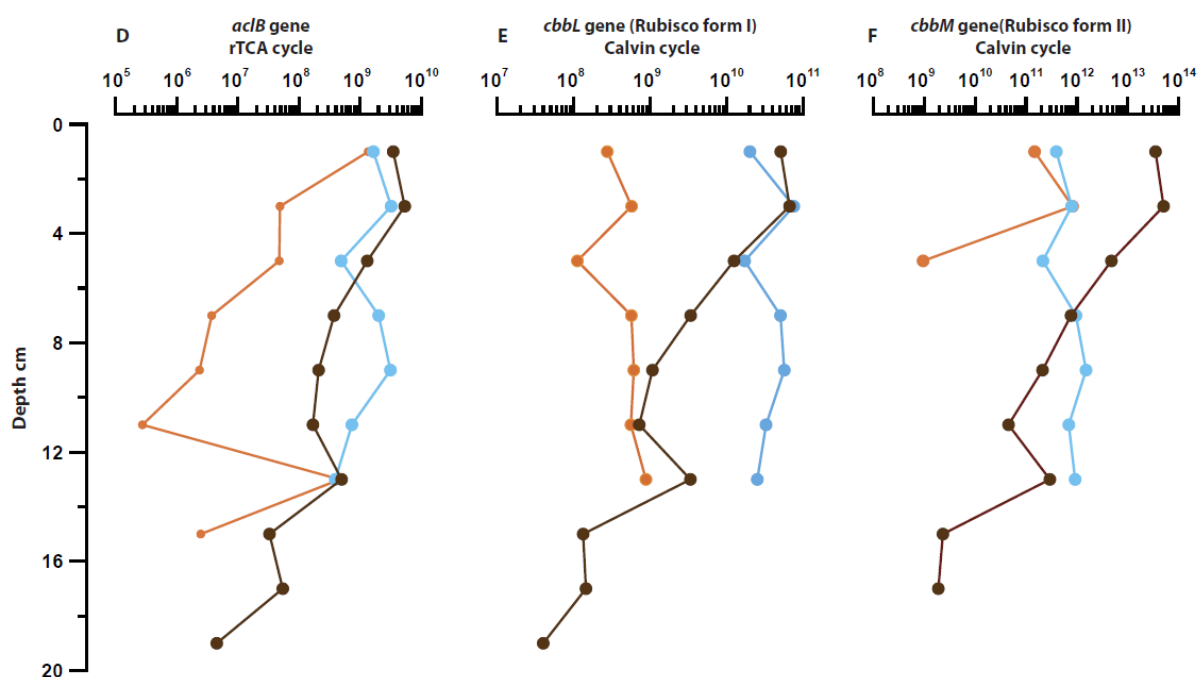


Figure 17. How the different carbon pathway activities change through depth in the different sites, where the orange line is for the white microbial mat site; the brown line for the brown microbial mat site; and the blue line for the sand sediment reference site (from Dr. N. Callac, unpublished data).

Tables 4. Summary of the concentrations [ng g<sup>-1</sup> dw] of the lipid biomarkers as a function of depth for each investigated sediment type.

<b>Biomarker</b>	<i>Core from White mat</i>			<i>Core from Brown mat</i>			<i>Core from Sand sediment</i>		
	1	7	13	1	7	17	1	7	11
<b>Archaea derived</b>									
<i>Archaeol</i>	3.94	1.62	nd	nd	nd	nd	nd	nd	nd
<i>GDGT-0</i>	1.42	1.35	0.04	nd	nd	nd	nd	nd	nd
<i>GDGT-1</i>	nd	1.21	nd	nd	nd	nd	nd	nd	nd
<i>GDGT-2</i>	nd	2.34	0.29	nd	nd	nd	nd	nd	nd
<i>GDGT-3</i>	0.03	1.36	0.10	nd	nd	nd	nd	nd	nd
<i>Crenarchaeol</i>	1.11	0.13	0.18	nd	nd	nd	nd	nd	nd
<b>Bacteria derived</b>									
<i>aiC<sub>12:0</sub>15Me</i>	-	-	-	161.86	nd/-	nd/-	180.67	78.20	52.28
<i>iC<sub>15:0</sub>17Me</i>	-	-	-	140.15	nd/-	nd/-	295.12	82.75	111.88
<i>Diploptene</i>	Low	nd/-	nd/-	Low	nd/-	nd/-	Low	nd/-	nd/-
<i>17β.21β-C<sub>32</sub> homohopanoic fatty acid</i>	Low	nd/-	nd/-	Low	nd/-	nd/-	Low	nd/-	nd/-
<i>17α.21β-C<sub>32</sub> bishopanoic fatty acid</i>	Low	nd/-	nd/-	Low	nd/-	nd/-	Low	nd/-	nd/-
<i>17β.21β-C<sub>32</sub> bishopanoic fatty acid</i>	Low	nd/-	nd/-	Low	nd/-	nd/-	Low	nd/-	nd/-
<b>Eukaryote derived</b>									
<i>Cholesterol Δ<sup>5</sup></i>	108.63	226.72	34.19	277.23	123.28	nd/-	181.59	132.76	116.22
<i>Sterol Δ<sup>5 22</sup></i>	120.02	nd/-	nd/-	122.54	120.49	nd/-	171.45	54.13	141.60
<i>Stigmasterol Δ<sup>5 22</sup></i>	75.78	nd/-	nd/-	234.84	174.61	nd/-	299.54	31.62	147.07
<i>.beta Sitosterol Δ<sup>5</sup></i>	199.33	nd/-	nd/-	697.11	279.29	nd/-	353.40	58.00	173.86
<b>Eukaryote and bacteria derived</b>									
<i>9-Hexadecenoic acid (9-16:1)</i>	112.11	nd/-	nd/-	1423.40	115.04	nd/-	3759.98	359.93	415.08
<i>Hexadecanoate C<sub>16</sub></i>	606.33	435.04	332.93	2770.78	630.21	232.52	4054.81	1255.96	1034.95
<i>Octadecanoate (stearate) C<sub>18</sub></i>	484.01	422.59	332.70	664.58	820.99	368.12	817.73	706.80	587.80

nd= below detection limit; ‘-’= not present.

Table 5. Carbon isotope signature ( $\text{‰} \delta^{13}\text{C}$  vs VPDB) of lipids together with their isotopic fractionation.

	Surface sample from white mat		Surface sample from brown mat		Surface sample from sand sediment	
	$\text{‰} \delta^{13}\text{C}$ (vs VPDB)	$[\Delta]$ DIC-lipid	$\text{‰} \delta^{13}\text{C}$ (vs VPDB)	$[\Delta]$ DIC-lipid	$\text{‰} \delta^{13}\text{C}$ (vs VPDB)	$[\Delta]$ DIC-lipid
<b>Bacteria</b>						
aiC <sub>12:0</sub> 15Me	-	-	nd	-	-19.73	25.51
iC <sub>15:0</sub> 17Me	-	-	nd	-	-22.58	28.50
<b>Eukaryotes and bacteria</b>						
9-Hexadecenoic acid (9-16:1)	-15.65	16.55	-29.52	35.30	-19.38	25.15
Hexadecanoate C <sub>16</sub>	-25.51	26.84	-29.58	35.37	-19.89	25.68
Octadecanoate (stearate) C <sub>18</sub>	nd	-	-31.63	37.55	-25.68	31.78

nd= below detection limit; '-'= not present.

## 6. Discussion

### 6.1. DIC and POC

The isotopic signatures of the DIC in the two microbial mats had an enriching trend with depth, which was not seen in the sand reference site which had none changing values through depth. Furthermore, the isotopic signatures of POC did not deviate noticeable with depth (average of -19‰ in the mats and 18‰ in the sand reference). Usually a correlation between the  $\delta^{13}\text{C}$ -DIC and -POC, influenced by marine algae (Henley et al., 2012; Rau et al., 1989; 1991), can be seen. This through the uptake of lighter  $\text{CO}_2$  enriching the inorganic carbon (DIC). This correlation cannot be seen here, as these two values do not inversely change together with depth. What can be noted from the DIC and POC's isotopic values, not changing inversely with depth in any site, is that the biological activities are not having a big impact on the isotopic values.

The biggest differences observed in the microbial mats, compared to the sand reference, are the temperature increase and the pH decrease with depth. The DIC ( $\text{H}_2\text{CO}_3$ ,  $\text{HCO}_3^-$  and  $\text{CO}_3^{2-}$ ) abundances are very dependent on pH, while the isotopic differences are strongly dependent on temperature (Eby 2004; Hayes 1993; 2001). Therefore, a correlation between the temperature and the enrichment of  $\delta^{13}\text{C}$ -DIC with depth can be estimated. Through the increase in temperature, with depth, a kinetic isotopic fractionation between the aquatic-DIC and the gaseous- $\text{CO}_2$  is pushing more depleted  $\delta^{13}\text{C}$  into  $\text{CO}_2$  ( $_{\text{gas}}$ ) and leaving more enriched  $\delta^{13}\text{C}$ -DIC behind, seen from our results. This analogy was also recorded in the NE Pacific deep-sea hydrothermal vent of Axial Volcano (Levesque et al., 2005), observing enrichments in  $\delta^{13}\text{C}$ -DIC with increasing fluid vent temperatures. Therefore the isotopic DIC values are presumed to be affected by the temperature increases through depth, in the microbial mats.

### 6.2. Lipid abundances affected by hydrothermal transition zones.

The lipid analysis varied in abundances but also in the diversity of different lipid types, between the different sites. In each site the lipid abundances seemed to decrease with depth. The lipid analysis performed in this study has contributed to the notion, suggested by Sievert et al. (1999), that the different sampled sites were separated by transitional zones caused by differences in hydrothermal conditions (e.g. temperature and physico-chemical conditions). The further away from the white mats (most active part of the hydrothermal area), a clear increase in lipid diversity and abundance can be

observed, which was also observed by Sievert et al. (1999) and Giovannelli et al. (2013), both studying the microbial diversity in the Palaeochori Bay's shallow hydrothermal area. Furthermore, higher sedimentation rates have been recorded outside the hydrothermally active areas of the Palaeochori bay, using  $^{210}\text{Pb}$ -dating methods (Ugür et al., 2003), compared to the most hydrothermally active area, suggesting a similar setting here. This correlates well with the identified lipid abundances, as higher abundances are seen further away from the vent field. The recorded high lipid content through depth for the sand sediment is most likely related to normal marine environmental conditions (i.e. neutral pH,  $\sim 20^\circ\text{C}$ , no hydrothermal activity, etc.). This environment promotes a larger diversity of organisms (seen from the diversity of lipid biomarkers). There is also a minor effect from the ongoing convection caused by the hydrothermal outgassing in the vent field (O'Hara et al., 1995; Dando et al., 1995a; Wenzhöfer et al., 2000) together with higher accumulation rates (Ugür et al., 2003), contributing to a higher abundance of organic matter in the site outside the hydrothermal vent field (i.e. sand sediment site). This higher abundance of lipids in the sand reference also correlates well with the TOC, as the TOC was relatively higher at the sand reference site compared to the other sites. However there was an exception at 7 cm, where the highest TOC was from the brown microbial mat site, followed by the white mat and the sand site having the lowest. This increase in the mats and decrease in the reference cannot be explained from the obtained results, but it is very interesting as this effected all sites, thus further research is needed to understand this increase.

The two straight chain fatty acids recovered in all samples (hexadecanoate and octadecanoate) are usually ubiquitous, and are unfortunately not used as biomarkers for specific organisms (Volkman 1998), since they can be produced by all organisms.

The identification of the different branched chain fatty acids (iso and anteiso) were most likely originating from prokaryotes (e.g. chemoautotrophic anaerobic bacteria). These lipids were only seen in the sand sediment and the brown mat, with higher concentrations through depth in the sand sediment, compared to the brown, which only had concentrations in the surface. Price et al. (2013a), Wenzhöfer et al. (2000) and Sievert et al. (1999) have all studied the seep fluids of sediments in the hydrothermal vent areas of Milos, Greece, and showed that in both microbial mat areas (white and brown) the temperature increased sharply with depth. The white mats temperature

increased on average from 40-60°C at the sediment surface to about 70°C at 2.5 cm sediment depth (Sievert et al., 1999 recorded temperatures up to 103°C at 10 cm sediment depth), with a decrease in pH from 7 to 3.8. The brown mats temperature stayed around 20°C in the sediment surface to about 1.5 cm with a decrease in pH of 7 to 4.5, where after, the temperature steadily increased though not as high as in the white mat site. The temperature in the sand reference site stays steadily in the range of 20°C to 25°C (Price et al. 2013a, Wenzhöfer et al. 2000 and Sievert et al. 1999). Temperature increasing with depth, in the brown and white mat (Wenzhöfer et al. 2000; Sievert et al. 1999), could be a reason for the absence of the iso and anteiso fatty acids in the deeper parts of the brown mat and the complete absence in the white mat. Furthermore, the abundance increase of prokaryotes towards the edges and outer regions of the main vent field, and decrease with depth, coincides with Giovannelli et al. (2013)'s study showing the same with the bacteria diversity in the Palaeochori Bay.

The monoenoic fatty acid 9-hexadecanoate (9-16:1), is seen in all sites, but is also considered ubiquitous (Volkman 1998), as it can be produced by all organisms. However, the decrease with depth among the different areas could be due to the temperature increase with depth (Wenzhöfer et al 2000) in the microbial mats.

### 6.3. The presence of Sterols.

The identified sterols from this study were *cholesterol*, *sterol*  $\Delta^{5,22}$ , *stigmasterol* and *sitosterol* occurring in all sampled sites, with the white mat having the lowest abundances of the sterols. The phytosterols (*sterol*  $\Delta^{5,22}$ , *stigmasterol* and *sitosterol*) in the white microbial mat were only seen in the surface sediment. Going down core these sterols were all absent, which could be because the sediment conditions were immediately more anoxic (Wenzhöfer et al., 2000). This lack of oxygen was thus inhibiting the synthesis of the sterols (Galea & Brown 2009). Although this anoxic trend was also seen in the brown mat, there were still sterol abundances present at 7cm, even though the sediment was anoxic. Out of all the sterols, the beta-sitosterol was the most abundant in all sites (relative to the other sterols in the same site). Sterol lipids are associated with algal membranes and the sterols observed in these different sites can be attributable to microalgae (as these utilize C<sub>29</sub> sterols in their biosynthesis) but also to diatoms (Volkman 1998).

#### 6.4. The presence of Hopanoids.

The identified hopanes in this study were *diploptene*, *17 $\beta$ H.21 $\beta$ H-bishomohopanoic acid*, *17 $\alpha$ H.21 $\beta$ H-bishomohopanoic acid* and *17 $\beta$ H.21 $\beta$ H-homohopanoic acid*. Though these only appear in the surface samples, the sand reference and brown habitat had all of these hopanes, while the white habitat only had diploptene and *17 $\beta$ H.21 $\beta$ H-bishomohopanoic acid*. The bishomohopanooids and homohopanooids are derived from complex hopanooids structures (Härtner et al., 2005). The 17 $\beta$ H.21 $\beta$ H structures of the hopanooids are the least thermodynamically stable structures (Barakat & Rullkötter 1995), therefore, with this in mind, it was not surprising that the overall relative predominance was that of the 17 $\beta$ H.21 $\beta$ H hopanooid components in all surface sites, as this would indicate that the surface sediments are not mature. Although, hopanooids are, to a large extent, biomarkers for bacterial organisms (relative abundances found in i.e. cyanobacteria, methanotrophic bacteria and members of the  $\alpha$ -proteobacteria), the knowledge regarding their taxonomic classification is not clear (Peters et al., 2005). However, these could be attributable to the sulfur-oxidizing proteobacterial organisms which had been identified in the Palaeochori Bay area (Sievert 1999). The identified diploptene hopanooid, one of the most common C<sub>30</sub> hopanooid compound in bacterial biosynthesis (Kannenberg et al., 1999), can be attributed to many organisms. Though here, alone, it cannot be set to any specific organisms.

#### 6.5. The identified GDGTs.

The identified abundances of GDGT-0 and crenarchaeol (GDGT-5), in the surface, could be biomarkers for the non-thermophilic Crenarchaeota (Smittenberg et al., 2005b; Schouten et al., 2013) classified as Thaumarchaeota. However, the low abundance of GDGT-3 and absence of GDGT-1; -2 and absence of the regio-isomer of crenarchaeol, together with the high temperature environment, suggests that these GDGTs are biomarkers for some other archaeal.

As mentioned, it has been suggested that the crenarchaeol may also be a biomarker for the biosynthesis of a thermophilic ammonia oxidizing crenarchaeon "*Candidatus Nitrosocaldus yellowstonii*" (Pearson et al., 2008; Lincoln et al 2013) which grows optimally in alkaline pH conditions with ammonia and oxygen present. Consequently this could be the reason for why the concentration of the crenarchaeol is higher in the oxic-anoxic interface between the seawater and the vent fluids (Yücel et al., 2013; Wenzhöfer et al., 2000), where Fitzsimons et al., (1997) recorded high abundances of

ammonia and oxygen in the white surface area. One of the reasons for the crenarchaeols immediate decrease in the white microbial mat could be the more acidic pH conditions, as studied by Wenzhöfer et al., (2000), in deeper parts of the sediment as this would inhibit the growth for the archaea.

The high abundance of GDGT-0 and crenarchaeol, and the relatively smaller abundances of the cyclic GDGTs (GDGT-1; -2; -3), found in the white mat site show a characteristic marine archaeal profile (as seen in Schouten et al 2000; Xiao-Lei Liu 2011), which has also been seen in other hydrothermal areas, e.g. the spreading ridge of Eastern Lau in the South Pacific Ocean (Hu et al., 2012) and the Lost city hydrothermal field near the mid-Atlantic ridge (Lincoln et al., 2013). Also as no branched GDGTs were identified (produced by bacteria (Xiao-Lei Liu 2011)), this suggests that the main biosynthesizes of the GDGTs here are archaeal organisms. The hydrothermal surface environment in this study suggests that the crenarchaeol, and the absence of the GDGTs mentioned above, is most likely a biomarker for the thermophilic ammonia oxidizing crenarchaeon "*Candidatus Nitrosocaldus yellowstonii*". However, it should be noted that the understanding of the biological sources of GDGTs is still in its early stages, as there has not been extensive research surrounding this (Xia-Lei Liu; Hu et al., 2012; Lincoln et al 2013).

The identified abundances of Ar (GDD with m/z 653, see figure 16) is the most commonly observed archaeal diether lipid (Xia-Lei Liu 2011) and can be attributable to methanotrophic archaea (Xia-Lei Liu 2011 and references therein). If similar ring moiety distribution would have been seen in the GDDs as well as the GDGTs, it could have been suggested that they have the same biological sources (Xia-Lei Liu 2011; Liu et al 2012), though this is not the case here. When relating the abundances of Ar to the different GDGTs identified, the Ar abundances are higher, in the surface sediment of the white microbial mat, with only one Ar (GDD-0) present. Liu 2011 recorded high abundances of specific H-shaped GDGTs (molecular weight + hydrogen mass) together with H-shaped GDDs in hydrothermal vent sediments. Another reason for the Ar presence in this study could be due to a diagenesis process by the GDGTs, as it has been reported by Takano et al., (2010) that benthic archaea can recycle GDGTs into GDDs. By this contrast GDDs can be indicators for archaeal lipid membranes or a diagenesis process by which the archaeal follow.

Moreover, the brown mat and sand reference samples did not show any abundances for GDGTs. Even though Fitzsimons et al., (1997) recorded 10 times lower ammonia levels in the brown mat, compared to the white mat, this is most likely not the reason for the absence of the biomarker. Even though the environment is different in the two other sites, there should still have been some signs of marine archaeal presence. Another possibility for the absence of the GDGTs in the brown and sand samples could be a methodological error (e.g. a low concentration of GDGTs in the samples, detection limits from the instrument or filtration issues in the method) causing the samples to not show identifiable signs for the GDGTs.

Based on the discussion above, the only definitive conclusion is that the presence of archaeal lipid membranes are present in the white microbial mat, and speculation on their biological source would suggest that they are biosynthesized by the thermophilic ammonia oxidizing crenarchaeon "*Candidatus Nitrosocaldus yellowstonii*". Further evidence for this is that the Crenarchaeota was measured in abundances, in this area, by Price et al (2013a). Also the recorded high abundance of GDGTs and GDD, in the surface sediment of the most active hydrothermal field area in this study, suggests that these biomarker lipids are important archaeal lipids that can be targeted in future hydrothermal studies.

Acquiring additional results from the other sites, a comparison between the different environments could be better understood, though this would imply further research on other sites.

## 6.6. Culture lipid analysis

The lipid analysis on the cultures was made to correlate specific lipid to those that were identified in the sediment samples. However, being that the lipids identified in the cultures were mostly ubiquitous, this correlation was not possible. Thus this is not discussed furtherly as there are no results that are discussable.

## 6.7. Isotopic lipid signatures indicating a mixed source from methanotrophs

When comparing the results from the brown microbial mat with the sand reference (no hydrothermal activity) the  $\delta^{13}\text{C}$  values are 10‰ more depleted, indicating that these systems has to have some other/mixed carbon source.

The organisms in the microbial mats can theoretically get their carbon source for

biosynthesis from three sources, bicarbonate; methane; and dissolved CO<sub>2</sub>. Carbon fixation of bicarbonate (Hayes 1993; 2001) in this system is one possibility (seen in deep-sea hydrothermal vent systems (Minic & Thongbam 2011)). However, through this biosynthesis the lipids isotopic signature would have smaller isotopic fractionation from their carbon source (bicarbonate), and thus be more enriched in <sup>13</sup>C compared to the dissolved CO<sub>2</sub>. For this reason the assimilation through this process is not proposed here, as this would mean that the δ<sup>13</sup>C results, from the lipids, would have less depleted (heavier) signals compared to the results gathered here.

Another possible carbon source could be from the biosynthesis of methane, by methanotrophs (Hanson & Hanson 1996), from the vent outgassing (<9%) (Dando et al., 1995). Several studies have been made identifying the different bacterial and archaeal organisms (Price et al., 2013a; Giovannelli et al., 2013), in the hydrothermal vent system of Milos, though there has not been any identification of methanotrophs. Methanotrophs are from the gamma- (ribulose monophosphate pathway) and alpha- (serine pathway) proteobacteria family (Hanson & Hanson 1996), and these family groups have been identified from this area (Price et al., 2013; Giovannelli et al., 2013), though not methanotrophs specifically. With optimum growth conditions, for methanotrophic bacteria, being within a temperature range of 25 to 35°C, pH values around 7 to 7.6, methane availability and ammonia concentrations ranging between 12 and 61 mM (Hanson & Hanson 1996), there is a possibility for them to be present in the microbial mats. Aerobic methanotrophs utilizing oxygen (which would be on top of the sediment due to anoxic condition in the sediment (Wenzhöfer et al., 2000)) and methane (coming from hydrothermal areas), which would yield δ<sup>13</sup>C lipid values ranging from -40 to -75‰ (these lipid values were found in mud volcanoes at the Mediterranean Ridge (Pancost et al., 2000)). Thus the available carbon source (HCO<sub>3</sub><sup>-</sup>) would be subsequently depleted. However, this would have been shown in the results, with much more depleted (lighter) δ<sup>13</sup>C signals from the lipids. Though, there is a possibility to suggest for a mixed carbon source isotopic signal (with one of them being from methanotrophs) in this environment, as the identified Ar GDD was high in abundance in the surface of the white microbial mat which could be attributable to methanotrophs. Though this would need further research to be able to propose these conditions.

The last possible carbon source is the dissolved CO<sub>2</sub>, which is the most plausible one in this environment because of the constant CO<sub>2</sub> vent gassing from the hydrothermally

active areas (white and brown mats) (Dando et al., 1999; 1995a). This CO<sub>2</sub> would permit for the easiest carbon fixation by the organisms (Hayes 1993; 2001). This is the argument for the values in the white and brown mats from this study. In these conditions the organisms would fractionate more readily, due to the large reservoir of the CO<sub>2</sub>, discriminating the <sup>13</sup>C in their assimilation (Hayes 2001), thus producing the depleted δ<sup>13</sup>C signals seen from the results. While the sand reference has a 10‰ more enriched signal, this is most likely due to the low reservoir of CO<sub>2</sub> (compared with the mats in the vent fields) and overall higher abundance of lipids and microbes (Price et al., 2013a; Giovannelli et al., 2013), causing the discrimination of carbon to not be as efficient.

A more broad study of this kind is needed, where the targeted lipids are not ubiquitous, as in this study, and can be linked to more specific organisms.

#### 6.8. RuBisCO (II) dominated throughout the sites

It has been proven that the rTCA cycle is the most dominant carbon fixation pathway for organisms in deep-sea hydrothermal vent systems (Campbell & Cary 2004), with only weak to no signal for both RuBisCO I and II. These deep-sea systems are mostly inhabited by chemolithoautotrophs while the photoautotrophic activity is limited. On the contrary, shallow submarine hydrothermal systems, such as in Milos, are in the photic zone and are influenced by photoautotrophic and chemoautotrophic organisms (Price et al., 2013a; Giovannelli et al., 2013), though these are highly affected by the dynamic hydrodynamics (tides, storms, microearthquakes and currents) that are present (Wenzhöfer et al., 2000). Here the microbial mats have nutrients and constant CO<sub>2</sub> vent outgassing (Dando et al., 1999; 1995a), making these areas practically non-limiting CO<sub>2</sub> reservoirs. The results, from the genes sequences of these areas, show that the RuBisCO form II is dominating in the Milos sediment, regardless of sample site, with rTCA having the lowest activity in all sites (except for the white mat). The highest levels of RuBisCO (II) and (I) were seen in the brown microbial mat, most likely due to the nutrient availability, non-limiting CO<sub>2</sub> environment (O'Leary & Roeske 1985; Staal et al., 2007), higher abundance microbial organisms (Giovannelli et al., 2013) seen from the lipid analysis as well (compared to the white microbial mat), and the less extreme environment (also compared to the white mat) (see figure 19). The white microbial mat also had higher RuBisCO (II) compared with the rTCA, though here the RuBisCO (I) had

decreased rapidly making it the third highest carbon fixation pathway (out of the three measured). The sand reference site had similar RuBisCO (II) activities as the white microbial mat, most likely due to the “marine” like environment, promoting a higher diversity of microorganisms, also seen from the lipid analysis. While the rTCA was at its lowest point in this sediment site (see figure 19). The discussion only entails to the surface values and not the deeper activities of the different genes.

This is the first study showing that the RuBisCO (II) is the most active carbon fixation pathway for organisms, in all regions (including the non-affected sand reference site) of the shallow submarine hydrothermal vent system of Milos Island. Furthermore, not all pathways for carbon fixation have been measured in this area (e.g. carboxylase, acetyl-CoA), and this would provide a more in-depth understand of this environment and the organisms inhabiting it.

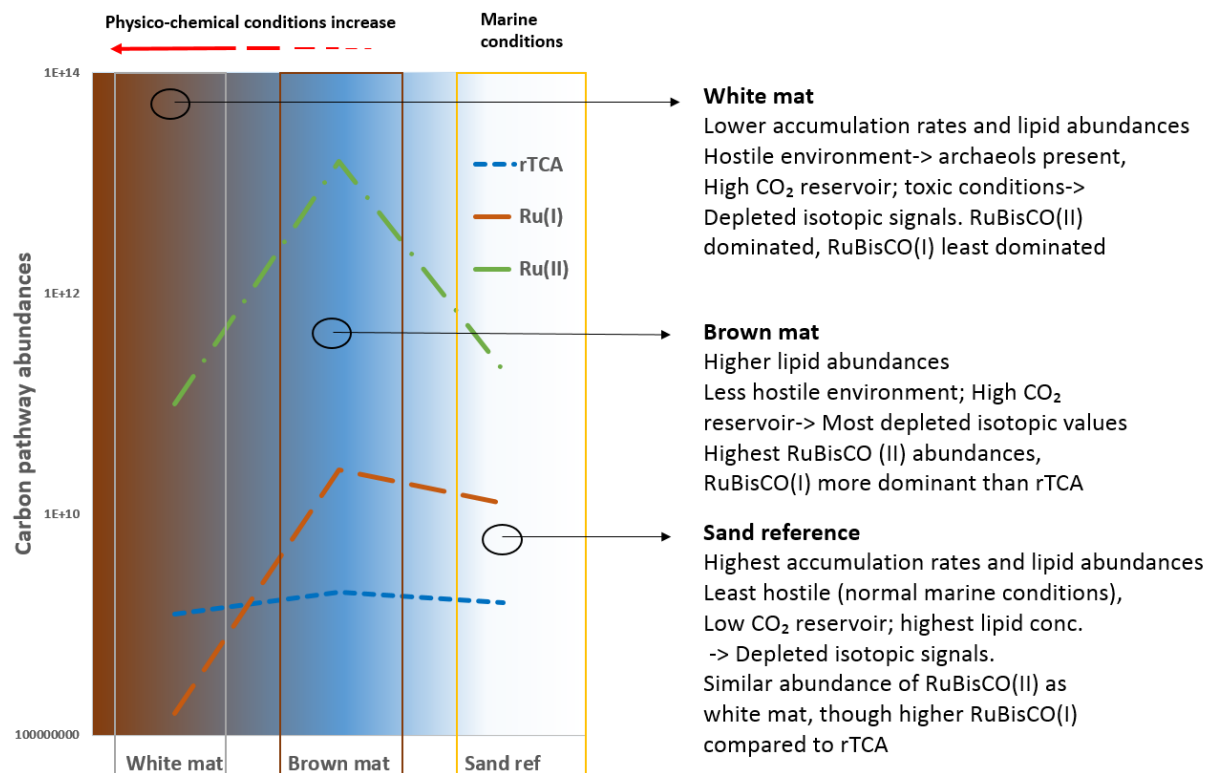


Figure 19. Detailed rendered summary figure of the different sediment surface sites recovered for analysis, with each sites results summarized. The color gradient of blue going in to red-brownish indicates the transition of entering into more hydrothermally active conditions, with physico-chemical conditions increasing (i.e. increasing temperature; seep fluid intrusions; more anoxic sediments; higher arsenic levels). The sand reference is the only area in the figure that has no hydrothermal activity (marine conditions), as it is situated further away from the other sites. Accumulation rates acquired from Ugür et al (2003). Carbon pathway abundances are in logarithmic scales.

## 7. Conclusions

From the arsenic rich hydrothermally active region of Milos, a comprehensive lipid biomarker interpretation was made. Interpreting these different lipid abundances, a clear correlation could be made together with the physico-chemical conditions of the environment. This indicated that the organism's abundance and diversity increase in the periphery and the outer regions of the hydrothermal vent field. The same is seen through depth in the different regions, with the microbial mats most likely affected by the sharp temperature rise. Furthermore these conclusions coincide with results from Giovanneli et al. (2013), which suggested the same conclusions. Similarly, the enriching isotope values of DIC with depth, in the microbial mats, are also most likely due to temperature increase which is affecting the isotopic fractionation of DIC. This permits more depleted CO<sub>2</sub> release, leaving more enriched DIC values in the deeper and higher temperature sediments.

The carbon isotope values from the two microbial mat lipids indicated that the most likely carbon source for organism's biosynthesis is dissolved CO<sub>2</sub>. This is concluded from the more depleted lipid signatures in the microbial mats, compared with the unaffected site, and the large reservoir of CO<sub>2</sub>, causing higher discrimination of <sup>13</sup>C compared to <sup>12</sup>C. These conditions do not appear to change through depth indicating small fluctuations in recent hydrodynamic processes.

The most important discovery from this study, is the demonstration that the RuBisCO (form II) is the most important carbon fixation pathway for chemoautotrophic and photoautotrophic organisms living in the arsenic rich shallow submarine hydrothermal system in Spathi Bay of Milos, Greece. Even though rTCA is favored by free-living microorganisms in deep-sea hydrothermal vent systems (e.g. Campbell & Cary 2004; Elsaied & Naganumna 2001), the key gene sequences targeted here (cbbL, cbbM and acIB) are showing a dominance for RuBisCO (especially form II) in these hydrothermally affected microbial mats. These are the first documented results indicating that the RuBisCO (II) is the most actively used enzyme, for biosynthesis, in a shallow submarine hydrothermal vent field area. However, the two RuBisCO forms diminish rapidly as the physico-chemical conditions increase and the environment become more extreme, while the rTCA is not affected as severely.

For future studies involving carbon fixation pathways in submarine hydrothermal vent systems, the hydrothermal vent field around the island of Milos is an ideal research location with high RuBisCO (II) activities. If there is a connection between RuBisCO (II) and arsenic in the environment these future studies could give a better understanding of how organisms survived in the early Earth environments.

## 8. Acknowledgements

I would like to thank my main-supervisor Ernest Chi Fru, co-supervisor Jayne Rattray and co-advisor Rienk Smittenberg for all their help and guidance throughout this thesis. I also want to acknowledge Nolwenn Callac, Heike Siegmund and Kweku Afrifa Yamoah for their laboratory assistants and support. During these 5 year at Stockholms University I have received a lot of help for the administrators, technical staff and professors from the Department of Geological Sciences, and would like to thank them as well. Lastly I would like to thank my mother, family members and friends, and a really big special thanks to Camilla Olsson who had the patience to help and encourage me throughout the thesis. I'm done and out (mic drop)!

## 9. References

- Aközcan, S. & Uğur Görgün, A. 2012, 'Trace metal and radionuclide pollution in marine sediments of the Aegean Sea (Izmir Bay and Didim)', *Environmental Earth Sciences*, p. 1-5
- Alfieris, D., Voudouris, P. & Spry, P. 2013, 'Shallow submarine epithermal Pb–Zn–Cu–Au–Ag–Te mineralization on western Milos Island, Aegean Volcanic Arc, Greece: Mineralogical, geological and geochemical constraints', *Ore Geology Reviews*, 53, pp. 159-180
- Amend JP., McCollom TM., Hentscher M. & Bach W. 2011. 'Catabolic and anabolic energy for chemolithoautotrophs in deep-sea hydrothermal systems hosted in different rock types'. *Geochim Cosmochim Acta*, 75, pp. 5736–5748
- Baker-Austin, C. & Dopson, M. 2007, 'Review: Life in acid: pH homeostasis in acidophiles', *Trends In Microbiology*, 15, pp. 165-171.
- Barakat AO. & Rullkötter J. (1995) Extractable and bound fatty acids in core sediments from the Nördlinger Ries, southern Germany. *Fuel* 74: 416–425
- Begy, R., Cosma, C., & Timar, A. 2009, 'Recent changes in Red Lake (Romania) sedimentation rate determined from depth profiles of <sup>210</sup>Pb and <sup>137</sup>Cs radioisotopes', *Journal Of Environmental Radioactivity*, 100, 8, pp. 644-648.
- Bekker, A., Slack, J.F., Planavsky, N., Krapež, B., Hofmann, A., Konhauser, K.O., Rouxel, O.J., 2010. Iron formation: The sedimentary product of a complex interplay among mantle, tectonic, oceanic, and biospheric processes. *Econ. Geol.* 105, 467-508.
- Bennett, S, Statham, P, Green, D, Le Bris, N, McDermott, J, Prado, F, Rouxel, O, Von Damm, K, & German, C 2011, 'Dissolved and particulate organic carbon in hydrothermal plumes from the East Pacific Rise, 9°50'N', *Deep-Sea Research Part I*, 58, pp. 922-931
- Berg, I., Kockelkorn, D., Ramos-Vera, W., Say, R., Zarzycki, J., Hügler, M., Alber, B. & Fuchs, G. 2010, 'Autotrophic carbon fixation in archaea', *Nature Reviews Microbiology*, 8, 6, pp. 447-460

- Breuer, C. & Pichler, T. 2013, 'Arsenic in marine hydrothermal fluids', *Chemical Geology*, 348, Arsenic in marine hydrothermal systems: Source, fate and environmental implications, pp. 2-14
- Cahnmann, H. 1957, 'Partially deactivated silica gel columns in chromatography: Chromatographic behavior of benzo[a]pyrene', *Analytical Chemistry*, 29, 9, p. 1307-1311.
- Cambray, R., Eakins, J., Harkness, J., & Pennington, W. 1976, 'Radionuclide dating of the recent sediments of Blelham Tarn', *Freshwater Biology*, 6, 4, p. 317.
- Campbell, B. & Gary, S. 2004, 'Abundance of reverse tricarboxylic acid cycle genes in free-living microorganisms at deep-sea hydrothermal vents', *Applied And Environmental Microbiology*, 70, 10, p. 6282-6289.
- Campbell, B., Cary, S. & Stein, J. 2003. 'Evidence of chemolithoautotrophy in the bacterial community associated with *Alvinella pompejana*, a hydrothermal vent polychaete', *Applied And Environmental Microbiology*, 69, 9, p. 5070-5078
- Castaneda, I., & Schouten, S., 2011, 'A review of molecular organic proxies for examining modern and ancient lacustrine environments', vol 30, pp. 2851, *Quaternary Science Reviews*, 125, pp. 174-176.
- Coolen MJL. & Gibson JAE. 2009. 'Ancient DNA in lake sediment records' *PAGES News*, 17, pp. 104–106
- Coolen, M. J. L., Muyzer, G. Rijpstra, W. I. C., Schouten, S., Volkman, J. K. and Sinninghe Damste J. S. 2004 'Combined DNA and lipid analyses of sediments reveal changes in Holocene haptophyte and diatom populations in an Antarctic lake'. *Earth Planet Sci. Lett.*, 223, 225–239
- Cronan, D., Varnavas, S., & Perissoratis, C., 1995, 'Hydrothermal Sedimentation in the Caldera of Santorini, Hellenic Volcanic Arc', *Terra Nova*, 7, 2, pp. 289-293.
- Dando, P., Hughes, J. & Thiermann, F. 1995b, 'Preliminary observations on biological communities at shallow hydrothermal vents in the Aegean Sea', *Geological Society, London, Special Publications*, vol. 87, issue 1, pp. 303-317

- Dando, P., Hughes, J., Leahy, Y., Niven, S., Taylor, L., & Smith, C., 1995a, 'Gas venting rates from submarine hydrothermal areas around the island of Milos, Hellenic Volcanic Arc', *Continental Shelf Research*, 15, 8, p. 913-929.
- Dando, P., Stüben, D. & Varnavas, S. 1999, 'Hydrothermalism in the Mediterranean Sea', *Progress In Oceanography*, 44, pp. 333-367
- DeLong, E.F. 1998, 'Everything in moderation: archaea as 'non-extremophiles'', *Current Opinion In Genetics & Development*, vol. 8, no. 6, pp. 649-654.
- E. Chi Fru., M. Ivarsson., S. P. Kiliyas., P. J. Frings., C. Hemmingsson., C. Broman., S. & Bengtson., E. Chatzitheodoridis. 2015. Biogenicity of an Early Quaternary iron formation, Milos Island, Greece. *Geobiology* 13, 225–244.
- Eby, G. Nelson. (2004). *Principles of environmental geochemistry*. Pacific Grove, Calif.: Thomson-Brooks/Cole
- Elsaied, H. & Naganuma, T. 2001, 'Phylogenetic diversity of ribulose-1,5-bisphosphate carboxylase/oxygenase large-subunit genes from deep-sea microorganisms', *Applied And Environmental Microbiology*, 67, 4, pp. 1751-1765
- Ernest Chi Fru, Magnus Ivarsson, Stephanos P. Kiliyas, Stefan Bengtson, Veneta Belivanova, Federica Marone, Danielle Fortin, Curt Broman, Marco Stampanoni. 2013. Fossilized iron bacteria reveal a pathway to the biological origin of banded iron formation. *Nature Communications* 4, 2050 doi:10.1038/ncomms3050.
- Fitzsimons, M., Pratt, S., Dando, P., Hughes, J., Thiermann, F., & Akoumianaki, I., 1997, 'Submarine hydrothermal brine seeps off Milos, Greece: Observations and geochemistry', *Marine Chemistry*, 57, 3-4, p. 325-340.
- Gaines, Susan M., Eglinton, Geoffrey & Rullkötter, Jürgen 2009. *Echoes of life: what fossil molecules reveal about earth history*. Oxford: Oxford University Press
- Galea, A. & Brown, A. 2009, 'Hypothesis Paper: Special relationship between sterols and oxygen: Were sterols an adaptation to aerobic life?', *Free Radical Biology And Medicine*, 47, pp. 880-889
- Gilhooly, W., Fike, D., Druschel, G., Kafantaris, F., Price, R. & Amend, J. 2014. 'Sulfur and oxygen isotope insights into sulfur cycling in shallow-sea hydrothermal vents, Milos, Greece', *Geochemical Transactions*, 15, doi: 10.1186/s12932-014-0012-y

- Godelitsas, A., Price, R., Pichler, T., Amend, J., Gamaletsos, P. & Göttlicher, J. 2015, 'Amorphous As-sulfide precipitates from the shallow-water hydrothermal vents off Milos Island (Greece)', *Marine Chemistry*, 177, Part 5, pp. 687-696
- Hanson, R. & Hanson, T. 1996, 'Methanotrophic Bacteria', *Microbiological reviews*, 60, 2, pp. 439-471
- Härtner, T., Kannenberg, E., & Straub, K. 2005, 'Occurrence of hopanoid lipids in anaerobic *Geobacter* species', *FEMS Microbiology Letters*, 243, 1, p. 59-64
- Harwood, J. & Russell, N. 1984. Lipids in plants and microbes. Department of Biochemistry, University College of Wales, Cardiff, UK, George Allen & Unwin (Publishers) Ltd
- Hayes, J. 1993, 'Factors controlling  $^{13}\text{C}$  contents of sedimentary organic compounds: Principles and evidence', *Marine Geology*, 113, 1-2, p. 111-125
- Hayes, J. 2001, 'Fractionation of Carbon and Hydrogen Isotopes in Biosynthetic Processes', *Reviews in Mineralogy and Geochemistry*, 43, p. 225-277
- Hein JR., Stamatakis MG. & Dowling JS. (2000) Trace metal-rich Quaternary hydrothermal manganese oxide and barite deposit, Milos Island, Greece. *Applied Earth Science: Transactions of the Institutions of Mining and Metallurgy: Section B* 109, 67-76.
- Henley, S., Annett, A., Ganeshram, R., Carson, D., Weston, K., Crosta, X., Tait, A., Dougans, J., Fallick, A. & Clarke, A. 2012, 'Factors influencing the stable carbon isotopic composition of suspended and sinking organic matter in the coastal Antarctic sea ice environment', *Biogeosciences*, 9, 3, p. 1137-1157
- Hewitt, W., 2000, 'Determining the Ages of the Recent Sediments using Measurements of Trace Radioactivity', *Terra et Aqua*, Number 78
- Hu, J., Meyers, P., Chen, G., Peng, P. & Yang, Q. 2012, 'Archaeal and bacterial glycerol dialkyl glycerol tetraethers in sediments from the Eastern Lau Spreading Center, South Pacific Ocean', *Organic Geochemistry*, 43, pp. 162-167

- Jungblut, A., Allen, M., Burns, B. & Neilan, B. 2009, 'Lipid biomarker analysis of cyanobacteria-dominated microbial mats in meltwater ponds on the McMurdo Ice Shelf, Antarctica', *Organic Geochemistry*, 40, pp. 258-269
- Kannenbergh, E., & Poralla, K. 1999, 'Hopanoid biosynthesis and function in bacteria', *Naturwissenschaften*, 86, 4, pp. 168-176
- Karner, M., DeLong, E. F. and Karl, D. M. 2001 Archaeal dominance in the mesopelagic zone of the Pacific Ocean. *Nature* 409, 507–510.
- Kelley, D, Karson, J, Blackman, D, Fruh-Green, G, Butterfield, D, Lilley, M, Olson, E, Schrenk, M, Roe, K, Lebon, G, & Rivizzigno, P 2001, 'An off-axis hydrothermal vent field near the Mid-Atlantic Ridge at 30 degrees N', *Nature*, 412, 6843, p. 145-149
- Kilias, S., Nomikou, P., Papanikolaou, D., Polymenakou, P., Godelitsas, A., Argyraki, A., Carey, S., Gamaletsos, P., Mertzimekis, T., Stathopoulou, E., Goettlicher, J., Steininger, R., Betzelou, K., Livanos, I., Christakis, C., Bell, K., & Scoullou, M., 2013, 'New insights into hydrothermal vent processes in the unique shallow-submarine arc-volcano, Kolumbo (Santorini), Greece', *Scientific Reports*, 3. DOI: 10.1038/srep02421
- Kim, J., van der Meer, J., Schouten, S., Helmke, P., Willmott, V., Sangiorgi, F., Koç, N., Hopmans, E. & Damsté, J. 2010, 'New indices and calibrations derived from the distribution of crenarchaeal isoprenoid tetraether lipids: Implications for past sea surface temperature reconstructions', *Geochimica Et Cosmochimica Acta*, 74, pp. 4639-4654
- Kuenen, G. 2009. Oxidation of Inorganic Compounds by Chemolithotrophs. In Lengeler, J.; Drews, G.; Schlegel, H. *Biology of the Prokaryotes*. John Wiley & Sons. p. 242
- Lanekoff, I., Karlsson, R., 2010. Analysis of intact ladderane phospholipids, originating from viable anammox bacteria, using RP-LC-ESI-MS. *Analytical and Bioanalytical Chemistry* 397, 3543-3551.
- Lerman, A. & Baccini, P. (red.) 1978. *Lakes: chemistry, geology, physics*. New York: Springer-Vlg
- Levesque, C., Limén, H. & Juniper, S. 2005, 'Origin, composition and nutritional quality of particulate matter at deep-sea hydrothermal vents on Axial Volcano, NE Pacific', *Marine Ecology Progress Series*, 289, p. 43-52

- Lincoln, S., Bradley, A., Newman, S. & Summons, R. 2013, 'Archaeal and bacterial glycerol dialkyl glycerol tetraether lipids in chimneys of the Lost City Hydrothermal Field', *Organic Geochemistry*, 60, pp. 45-53
- Liu, X., Lipp, J., Schröder, J., Summons, R. & Hinrichs, K. 2012, 'Isoprenoid glycerol dialkanol diethers: A series of novel archaeal lipids in marine sediments', *Organic Geochemistry*, 43, pp. 50-55
- Mackenzie, A.S., Brassell, S.C., Eglinton, G., & Maxwell J.R., 1982, 'Chemical Fossils: The Geological Fate of Steroids', *Science*, vol. 217, no. 4559, pp. 491-504.
- Minic, Z., & Thongbam, P. 2011, 'The Biological Deep Sea Hydrothermal Vent as a Model to Study Carbon Dioxide Capturing Enzymes', *Marine Drugs*, 9, 5, pp. 719-738
- Nakagawa, S., & Takai, K., 2008, 'Deep-sea vent chemoautotrophs: diversity, biochemistry and ecological significance', *Fems Microbiology Ecology*, 65, 1, pp. 1-14
- O'Hara, S., Dando, P., Schuster, U., Bennis, A., Boyle, J., Chui, F., Hatherell, T., Niven, S. & Taylor, L. 1995, 'Gas seep induced interstitial water circulation: observations and environmental implications', *Continental Shelf Research*, 15, 8, p. 931-948
- O'Leary, M. & Roeske, C. 1985, 'Carbon isotope effect on carboxylation of ribulose biphosphate catalyzed by ribulosebiphosphate carboxylase from *Rhodospirillum rubrum*', *Biochemistry*, 24, 7, p. 1603-1607
- Othman, I., Al-Masri, M., & Al-Rayyes, A. 2000, 'Sedimentation rates and pollution history of the eastern Mediterranean Sea: Syrian coast', *Science Of The Total Environment*, 248, pp. 27-35
- Oulas, A., Polymenakou, P., Mandalakis, M., Christakis, C., Kotoulas, G., Magoulas, A., Seshadri, R., Tripp, H., Paez-Espino, A., Pati, A., Ivanova, N., Kyrpides, N., Chain, P., Nomikou, P., Kiliass, S. & Carey, S. 2016, 'Metagenomic investigation of the geologically unique Hellenic Volcanic Arc reveals a distinctive ecosystem with unexpected physiology', *Environmental Microbiology*, 18, 4, p. 1122-1136
- Pancost, R., Sinninghe Damsté, J., de Lint, S., van der Maarel, M. & Gottschal, J. 2000. 'Biomarker evidence for widespread anaerobic methane oxidation in Mediterranean sediments by a consortium of methanogenic archaea and bacteria.

- The Medinaut Shipboard Scientific Party', *Applied And Environmental Microbiology*, 66, 3, pp. 1126-1132
- Pearson, A., Pi, Y., Li, S., Zhao, W., Li, Y., Romanek, C., Zhang, C., Li, W., Inskeep, W. & Perevalova, A. 2008, 'Factors controlling the distribution of archaeal tetraethers in terrestrial hot springs', *Applied And Environmental Microbiology*, 74, 11, p. 3523-3532
- Peters, K. E., Walters, C. C. & Moldowan, J. M. (red.) 2005. The Biomarker Guide / Volume 1. Biomarkers and Isotopes in the Environment and Human History., Cambridge University Press, Cambridge
- Price RE., Lesniewski R., Nitzsche KS., Meyerdierks A., Saltikov C., Pichler T. & Amend JP. 2013a. Archaeal and bacterial diversity in an arsenic-rich shallow-sea hydrothermal system undergoing phase separation. *Frontiers in microbiology*, 4. doi: 10.3389/fmicb.2013.00158
- Price RE., Savov I., Planer-Friedrich B., Bühring SI., Amend J. & Pichler T. 2013b. Processes influencing extreme As enrichment in shallow-sea hydrothermal fluids of Milos Island, Greece. *Chemical Geology*, 348, 15-26.
- Rattray, J., Iñiguez, E., Yamoah, K., Muschitiello, F., Sawicka, J., Smittenberg, R. 'A high-throughput reverse phase UHPLC-MS method for the analysis of GDGTs'. In prep.
- Rau, G. H., Froelich, P. N., Takahashi, T., and Des Marais, D. J. 1991: Does sedimentary organic  $\delta^{13}\text{C}$  record variations in Quaternary ocean  $[\text{CO}_2(\text{aq})]$ ? *Paleoceanography*, 6, 335–347, 1991.
- Rau, G. H., Takahashi, T., and Des Marais, D. J. 1989: Latitudinal variations in plankton  $\delta^{13}\text{C}$ : implications for  $\text{CO}_2$  and productivity in past oceans, *Nature*, 341, 516–518
- Schouten, S., Hopmans, E., & Sinninghe, Damsté, J. 2013, 'Review: The organic geochemistry of glycerol dialkyl glycerol tetraether lipids: A review', *Organic Geochemistry*, 54, pp. 19-61
- Schouten, S., Hopmans, E., Schefuß, E. & Sinninghe Damsté, J. 2002, 'Distributional variations in marine crenarchaeotal membrane lipids: a new tool for reconstructing ancient sea water temperatures?', *Earth And Planetary Science Letters*, 204, pp. 265-274

- Schouten, S., Hopmans, E.C., Pancost, R.D., Sinninghe Damsté, J.S., 2000. Widespread occurrence of structurally diverse tetraether membrane lipids: evidence for the ubiquitous presence of low-temperature relatives of hyperthermophiles. *Proceedings of the National Academy of Sciences USA* 97, 14421–14426
- Schouten, S., Van Der Meer, M., Hopmans, E., Rijpstra, W., Damsté, J., Reysenbach, A. & Ward, D. 2007, 'Archaeal and bacterial glycerol dialkyl glycerol tetraether lipids in hot springs of Yellowstone National Park', *Applied And Environmental Microbiology*, 73, 19, p. 6181-6191
- Sievert, S., Kuever, J., Brinkhoff, T., Muyzer, G. & Ziebis, W. 1999, 'Spatial heterogeneity of bacterial populations along an environmental gradient at a shallow submarine hydrothermal vent near Milos island (Greece)', *Applied And Environmental Microbiology*, 65, 9, p. 3834-3842
- Sjöberg S. 2014, 'Characterization of an REE-enriched black substance in fractured bedrock in the Ytterby Mine', Stockholm University, Master thesis
- Smittenberg, R. H., Baas, M., Schouten, S. and Sinninghe Damsté, J. S. 2005 'The demise of the alga *Botryococcus braunii* from a Norwegian fjord was due to early eutrophication'. *The Holocene*, 15, 133-140
- Smittenberg, R., Baas, M., Green, M., Hopmans, E., Schouten, S. & Sinninghe Damsté, J. 2005, 'Pre- and post-industrial environmental changes as revealed by the biogeochemical sedimentary record of Drammensfjord, Norway', *Marine Geology*, 214, pp. 177-200
- Staal, M., Thar, R., Kuhl, M., van Loosdrecht, M., Wolf, G., de Brouwer, J. & Rijstenbil, J. 2007. 'Different carbon isotope fractionation patterns during the development of phototrophic freshwater and marine biofilms', *Biogeosciences*, 4, 4, pp. 613-626
- Stan-Lotter, H., & Fendrihan, S., 2012. *Adaption of Microbial Life to Environmental Extremes: Novel Research Results and Application*. Vienna: Springer Vienna
- Starr, M.P., (red.) 1981. *The prokaryotes: a handbook on habitats, isolation, and identification of bacteria*. Berlin: Springer-Vlg.

- Takano, Y., Chikaraishi, Y., Ogawa, O.N., Nomaki, H., Morono, Y., Inagaki, F., Kitazato, H., Hinrichs, K.-U., Ohkouchi, N., 2010. Sedimentary membrane lipids recycled by deep-sea benthic archaea. *Nature Geoscience* 3, 858–861
- Timmis, K. N. 2010. *Handbook of Hydrocarbon and Lipid Microbiology*. Berlin, Heidelberg: Springer Berlin Heidelberg
- Uğur, (Tanbay) A., & Yener, G. 2001, 'Accumulation rates and sediment deposition in the Gökova Bay in Aegean Sea Turkish Coast', *Applied Radiation And Isotopes*, 55, pp. 581-588
- Uğür, A., Miquel, J., Fowler, S., & Appleby, P. 2003, 'Radiometric dating of sediment cores from a hydrothermal vent zone off Milos Island in the Aegean Sea', *Science Of The Total Environment*, 307, pp. 203-214
- Volkman, J., Barrett, S., Blackburn, S., Mansour, M., Sikes, E. & Gelin, F. 1998, 'Microalgal biomarkers: A review of recent research developments', *Organic Geochemistry*, 29, 5-7, pp. 1163-1179
- Wenzhöfer, F., Holby, O., Glud, R., Nielsen, H., & Gundersen, J., 2000, 'In situ microsensor studies of a shallow water hydrothermal vent at Milos, Greece', *Marine Chemistry*, 69, pp. 43-54.
- Woese, Carl R., Kandler, O, Wheelis, M. 1990. 'Towards a natural system of organisms: proposal for the domains Archaea, Bacteria, and Eucarya'. *Proc Natl Acad Sci USA* 87 (12): 4576–4579
- Yamoah, K., Chabangborn, A., Chawchai, S., Väiliranta, M., Wohlfarth, B. & Smittenberg, R. 2016, 'Large variability in n-alkane  $\delta^{13}\text{C}$  values in Lake Pa Kho (Thailand) driven by wetland wetness and aquatic productivity', *Organic Geochemistry*, 97, pp. 53-60
- Yücel, M., Sievert, S., Vetriani, C., Foustoukos, D., Giovannelli, D. & Le Bris, N. 2013, 'Eco-geochemical dynamics of a shallow-water hydrothermal vent system at Milos Island, Aegean Sea (Eastern Mediterranean)', *Chemical Geology*, 356, pp. 11-20
- Zhu, C., Lipp, J.S., Wormer, L., Becker, K.W., Schroder, J., Hinrichs, K.U., 2013. 'Comprehensive glycerol ether lipid fingerprints through a novel reversed phase liquid chromatography-mass spectrometry protocol'. *Organic Geochemistry* 65, 53-62.

Zimmerman, A. R., and Canuel, E. A. 2000 'A geochemical record of eutrophication and anoxia in Chesapeake Bay sediments: anthropogenic influence on organic matter composition'. Mar Chem. 69, 117-137

### **Lipid references**

AOCS lipid library- <http://lipidlibrary.aocs.org/index.cfm>

GCMS library- From the installed program on Shimadzu GCMS-QP2010 Ultra.

Mass spectra library- A large diverse group of spectra's acquired over time at Stockholm University

Sjöberg S. 2014, 'Characterization of an REE-enriched black substance in fractured bedrock in the Ytterby Mine', Stockholm University, Master thesis

### **Electronic resources**

HTML 1: <http://lipidlibrary.aocs.org/History/content.cfm?ItemNumber=40363>

## 10. Appendix

**Detailed description of how to identify lipids together with abundances from this study.** Saturated straight-chain fatty acids (also known as: fatty acid methyl esters = FAmEs) have higher  $m/z$  ratios of  $M^+-31$  peak compared to  $M^+-23$  (see appendix figure 22), where  $M^+-x$  is the molecular weight of that compound minus  $x$ . Apart from normal FAmEs, saturated branched-chain fatty acid methyl esters (iso- and anteiso) were also detected. When distinguishing them from normal FAmE, of the same carbon number, these exhibited slight spectral differences (see difference between figure 22 & 23). Iso FAmEs show relatively enhanced  $M^+-43$  and almost equal heights in  $M^+-31$  and  $M^+-29$ , while anteiso FAmEs show a higher  $M^+-29$  compared to  $M^+-31$ , and have a raised  $M^+-57$ . The unsaturated monoenoic fatty acids (figure 24) were identified using different mass spectra libraries (e.g. GCMS library and lipid-database online). The sterols were identified using a mass spectra library, and the diagnostic ions for identification can be seen in table 6 (also see figures 25 to 28). Due to the low TOC % the hopanoids (triterpenoids) were only identified after the SIM GCMS analysis, targeting specific ions (i.e. 189 and 191). The diagnostic ions for the identification of the hopanoids are presented in table 7 (also figure 29).

Figures 20 & 21 show the total volumes of the peaks identified from the two GCMS methods. The surface samples are described in detail since the highest number and highest amounts of compounds were identified here. In all surface samples from the normal GCMS method, the highest volume of lipids were the straight chain fatty acids accounting for more the half of the identified peak (57%, 60% and 53% for sand, brown mat and white mat, respectively). The second highest lipid abundance were the unsaturated fatty acids for both the sand sediment- and brown microbial mat samples corresponding to 35% and 34%, respectively. The white mat sample had a much lower volume of unsaturated fatty acids, making up only 4%. The branched fatty acids were only present in the sand sediment- and brown mat samples, constituting 6% and 3%, respectively. Finally the “other” category accounts for unknown compounds that do not fit in with the other categories. For the sand sediment- and the brown mat samples this volume was low, making up 2% and 3%, respectively, while the white mat sample had almost half of the total volume, accounting for 43% “other” lipids. However, it is worth noting that overall significantly more and greater peaks were found in the sand sediment and brown mat (i.e. higher concentrations compared with the white sample),

especially in fraction 3a. Although more lipids were identified using the SIM method, it should be noted again that most of these lipid biomarkers are significantly lower in volume than the lipid biomarkers identified from the normal GCMS method.

For the sand sediment sample the highest volume of lipids were the triterpenoids accounting for 34%, followed by the straight chain fatty acids, 27% and two propyl esters (hexadecanoic 2,3-bis[(trimethylsilyl)oxy] propyl ester and octadecanoic 2,3-bis[(trimethylsilyl)oxy] propyl ester), accounting for 18%. Here the “other” category made up 11% and the branched fatty acids, 10%.

In the brown mat the highest volume of the lipids were also the triterpenoids accounting for 31% of the total volume, followed by the straight chain fatty acids, 26%. The “other” category, two propyl esters, the branched fatty acids and the unsaturated fatty acids constituted 21%, 12%, 8% and 2%, respectively.

Lastly the white mat had a lower diversity, where the two propyl esters accounted for 49%, the triterpenoids, 27% and the “other” category, 24%.

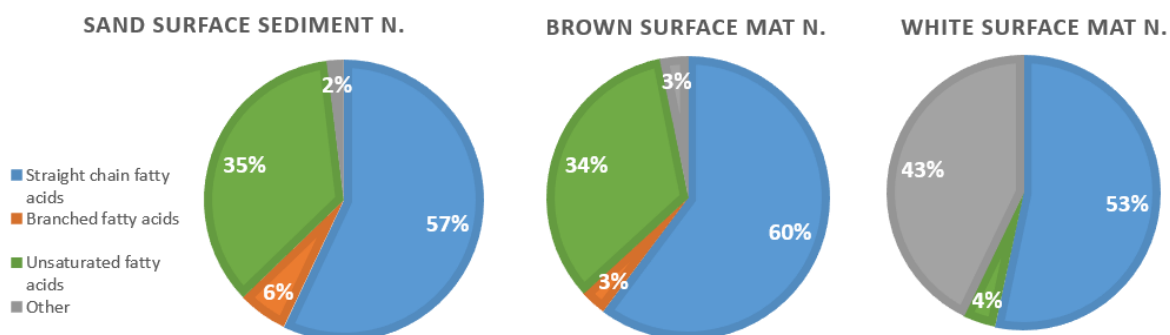


Figure 20. Pie chart distribution of total lipid biomarker volumes for the sand sediment-, brown mat-, and white mat surface samples. Above figure labeled with the “N.” illustrate the lipid biomarkers identified using the “normal” total ion GCMS method.

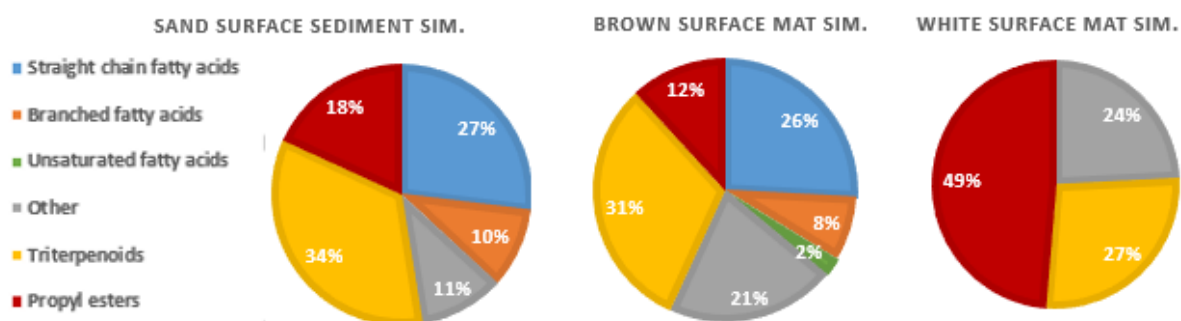


Figure 21. Pie chart distribution of total lipid biomarker volumes for the sand sediment-, brown mat-, and white mat surface samples. The figure is labeled with the “SIM.” illustrate the lipid biomarkers identified

using the "SIM" ion GCMS method.

\*Note that not all peaks have been identified from the chromatograph, due to low volumes, and are thus not accounted for in the total volume of the samples, however some unidentified peaks have been accounted for due to their high volumes and are represented in the "other" category.

### hexadecanoate (16:0)

#### Methyl Esters - Archive of Mass Spectra

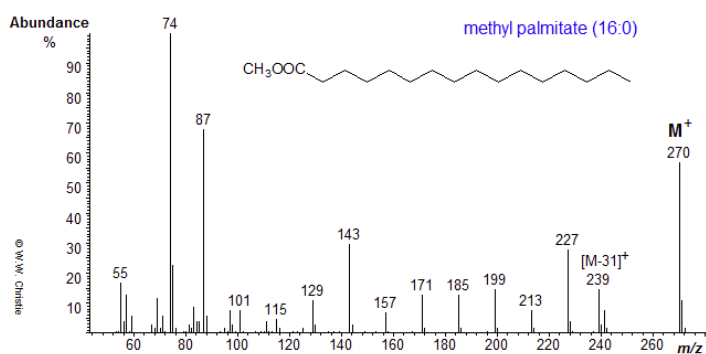


Figure 22. Mass spectra for Hexadecanoate (from AOCS lipid library)

### 14-methyl-pentadecanoate (iso)

#### Methyl Esters - Archive of Mass Spectra

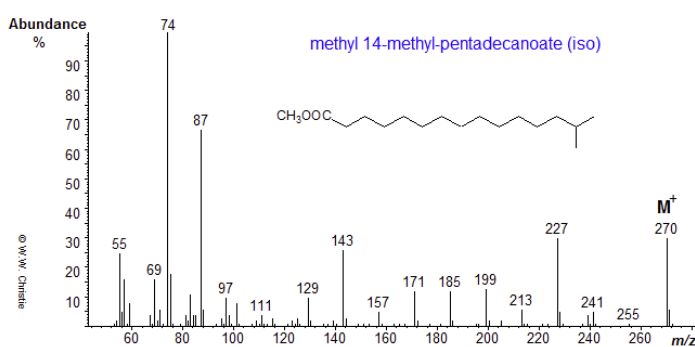


Figure 23. Mass spectra for 14-methyl pentadecanoate (iso) (from AOCS lipid library)

9-hexadecenoate (9-16:1)

Methyl Esters - Archive of Mass Spectra

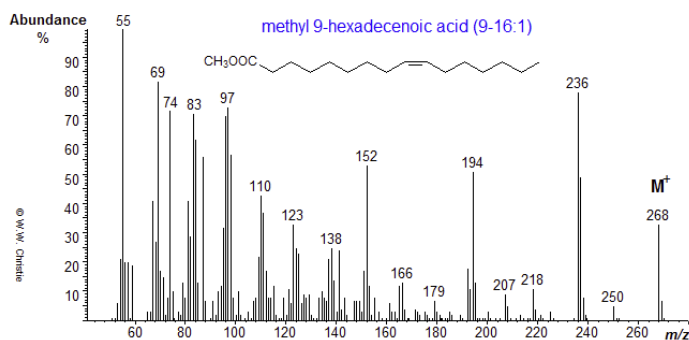


Figure 24. Mass spectra for 9-hexadecanoate (monoenoic FAmE) (from AOCs lipid library)

Table 6. List of sterols identified, underlining of diagnostic fragments refers to the base peak (highest peak).

Name	Carbon nr.	M <sup>+</sup>	Diagnostic fragments	Δ notation refers to position of double bond
Cholesterol	27	458	<u>129</u> ; 329; 353; 368; 443	Δ <sup>5</sup>
Sterol	28	470	<u>69</u> ; 125; 129; 255; 341; 365; 380	Δ <sup>5/22</sup>
Stigmasterol	29	484	<u>83</u> ; 129; 255; 351; 355; 379; 394	Δ <sup>5/22</sup>
.beta sitosterol	29	486	<u>129</u> ; 255; 357; 381; 396	Δ <sup>5</sup>

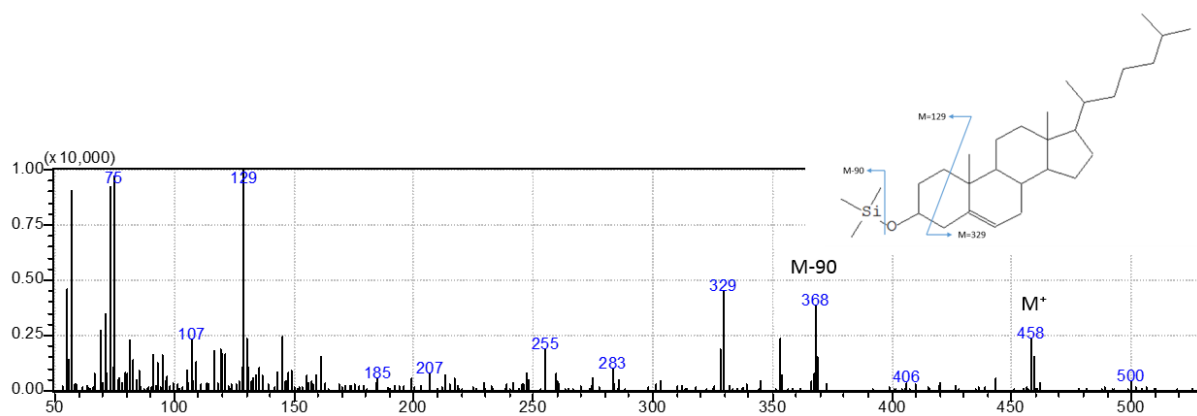


Figure 25. Spectrum for Cholesterol C<sub>27</sub> with Δ<sup>5</sup>.

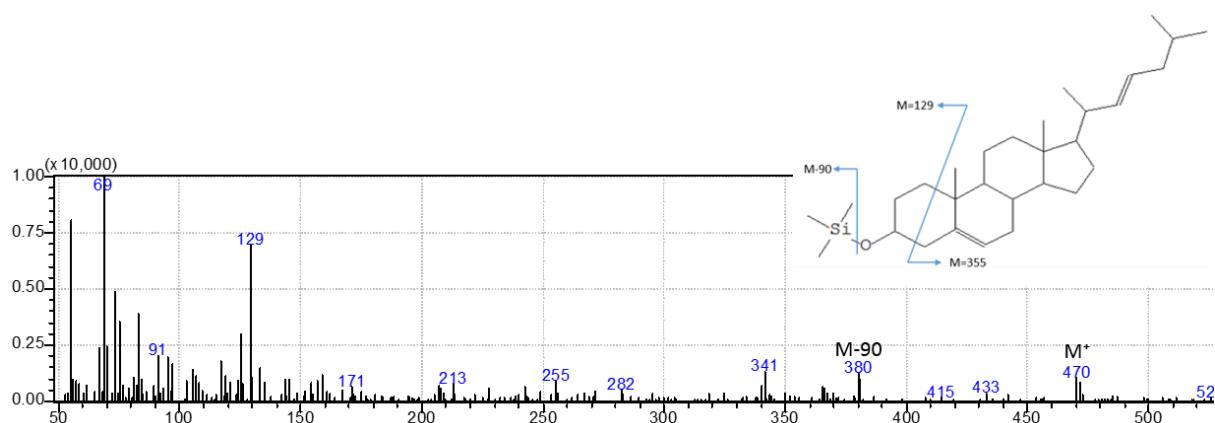


Figure 26. Spectrum for Sterol C<sub>28</sub> with  $\Delta^{5,22}$ .

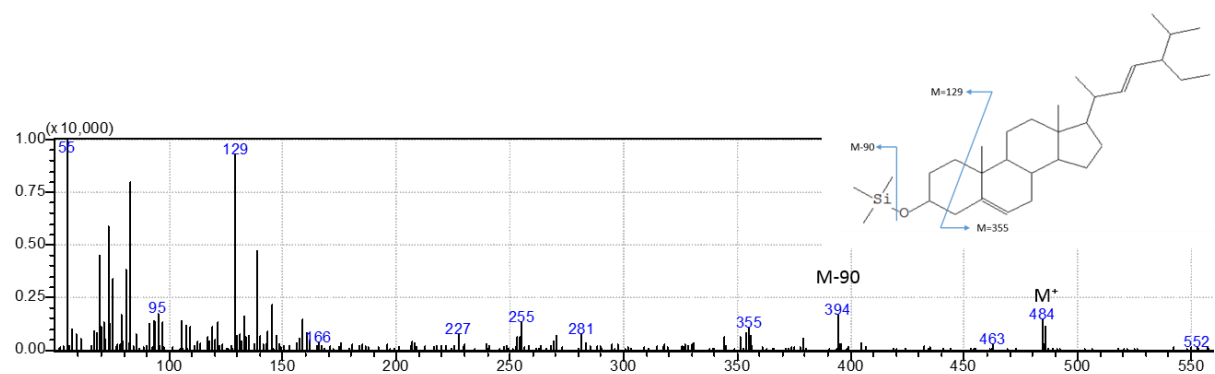


Figure 27. Spectrum for Stigmasterol C<sub>29</sub> with  $\Delta^{5,22}$ .

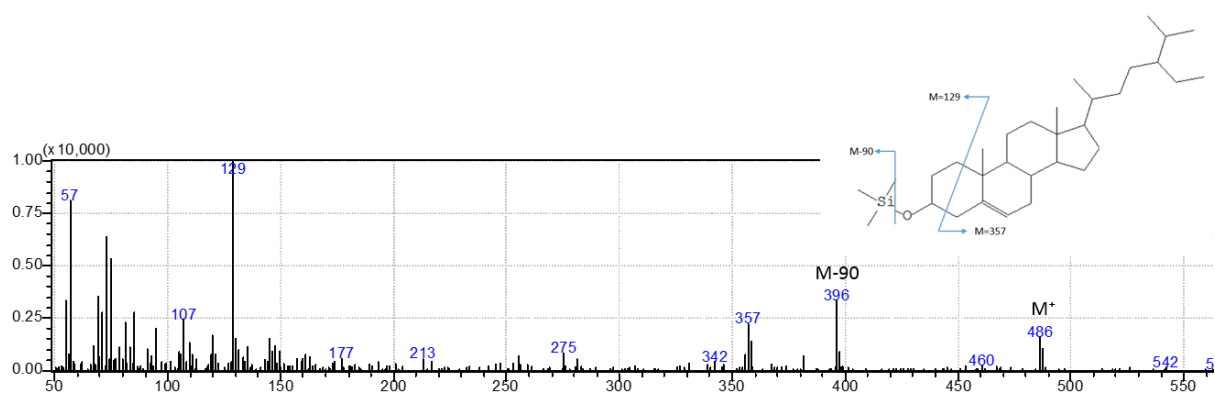


Figure 28. Spectrum for beta Sitosterol C<sub>29</sub> with  $\Delta^5$ .

Table 7. List of hopanes identified, underlining of diagnostic fragments refers to the base peak (highest peak).

Hopane	$M^+$	<u>Diagnostic fragments</u>
Diploptene	410	191
17 $\beta$ H,21 $\beta$ H-Homohopanoic fatty acid	470	<u>249</u> ; 191; 369; 455
17 $\alpha$ H,21 $\beta$ H-Bishomohopanoic fatty acid	484	<u>191</u> ; 263; 369; 469
17 $\beta$ H,21 $\beta$ H-Bishomohopanoic fatty acid	484	<u>263</u> ; 191; 369; 469

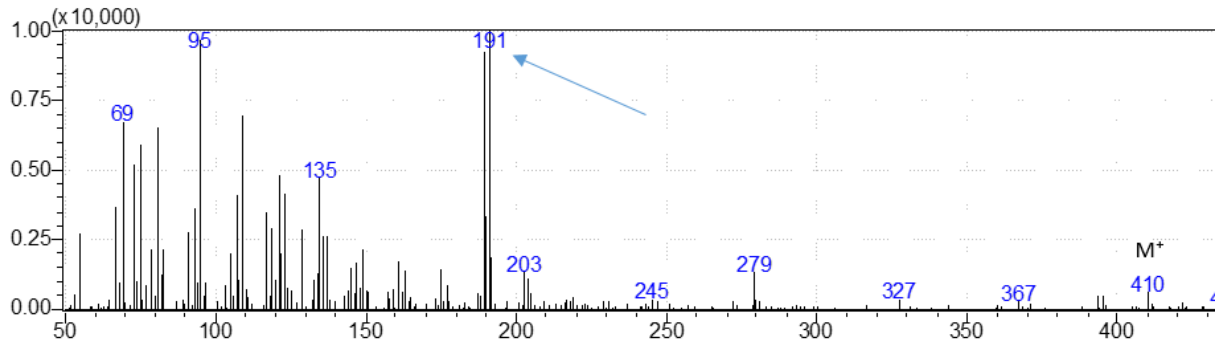


Figure 29. Spectrum for Diploptene, significant diagnostic fragments include: 191.

Table 8. Detailed list of the peaks from Brown mat shown in figure 30 fraction 3a.

Brown Mat	Surface Fraction 3a							
<i>Peak</i>	<i>Lipid biomarker</i>	<i>Identified compound</i>	<i>M*</i>	<i>Carbon nr</i>	<i>Formula</i>	<i>Known or postulated source</i>	<i>Area %</i>	<i>Reference</i>
1	S. Straight chain Fatty acid	Tetradecanoate	242	C <sub>14</sub>	C <sub>15</sub> H <sub>30</sub> O <sub>2</sub>	Eukaryote and Prokaryote	2.9% n.	Harwood & Russel (1984)
2	S. Straight chain Fatty acid	Pentadecanoate	256	C <sub>15</sub>	C <sub>16</sub> H <sub>32</sub> O <sub>2</sub>		1.7% n.	AOCS lipid library
3	Monoenoic Fatty acid	9-Hexadecenoic acid (9-16:1)	268	C <sub>16</sub>	C <sub>17</sub> H <sub>32</sub> O <sub>2</sub>	Eukaryote and Prokaryote	10.4% n.	Harwood & Russel (1984)
4	S. Straight chain Fatty acid	Hexadecanoate	270	C <sub>16</sub>	C <sub>17</sub> H <sub>34</sub> O <sub>2</sub>	Eukaryote and Prokaryote	20.2% n.	Harwood & Russel (1984)
5	S. Branched chain fatty acid	14-Methyl-hexadecanoate (anteiso)	284	C <sub>17</sub>	C <sub>18</sub> H <sub>36</sub> O <sub>2</sub>	Prokaryote. Anaerobic bacteria, e.g. Sulfate reducing bacteria	1.3% n.	Gaines (2009), AOCS lipid library
6	S. Branched chain fatty acid	15-Methyl-Hexadecanoate (iso)	284	C <sub>17</sub>	C <sub>18</sub> H <sub>36</sub> O <sub>2</sub>	Prokaryote. Anaerobic bacteria, e.g. Sulfate reducing bacteria	0.7% n.	Gaines (2009), AOCS lipid library
7	S. Straight chain Fatty acid	Heptadecanoate	284	C <sub>17</sub>	C <sub>18</sub> H <sub>36</sub> O <sub>2</sub>		1% n.	AOCS lipid library
8	Monoenoic Fatty acid	9-Octadecenoate (9-18:1)	296	C <sub>18</sub>	C <sub>19</sub> H <sub>36</sub> O <sub>2</sub>	Prokaryote	2.3% n.	Harwood & Russel (1984)
9	Monoenoic Fatty acid	11-Octadecenoate (11-18:1)	296	C <sub>18</sub>	C <sub>19</sub> H <sub>36</sub> O <sub>2</sub>	Prokaryote	2.9% n.	Harwood & Russel (1984)
10	S. Straight chain Fatty acid	Methyl Stearate, Octadecanoate	298	C <sub>18</sub>	C <sub>19</sub> H <sub>38</sub> O <sub>2</sub>		4.9% n.	AOCS lipid library
11	S. Branched chain fatty acid	18-Methyl-nonadecanoate (iso)	326	C <sub>20</sub>	C <sub>21</sub> H <sub>42</sub> O <sub>2</sub>	Prokaryote. Anaerobic bacteria, e.g. Sulfate reducing bacteria	2.6% SIM	Gaines (2009), AOCS lipid library
12	Monoenoic Fatty acid	13-Docosenoate	352	C <sub>22</sub>	C <sub>23</sub> H <sub>44</sub> O <sub>2</sub>		8.7% SIM	AOCS lipid library
13	S. Branched chain fatty acid	20-Methyl-heneicosanoate (anteiso)	354	C <sub>22</sub>	C <sub>23</sub> H <sub>38</sub> O <sub>2</sub>	Prokaryote. Anaerobic bacteria, e.g. Sulfate reducing bacteria	1.6% SIM	Gaines (2009), AOCS lipid library
14		Phthalic acid, di (2-propylpentyl) ester	390	C <sub>23</sub>	C <sub>24</sub> H <sub>38</sub> O <sub>4</sub>		0.4% SIM	AOCS lipid library
15		Eicosane	326	C <sub>19</sub>	C <sub>20</sub> H <sub>42</sub>		0.4% SIM	AOCS lipid library
16	S. Straight chain Fatty acid	Tricosanoate	368	C <sub>23</sub>	C <sub>24</sub> H <sub>48</sub> O <sub>2</sub>		0.9% SIM	AOCS lipid library
17		Squalene	422	C <sub>29</sub>	C <sub>30</sub> H <sub>62</sub>		7.6% SIM	AOCS lipid library
18	Monoenoic Fatty acid	15-Tetracosenoate (15-24:1)	380	C <sub>24</sub>	C <sub>25</sub> H <sub>48</sub> O <sub>2</sub>		2.5% SIM	AOCS lipid library
19	S. Straight chain Fatty acid	Tetracosanoate	382	C <sub>24</sub>	C <sub>25</sub> H <sub>50</sub> O <sub>2</sub>		7.3% SIM	AOCS lipid library
20	S. Straight chain Fatty acid	Pentacosanoate	396	C <sub>25</sub>	C <sub>26</sub> H <sub>52</sub> O <sub>2</sub>		1.9% SIM	AOCS lipid library
21		?			?		7.1% SIM	AOCS lipid library
22	S. Straight chain Fatty acid	Hexacosanoate	410	C <sub>26</sub>	C <sub>27</sub> H <sub>54</sub> O <sub>2</sub>		6.2% SIM	AOCS lipid library
23	S. Branched chain fatty acid	20-Methyl-Hexacosanoate	424	C <sub>27</sub>	C <sub>28</sub> H <sub>56</sub> O <sub>2</sub>		0.7% SIM	AOCS lipid library
24	S. Branched chain fatty acid	24-Methyl-Hexacosanoate (anteiso)	424	C <sub>27</sub>	C <sub>28</sub> H <sub>56</sub> O <sub>2</sub>	Prokaryote. Anaerobic bacteria, e.g. Sulfate reducing bacteria	0.9% SIM	Gaines (2009), AOCS lipid library
25	Monoenoic Fatty acid	19-Octacosenoate (19-28:1)	436		?		1.9% SIM	AOCS lipid library
26	S. Straight chain Fatty acid	Octacosanoate	438	C <sub>28</sub>	C <sub>29</sub> H <sub>58</sub> O <sub>2</sub>		3.5% SIM	AOCS lipid library
27	S. Straight chain Fatty acid	Triacosanoate	466	C <sub>30</sub>	C <sub>31</sub> H <sub>62</sub> O <sub>2</sub>	Eukaryote. Plant derived fatty alcohol	1.3% SIM	Gaines (2009), AOCS lipid library
28	S. Branched chain fatty acid	30-Methyl-Hentriacontanoate (iso)	494		?	Prokaryote. Anaerobic bacteria, e.g. Sulfate reducing bacteria	0.6% SIM	Mass spectra library
29	Hopanoid	17βH,21βH-Homohopanoic fatty acid	470	C <sub>31</sub>	?	Prokaryote, Aerobic bacteria	0.4% SIM	Mass spectra library
30	Hopanoid	17αH,21βH-Bishomohopanoic fatty acid	484	C <sub>32</sub>	?	Prokaryote, Aerobic bacteria	0.5% SIM	Mass spectra library
31	Hopanoid	17βH,21βH-Bishomohopanoic fatty acid	484	C <sub>32</sub>	?	Prokaryote, Aerobic bacteria	1.9% SIM	Mass spectra library

(S.= straight; n.= normal total ion GCMS method; SIM= SIM GCMS method)

Table 9. Detailed list of the peaks from Brown mat shown in figure 30 fraction 3b.

<b>Brown Mat</b>	<b>Surface Fraction 3b</b>							
<i>Peak</i>	<i>Lipid biomarker</i>	<i>Identified compound</i>	<i>M*</i>	<i>Carbon nr</i>	<i>Formula</i>	<i>Known or postulated source</i>	<i>Area %</i>	<i>Reference</i>
1		Glycerol	308	C <sub>3</sub>	C <sub>12</sub> H <sub>32</sub> O <sub>3</sub> Si <sub>3</sub>		1.4% n.	GCMS library
2		Nonanoic acid	230		C <sub>12</sub> H <sub>26</sub> O <sub>2</sub> Si		0.7% n.	GCMS library
3	S. Straight chain Fatty acid	Tetradecanoate	242	C <sub>14</sub>	C <sub>15</sub> H <sub>30</sub> O <sub>2</sub>	Eukaryote and Prokaryote	0.9% n.	Harwood & Russel (1984)
4	Monoenoic Fatty acid	9-Hexadecenoic acid (9-16:1)	268	C <sub>16</sub>	C <sub>17</sub> H <sub>32</sub> O <sub>2</sub>	Prokaryote	5.4% n.	Harwood & Russel (1984)
5	S. Straight chain Fatty acid	Hexadecanoate	270	C <sub>16</sub>	C <sub>17</sub> H <sub>34</sub> O <sub>2</sub>	Eukaryote and Prokaryote	5.8% n.	Harwood & Russel (1984)
6	S. Straight chain Fatty acid	Hexadecanoic acid. TMS ester	328		C <sub>19</sub> H <sub>40</sub> O <sub>2</sub> Si		2.1% n.	GCMS library
7	Monoenoic Fatty acid	10-Octadecenoate	296		C <sub>19</sub> H <sub>36</sub> O <sub>2</sub>	Prokaryote	1.3% n.	Harwood & Russel (1984)
8	S. Straight chain Fatty acid	Methyl Stearate	298	C <sub>18</sub>	C <sub>19</sub> H <sub>38</sub> O <sub>2</sub>		1.4% n.	GCMS library
9	Ester	Hexadecanoic acid. 2.3-bis propyl ester	474	C <sub>16</sub>	C <sub>25</sub> H <sub>54</sub> O <sub>4</sub> Si		5.3% SIM	GCMS library
10		Tetracosan-1-ol trimethylsilyl ether	426	C <sub>24</sub>	C <sub>27</sub> H <sub>58</sub> OSi		0.4% SIM	GCMS library
11	Ester	Octadecanoic acid. 2.3-bis propyl ester	502	C <sub>18</sub>	C <sub>27</sub> H <sub>58</sub> O <sub>4</sub> Si <sub>2</sub>		4.3% SIM	GCMS library
12		Squalene	422	C <sub>29</sub>	C <sub>30</sub> H <sub>62</sub>		1.1% SIM	GCMS library
13	Sterol	Cholesterol Δ <sup>5</sup>	458	C <sub>27</sub>	C <sub>30</sub> H <sub>54</sub> OSi	Eukaryote	3.6% SIM	Mass spectra library
14	Sterol	Sterol Δ <sup>5 22</sup>	470	C <sub>28</sub>	?	Eukaryote	3.3% SIM	Mass spectra library
15	Sterol	Stigmasterol Δ <sup>5 22</sup>	484	C <sub>29</sub>	C <sub>32</sub> H <sub>56</sub> OSi	Eukaryote	3.5% SIM	Mass spectra library
16	Sterol	.beta Sitosterol Δ <sup>5</sup>	484	C <sub>29</sub>	C <sub>32</sub> H <sub>58</sub> OSi	Eukaryote	10.6% SIM	Mass spectra library
17	Hopanoid	Diploptene	410	C <sub>30</sub>	C <sub>30</sub> H <sub>50</sub>	Prokaryote. Methanotrophic bacteria 13C-depleted	1% SIM	Sjöberg (2014). Gaines (2009)
18	Hopanoid	17βH.21βH-Bishomohopanoic fatty acid	484	C <sub>32</sub>	?	Prokaryote. Aerobic bacteria	0.7% SIM	Mass spectra library

(S.= straight; n.= normal total ion GCMS method; SIM= SIM GCMS method)

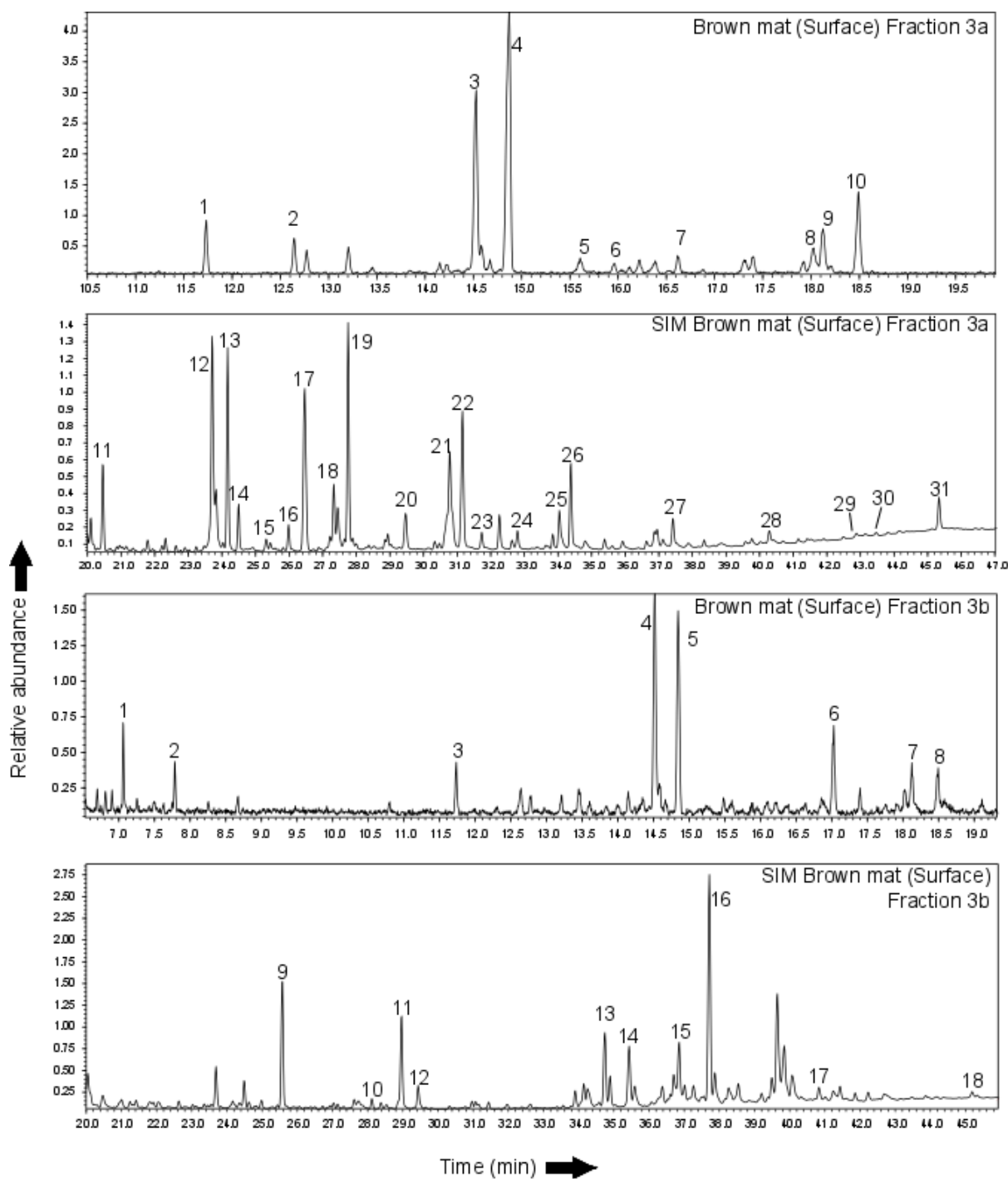


Figure 30. GCMS chromatogram of the total lipid extracts from brown mat's surface. The peaks are shown on tables 8 & 9.

Table 10. Detailed list of the peaks from Sand sediment shown in figure 31 fraction 3a.

<u>Sand sediment</u>	<u>Surface Fraction 3a</u>	<u>Identified compound</u>	<u>M<sup>+</sup></u>	<u>Carbon nr</u>	<u>Formula</u>	<u>Known or postulated source</u>	<u>Area %</u>	<u>Reference</u>
<u>Peak</u>	<u>Lipid type</u>							
1	S. Straight chain Fatty acid	Tetradecanoate	242	C <sub>14</sub>	C <sub>15</sub> H <sub>30</sub> O <sub>2</sub>	Eukaryote and Prokaryote	3.8% n.	Harwood & Russel (1984)
2	S. Branched chain fatty acid	12-Methyl-Tetradecanoate (anteiso)	256	C <sub>15</sub>	C <sub>16</sub> H <sub>32</sub> O <sub>2</sub>	Prokaryote. Anaerobic bacteria, e.g. Sulfate reducing bacteria	0.9% n.	Gaines (2009), AOCS lipid library
3	S. Straight chain Fatty acid	Pentadecanoate	256	C <sub>15</sub>	C <sub>16</sub> H <sub>32</sub> O <sub>2</sub>		3.8% n.	AOCS lipid library
4	Monoenoic Fatty acid	9-Hexacenoate (9-16:1)	268	C <sub>16</sub>	C <sub>17</sub> H <sub>32</sub> O <sub>2</sub>	Prokaryote	16% n.	Harwood & Russel (1984)
5	S. Straight chain Fatty acid	Hexadecanoate	270	C <sub>16</sub>	C <sub>17</sub> H <sub>34</sub> O <sub>2</sub>	Eukaryote and Prokaryote	17.2% n.	Harwood & Russel (1984)
6	S. Branched chain fatty acid	? ai14MeC <sub>16</sub> (anteiso)			?		0.8% n.	AOCS lipid library
7	S. Branched chain fatty acid	? 15-Methyl-Hexadecanoate (iso)	284	C <sub>17</sub>	C <sub>18</sub> H <sub>36</sub> O <sub>2</sub>	Prokaryote. Anaerobic bacteria, e.g. Sulfate reducing bacteria	0.3% n.	Gaines (2009), AOCS lipid library
8	S. Branched chain fatty acid	15-Methyl-Hexadecanoate (iso)	284	C <sub>17</sub>	C <sub>18</sub> H <sub>36</sub> O <sub>2</sub>	Prokaryote. Anaerobic bacteria, e.g. Sulfate reducing bacteria	1.3% n.	Gaines (2009), AOCS lipid library
9	S. Straight chain Fatty acid	Methyl Stearate	298	C <sub>18</sub>	C <sub>19</sub> H <sub>38</sub> O <sub>2</sub>		3.5% n.	AOCS lipid library
10	S. Straight chain Fatty acid	Heneicosanoate	340	C <sub>21</sub>	C <sub>22</sub> H <sub>44</sub> O <sub>2</sub>		2% SIM	AOCS lipid library
11	S. Straight chain Fatty acid	Docosanoate	354	C <sub>22</sub>	C <sub>23</sub> H <sub>46</sub> O <sub>2</sub>		3.1% SIM	AOCS lipid library
12	S. Straight chain Fatty acid	Tetracosanoate	382	C <sub>24</sub>	C <sub>25</sub> H <sub>50</sub> O <sub>2</sub>		7.5% SIM	AOCS lipid library
13		Squalene			?		1.9% SIM	AOCS lipid library
14	S. Branched chain fatty acid	14-methyl-hexacosanoate (anteiso)	284	C <sub>17</sub>	C <sub>18</sub> H <sub>36</sub> O <sub>2</sub>	Prokaryote. Anaerobic bacteria, e.g. Sulfate reducing bacteria	5.6% SIM	Gaines (2009), AOCS lipid library
15	S. Branched chain fatty acid	24-Methyl-Hexacosanoate (anteiso)	424	C <sub>27</sub>	C <sub>28</sub> H <sub>56</sub> O <sub>2</sub>	Prokaryote. Anaerobic bacteria, e.g. Sulfate reducing bacteria	0.5% SIM	Gaines (2009), AOCS lipid library
16	S. Straight chain Fatty acid	Octacosanoate	438	C <sub>28</sub>	C <sub>29</sub> H <sub>58</sub> O <sub>2</sub>		2.8% SIM	AOCS lipid library
17		Phosphate?			?		2.9% SIM	
18	S. Straight chain Fatty acid	Triacontanoic acid	466	C <sub>30</sub>	C <sub>31</sub> H <sub>62</sub> O	Eukaryote. Plant derived fatty alcohol	1.2% SIM	AOCS lipid library
19	Hopanoid	17βH,21βH-Homohopanoic fatty acid	470	C <sub>31</sub>	?	Prokaryote, Aerobic bacteria	0.7% SIM	Mass spectra library
20	Hopanoid	17αH,21βH-Bishomohopanoic fatty acid	484	C <sub>32</sub>	?	Prokaryote, Aerobic bacteria	0.8% SIM	Mass spectra library
21	Hopanoid	17βH,21βH-Bishomohopanoic fatty acid	484	C <sub>32</sub>	?	Prokaryote, Aerobic bacteria	2.7% SIM	Mass spectra library

(S.= straight; n.= normal total ion GCMS method; SIM= SIM GCMS method)

Table 11. Detailed list of the peaks from Sand sediment shown in figure 31 fraction 3b.

Sand sediment	Surface Fraction 3b	Identified compound	M <sup>+</sup>	Carbon nr	Formula	Known or postulated source	Area %	Reference
Peak	Lipid biomarker							
1		Glycerol	308	C <sub>3</sub>	C <sub>12</sub> H <sub>32</sub> O <sub>3</sub> Si <sub>3</sub>		0.7% n.	GCMS library
2	S. Straight chain Fatty acid	Tetradecanoate	242	C <sub>14</sub>	C <sub>15</sub> H <sub>30</sub> O <sub>2</sub>	Eukaryote and Prokaryote	0.7% n.	Harwood & Russel (1984)
3	S. Straight chain Fatty acid	Pentadecanoate	256	C <sub>15</sub>	C <sub>16</sub> H <sub>32</sub> O <sub>2</sub>		0.6% n.	AOCS lipid library
4		Phthalic acid. diisobutyl ester	278		C <sub>16</sub> H <sub>22</sub> O <sub>2</sub>		0.4% n.	GCMS library
5	Monoenoic Fatty acid	9-Hexadecenoic acid (9-16:1)	268	C <sub>16</sub>	C <sub>17</sub> H <sub>32</sub> O <sub>2</sub>	Prokaryote	4.3% n.	Harwood & Russel (1984)
6	S. Straight chain Fatty acid	Hexadecanoate	270	C <sub>16</sub>	C <sub>17</sub> H <sub>34</sub> O <sub>2</sub>	Eukaryote and Prokaryote	2.4% n.	Harwood & Russel (1984)
7	S. Straight chain Fatty acid	Hexadecanoic acid. TMS ester	328		C <sub>19</sub> H <sub>40</sub> O <sub>2</sub> Si		0.8% n.	AOCS lipid library
8		1-O-Hexadecylglycerol-bis ether derivative	460		C <sub>25</sub> H <sub>56</sub> O <sub>3</sub> Si		0.7% SIM	GCMS library
9		Phthalic acid. bis(2-ethylhexyl) ester	390		C <sub>24</sub> H <sub>38</sub> O <sub>4</sub>		0.5% SIM	GCMS library
10	Ester	Hexadecanoic acid. 2.3-bis propyl ester	474	C <sub>16</sub>	C <sub>25</sub> H <sub>54</sub> O <sub>4</sub> Si		6% SIM	GCMS library
11		Tetracosan-1-ol trimethylsilyl ether	426	C <sub>24</sub>	C <sub>27</sub> H <sub>58</sub> O <sub>2</sub> Si		0.5% SIM	GCMS library
12	Ester	Octadecanoic acid. 2.3-bis propyl ester	502	C <sub>18</sub>	C <sub>27</sub> H <sub>58</sub> O <sub>4</sub> Si <sub>2</sub>		4.6% SIM	GCMS library
13	Sterol	Cholesterol Δ <sup>5</sup>	458	C <sub>27</sub>	C <sub>30</sub> H <sub>54</sub> O <sub>2</sub> Si	Eukaryote	3% SIM	Mass spectra library
14	Sterol	Sterol Δ <sup>5 22</sup>	470	C <sub>28</sub>	?	Eukaryote	2.6 SIM	Mass spectra library
15	Sterol	Stigmasterol Δ <sup>5 22</sup>	484	C <sub>29</sub>	C <sub>32</sub> H <sub>56</sub> O <sub>2</sub> Si	Eukaryote	4.4% SIM	Mass spectra library
16	Sterol	.beta Sitosterol Δ <sup>5</sup>	484	C <sub>29</sub>	C <sub>32</sub> H <sub>58</sub> O <sub>2</sub> Si	Eukaryote	6.1% SIM	Mass spectra library
17	Hopanoid	Diploptene	410	C <sub>30</sub>	C <sub>30</sub> H <sub>50</sub>	Prokaryote. Methanotrophic bacteria 13C-depleted	0.6% SIM	Sjöberg (2014). Gaines (2009)

(S.= straight; n.= normal total ion GCMS method; SIM= SIM GCMS method)

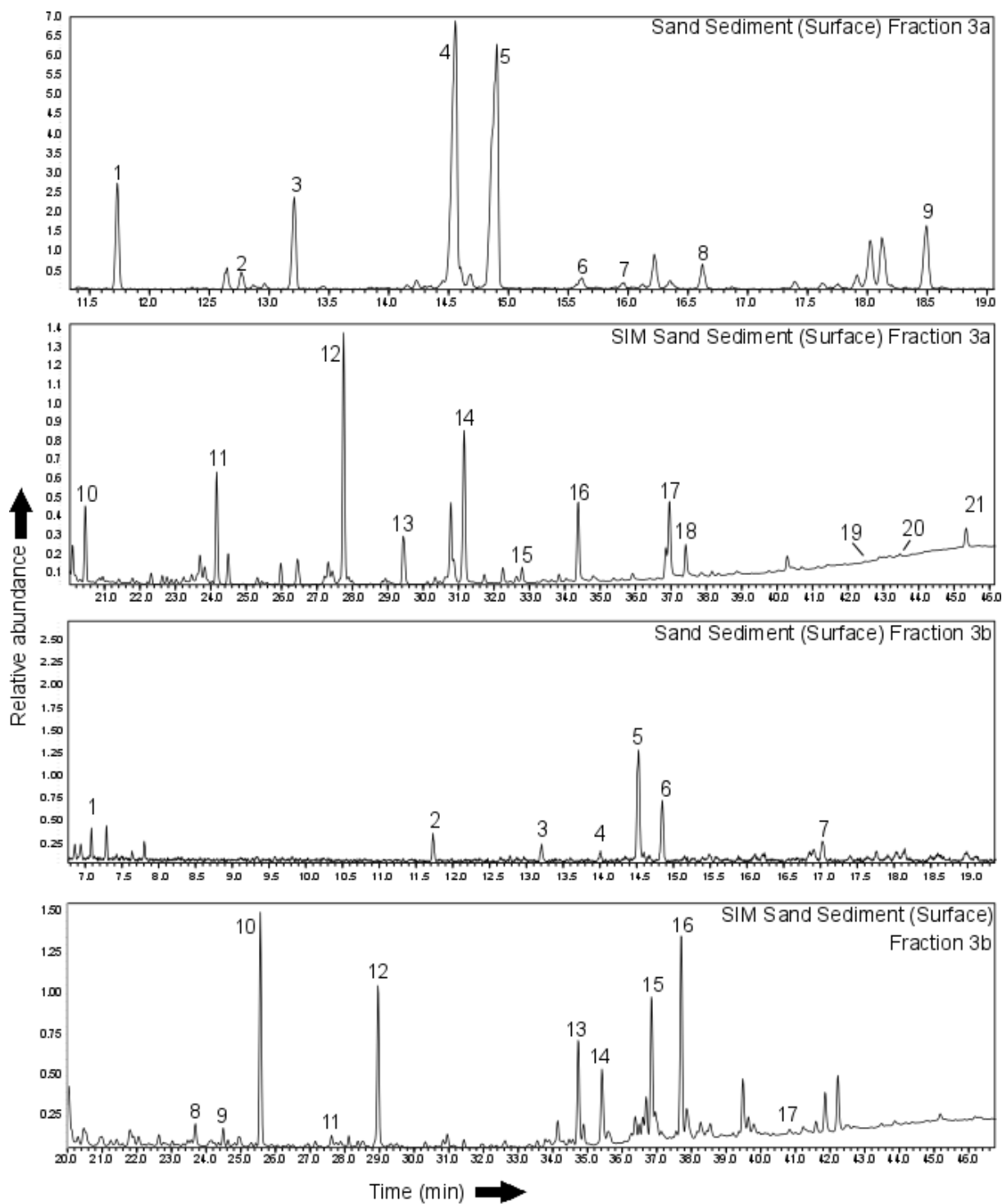


Figure 31. GCMS chromatogram of the total lipid extracts from sand sediment's surface). The peaks are shown on tables 10 & 11.

Table 12. Detailed list of the peaks from White mat shown in figure 32 fraction 3a.

White Mat	Surface Fraction 3a							
<i>Peak</i>	<i>Lipid biomarker</i>	<i>Identified compound</i>	<i>M*</i>	<i>Carbon nr</i>	<i>Formula</i>	<i>Known or postulated source</i>	<i>Area %</i>	<i>Reference</i>
1	Monoenoic Fatty acid	7-hexadecenoate	268		C <sub>17</sub> H <sub>32</sub> O <sub>2</sub>		1.6% n.	AOCS lipid library, GCMS library
2	S. Straight chain Fatty acid	Hexadecanoate	270	C <sub>16</sub>	C <sub>17</sub> H <sub>34</sub> O <sub>2</sub>	Eukaryote and Prokaryote	8.8% n.	Harwood & Russel (1984)
3		Sulfur contaminant			?		18% n.	GCMS library
4	S. Straight chain Fatty acid	Methyl Stearate	298	C <sub>18</sub>	C <sub>19</sub> H <sub>38</sub> O <sub>2</sub>		7% n.	GCMS library

(S.= straight; n.= normal total ion GCMS method; SIM= SIM GCMS method)

Table 13. Detailed list of the peaks from White mat shown in figure 32 fraction 3b.

White Mat	Surface Fraction 3b							
<i>Peak</i>	<i>Lipid biomarker</i>	<i>Identified compound</i>	<i>M*</i>	<i>Carbon nr</i>	<i>Formula</i>	<i>Known or postulated source</i>	<i>Area %</i>	<i>Reference</i>
1		Phthalic acid. di (2-propylpentyl) ester	390	C <sub>23</sub>	C <sub>24</sub> H <sub>38</sub> O <sub>4</sub>		0.9% n.	
2	Monoenoic Fatty acid	9-Hexadecenoic acid (9-16:1)	268	C <sub>16</sub>	C <sub>17</sub> H <sub>32</sub> O <sub>2</sub>	Prokaryote	0.3% n.	Harwood & Russel (1984)
3	S. Straight chain Fatty acid	Hexadecanoate	270	C <sub>16</sub>	C <sub>17</sub> H <sub>34</sub> O <sub>2</sub>	Eukaryote and Prokaryote	3.7% n.	Harwood & Russel (1984)
4	S. Straight chain Fatty acid	Hexadecanoic acid. TMS ester	328		C <sub>19</sub> H <sub>40</sub> O <sub>2</sub> Si		4.5% n.	AOCS lipid library. GCMS library
5	S. Straight chain Fatty acid	Methyl Stearate	298	C <sub>18</sub>	C <sub>19</sub> H <sub>38</sub> O <sub>2</sub>		2.4% n.	AOCS lipid library. GCMS library
6		Bis(2-ethylhexyl) phthalate			?		5.8% SIM	GCMS library
7	Ester	Hexadecanoic acid. 2.3-bis propyl ester	474	C <sub>16</sub>	C <sub>25</sub> H <sub>54</sub> O <sub>4</sub> Si		8.8% SIM	GCMS library
8	Ester	Octadecanoic acid. 2.3-bis propyl ester	502	C <sub>18</sub>	C <sub>27</sub> H <sub>58</sub> O <sub>4</sub> Si <sub>2</sub>		7% SIM	GCMS library
9		Squalene	422	C <sub>29</sub>	C <sub>30</sub> H <sub>62</sub>		1% SIM	GCMS library
10		Nonacosane	408		C <sub>29</sub> H <sub>60</sub>		1.3% SIM	GCMS library
11	Sterol	Cholesterol Δ <sup>5</sup>	458	C <sub>27</sub>	C <sub>30</sub> H <sub>54</sub> O <sub>Si</sub>	Eukaryote	2.6% SIM	Mass spectra library
12	Sterol	Sterol Δ <sup>5 22</sup>	470	C <sub>28</sub>	?	Eukaryote	2% SIM	Mass spectra library
13	Sterol	Stigmasterol Δ <sup>5 22</sup>	484	C <sub>29</sub>	C <sub>32</sub> H <sub>56</sub> O <sub>Si</sub>	Eukaryote	1% SIM	Mass spectra library
14	Sterol	.beta Sitosterol Δ <sup>5</sup>	484	C <sub>29</sub>	C <sub>32</sub> H <sub>58</sub> O <sub>Si</sub>	Eukaryote	0.5% SIM	Mass spectra library
15	Hopanoic acid	Diploptene	410	C <sub>30</sub>	C <sub>30</sub> H <sub>50</sub>	Prokaryote. Methanotrophic bacteria 13C-depleted	1.4% SIM	Sjöberg (2014). Gaines (2009)
16	Hopanoic acid	17βH.21βH-Bishomohopanoic fatty acid	484	C <sub>32</sub>	?	Prokaryote. Aerobic bacteria	1.4% SIM	Mass spectra library

(S.= straight; n.= normal total ion GCMS method; SIM= SIM GCMS method)

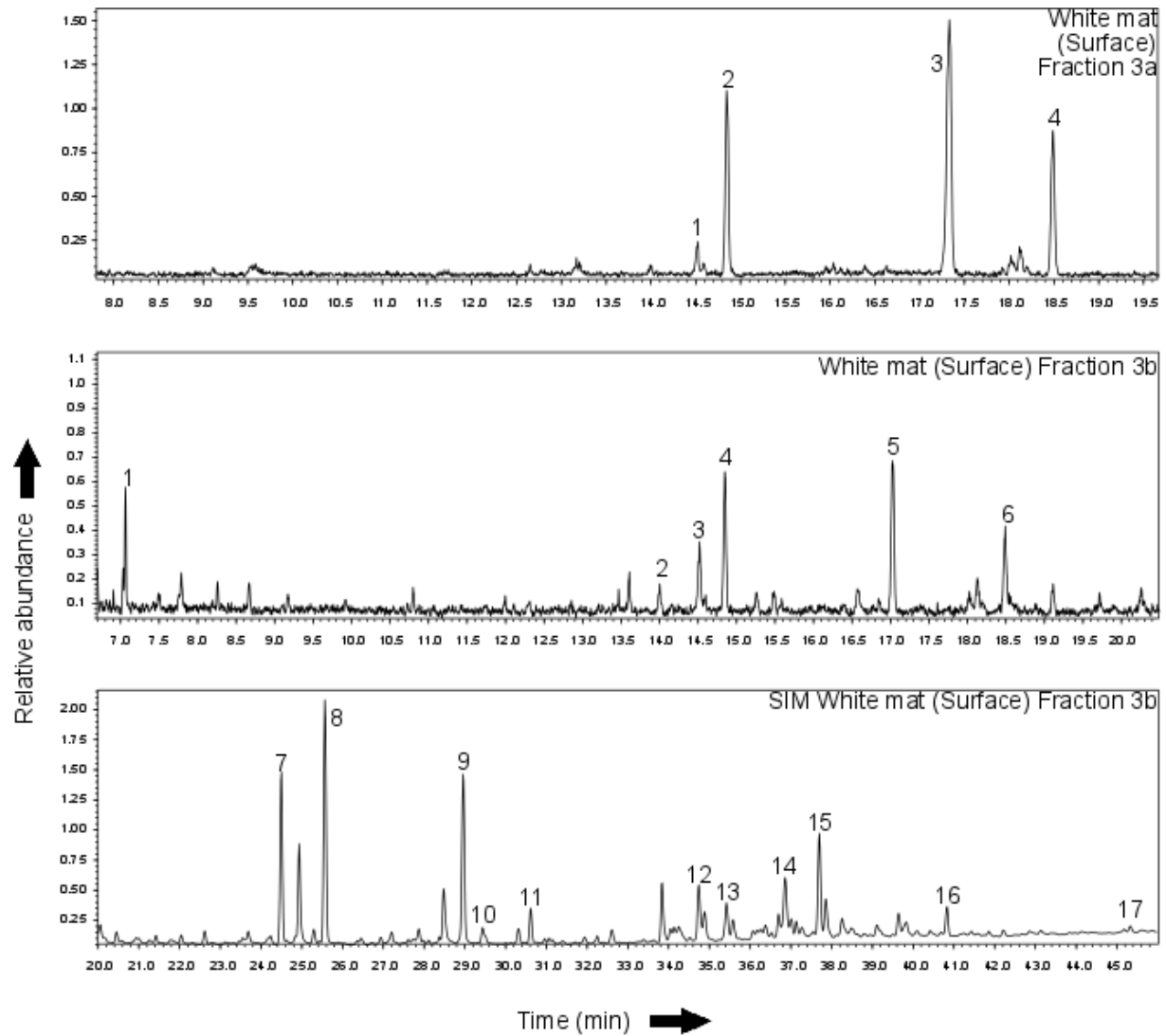


Figure 32. GCMS chromatogram of the total lipid extracts from white mat's surface. The peaks are shown on tables 12 & 13.

Table 14. Detailed lipid biomarker index acquired from the bacterial and archaeal cultures. Peaks are shown in figures 33 & 34. (S.= straight; n.= normal total ion GCMS method; SIM= SIM GCMS method)

<b>Geobacta</b>								
<b>Sulfurid</b>								
<u>Peak</u>	<u>Lipid type</u>	<u>Identified compound</u>	<u>M*</u>	<u>Carbon nr</u>	<u>Formula</u>	<u>Known or postulated source</u>	<u>Area %</u>	<u>Reference</u>
1		Dodecanoic acid. TMS ester	272		C <sub>15</sub> H <sub>32</sub> O <sub>2</sub>		1.2% n.	GCMS library
2	S. Straight chain Fatty acid	Tetradecanoate	242	C <sub>14</sub>	C <sub>15</sub> H <sub>30</sub> O <sub>2</sub>	Eukaryote and Prokaryote	1.7% n.	Harwood & Russel (1984)
3	S. Straight chain Fatty acid	Pentadecanoic acid	256				1.6% n.	GCMS library
4		Tetradecanoic acid. TMS ester	300				0.5% n.	GCMS library
5	Monoenoic Fatty acid	9-Hexadecenoic acid (9-16:1)	268			Eukaryote and Prokaryote	13.2% n.	Harwood & Russel (1984)
6	S. Straight chain Fatty acid	Hexadecanoate	270	C <sub>16</sub>	C <sub>17</sub> H <sub>34</sub> O <sub>2</sub>	Eukaryote and Prokaryote	20% n.	Harwood & Russel (1984)
7		Hexadecanoic acid. TMS ester	328		C <sub>19</sub> H <sub>40</sub> O <sub>2</sub> Si		5% n.	GCMS library
8	Monoenoic Fatty acid	11-Octadecenoate (11-18:1)	296			Eukaryote and Prokaryote	1.2% n.	Harwood & Russel (1984)
9	S. Straight chain Fatty acid	Methyl Stearate	298	C <sub>18</sub>	C <sub>19</sub> H <sub>38</sub> O <sub>2</sub>		10.1% n.	GCMS library
10		Octadecanoic acid. TMS ester	356				2.1% n.	GCMS library
11	Monoenoic Fatty acid	13-Docosenoate (13-22:1)	352		C <sub>23</sub> H <sub>44</sub> O <sub>2</sub>	Eukaryote and Prokaryote	2.2% SIM	Harwood & Russel (1984)
12	S. Straight chain Fatty acid	Docosanoate	354		C <sub>23</sub> H <sub>46</sub> O <sub>4</sub>		1.3% SIM	GCMS library
13	Ester	Hexadecanoic acid 2.3-bis propyl ester	474	C <sub>16</sub>	C <sub>25</sub> H <sub>54</sub> O <sub>4</sub> Si		10.3% SIM	GCMS library
14	Ester	Octadecanoic acid 2.3-bis propyl ester	502	C <sub>18</sub>	C <sub>27</sub> H <sub>58</sub> O <sub>4</sub> Si <sub>2</sub>		8.8% SIM	GCMS library
15		Squalene	422	C <sub>29</sub>	C <sub>30</sub> H <sub>62</sub>		1% SIM	GCMS library
<b>Mariprofundus</b>								
<u>Peak</u>	<u>Lipid type</u>	<u>Identified compound</u>	<u>M*</u>	<u>Carbon nr</u>	<u>Formula</u>	<u>Known or postulated source</u>	<u>Area %</u>	<u>Reference</u>
1	S. Straight chain Fatty acid	Hexadecanoate	270	C <sub>16</sub>	C <sub>17</sub> H <sub>34</sub> O <sub>2</sub>	Eukaryote and Prokaryote	13.2% n.	Harwood & Russel (1984)
2	S. Straight chain Fatty acid	Methyl Stearate	298	C <sub>18</sub>	C <sub>19</sub> H <sub>38</sub> O <sub>2</sub>		15.5% n.	
3	Ester	Hexadecanoic acid 2.3-bis propyl ester	474	C <sub>16</sub>	C <sub>25</sub> H <sub>54</sub> O <sub>4</sub> Si		19.3% SIM	GCMS library
4	Ester	Octadecanoic acid 2.3-bis propyl ester	502	C <sub>18</sub>	C <sub>27</sub> H <sub>58</sub> O <sub>4</sub> Si <sub>2</sub>		15% SIM	GCMS library
<b>Marinobacter</b>								
<b>Santorini</b>								
<u>Peak</u>	<u>Lipid type</u>	<u>Identified compound</u>	<u>M*</u>	<u>Carbon nr</u>	<u>Formula</u>	<u>Known or postulated source</u>	<u>Area %</u>	<u>Reference</u>
1	S. Straight chain Fatty acid	Hexadecanoate	270	C <sub>16</sub>	C <sub>17</sub> H <sub>34</sub> O <sub>2</sub>	Eukaryote and Prokaryote	5.7%	Harwood & Russel (1984)
2	S. Straight chain Fatty acid	Methyl Stearate	298	C <sub>18</sub>	C <sub>19</sub> H <sub>38</sub> O <sub>2</sub>		5.3%	
3	Ester	Hexadecanoic acid 2.3-bis propyl ester	474	C <sub>16</sub>	C <sub>25</sub> H <sub>54</sub> O <sub>4</sub> Si		3.2%	GCMS library
4	Ester	Octadecanoic acid 2.3-bis propyl ester	502	C <sub>18</sub>	C <sub>27</sub> H <sub>58</sub> O <sub>4</sub> Si <sub>2</sub>		1.8%	GCMS library
<b>Archaea</b>								
<u>Peak</u>	<u>Lipid type</u>	<u>Identified compound</u>	<u>M*</u>	<u>Carbon nr</u>	<u>Formula</u>	<u>Known or postulated source</u>	<u>Area %</u>	<u>Reference</u>
1		Propanoic acid	286		C <sub>16</sub> H <sub>30</sub> O <sub>4</sub>		0.9%	GCMS library
2	S. Straight chain Fatty acid	Tetradecanoate	242	C <sub>14</sub>	C <sub>15</sub> H <sub>30</sub> O <sub>2</sub>	Eukaryote and Prokaryote	0.8%	Harwood & Russel (1984)
3		1,2-Benzenedecarboxylic acid	278		C <sub>16</sub> H <sub>22</sub> O <sub>4</sub>		1.1%	GCMS library
4	S. Straight chain Fatty acid	Hexadecanoate	270	C <sub>16</sub>	C <sub>17</sub> H <sub>34</sub> O <sub>2</sub>	Eukaryote and Prokaryote	13.2%	Harwood & Russel (1984)
5	S. Straight chain Fatty acid	Octadecanoate	324		C <sub>21</sub> H <sub>40</sub> O <sub>2</sub>		0.8%	GCMS library
6	Monoenoic Fatty acid	9-Octadecenoate (9-18:1)	296	C <sub>18</sub>	C <sub>19</sub> H <sub>38</sub> O <sub>2</sub>	Prokaryote	0.8%	Harwood & Russel (1984)
7	S. Straight chain Fatty acid	Methyl Stearate	298	C <sub>18</sub>	C <sub>19</sub> H <sub>38</sub> O <sub>2</sub>		11.6%	GCMS library
8	S. Branched chain Fatty acid	18-Methyl-nonadecanoate	326	C <sub>20</sub>	C <sub>21</sub> H <sub>42</sub> O <sub>2</sub>	Prokaryote. Anaerobic bacteria. e.g. Sulfate reducing bacteria	0.13%	Gaines (2009). AOCs lipid library

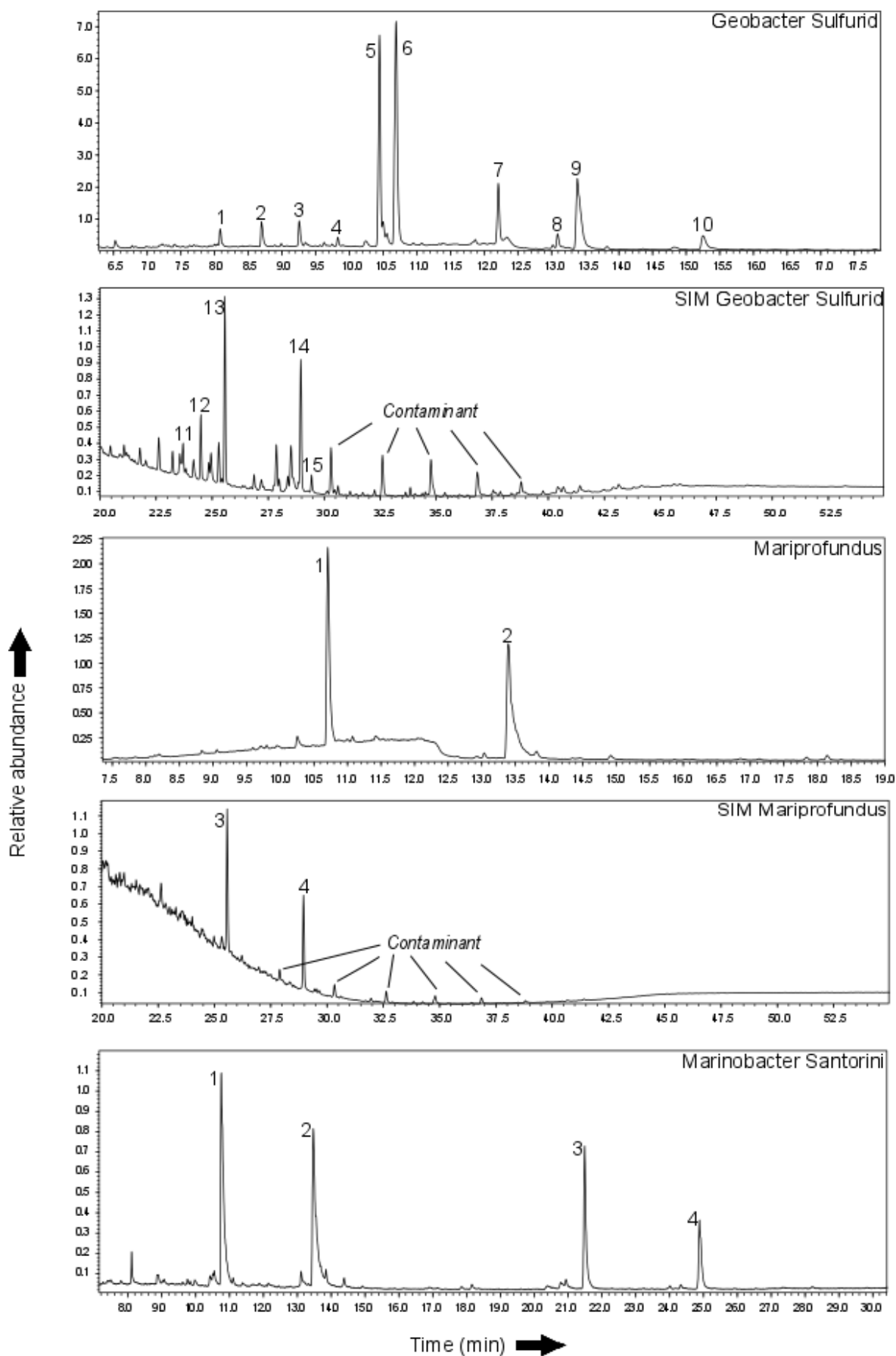


Figure 33. GCMS chromatogram of the pure bacteria and archaea cultures. Detailed list of peak in table 14.

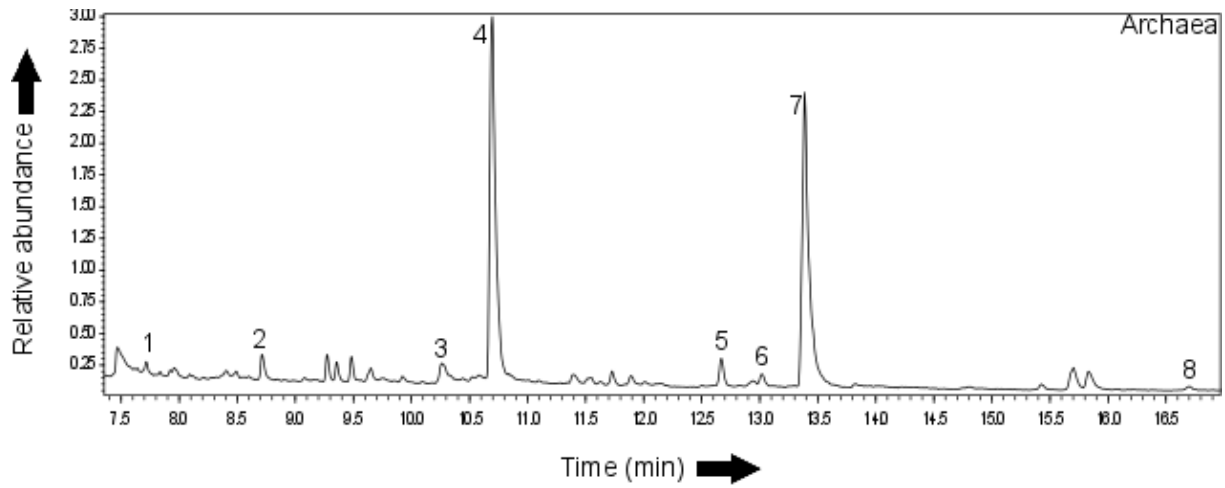


Figure 34. GCMS chromatogram of the pure bacteria and archaea cultures. Detailed list of peak in table 14.